PHOTOPHYSICAL AND PHOTOCHEMICAL STUDIES OF NOVEL THIOXANTHONE-FUNCTIONALIZED METHACRYLATES

by

Tuğçe Nur Eren

B.S., Chemistry, Boğaziçi University, 2013

Submitted to the Institute for Graduate Studies in
Science and Engineering in partial fulfillment of
the requirements for the degree of
Master of Science

Graduate Program in Chemistry

Boğaziçi University

2015

Dedicated to my family…

ACKNOWLEDGEMENTS

I would like to deeply thank my supervisor Prof. Duygu Avcı Semiz for her valuable guidance, advices, attention and encouragement throughout my project. I gained a lot of experience thanks to her and I am very appreciated to do master's degree under her supervision.

I would like to express my appreciation to Prof. Jacques Lalevée for welcoming me in the Institut of Materials Science of Mulhouse – National Center for Scientific Research (IS2M - CNRS) for a colloboration. I gained many experiences due to his guidance and advices. I also want to thank his group members for their helps and friendship.

I want to express my thanks to my committee members Prof. İlknur Doğan and Prof. Nilhan Kayaman Apohan for politely sparing their valuable time for reviewing the final manuscript and for their constructive interpretations and recommendations.

I wish to extend my great thanks to Sesil Çınar and Belgin Cesur due to their assistance and guidance particularly in my first experiences in the laboratory. I also thank to my dear group friends Fulya Köylü, Betül Bingöl, Melek Naz Güven and Ece Akyol for their help and friendship.

I would also like to thank all members of Chemistry Department for their helps.

I want to express my gratitude to my mother, father, grandmother, grandfather and all my family for their endless love, support and encouragement throughout my entire life.

Finally, I also want to thank to The Scientific and Technological Research Council of Turkey (TÜBİTAK) [113Z241] and Bogazici University Research Fund (7940) for their financial support for my research.

ABSTRACT

PHOTOPHYSICAL AND PHOTOCHEMICAL STUDIES OF NOVEL THIOXANTHONE-FUNCTIONALIZED METHACRYLATES

Five novel thioxanthone (TX) based monomeric photoinitiators (PIs) for free radical polymerization of acrylates were synthesized from reactions of *tert*-butyl α-bromomethacrylate with 2-hydroxy thioxanthone (TX1) and 1,4-dihydroxy thioxanthone (TX3); and by cleavage of their respective *tert*-butyl ester groups with trifluoro acetic acid (TX2 and TX4); and by reaction of the acid chloride derivative of TX2 with 2-hydroxy-1-[4-(2-hydroxyethoxy)phenyl]-2-methyl-1-propanone (Irgacure 2959) (TX5). This last monomeric PI possesses two side-chain photoinitiating groups. The photoinitiator TX1 has also been copolymerized with N,N-dimethylaminoethyl methacrylate (DMAEM) to give a polymeric photoinitiator. All these monomeric PIs absorb in the near UV-visible region (390-420 nm; absorption red-shift ~10-40 nm) with comparable ε values to TX. Their photoinitiating abilities of acrylate polymerizations are studied under LED exposure at 385 and 405 nm using real-time FTIR and under mercury lamp using photo-DSC. The performances of TX1 and TX2 are similar to isopropyl thioxanthone, and TX used as reference photoinitiators. The reactivities of TX3 and TX4 are lower, due to their difunctional character, which however makes it possible for them to simultaneously serve as crosslinking agents. The successful photoinitiating by TX5 under visible light proves that TX5 contains both photoinitiator and photosensitizer groups. The photochemical mechanisms are studied by electron spin resonance, steady state photolysis, laser flash photolysis experiments and cyclic voltammetry techniques.

ÖZET

YENİ TİYOKZANTON FONKSİYONEL METAKRİLATLARIN FOTOFİZİKSEL VE FOTOKİMYASAL İNCELEMELERİ

Akrilatların serbest radikal polimerizasyonunda kullanılmak üzere, beş yeni tiyokzanton (TX) bazlı monomerik fotobaşlatıcı, *tert*-bütil α-bromo metakrilatın 2-hidroksi tiyokzanton (TX1) ve 1,4-dihidroksi tiyokzanton (TX2) ile reaksiyonlarından; ve *tert*-bütil ester gruplarının trifloro asetik asit ile kırılmasından (TX2 ve TX4); TX2'nin asit klorür türevinin, 2-hidroksi-1-[4-(2-hidroksietoksi)fenil]-2-metil-1-propanon (Irgacure 2959) ile reaksiyonundan (TX5) sentezlendi. Bu son monomerik fotobaşlatıcı yan zincirinde iki fotobaşlatıcı gruba sahiptir. Fotobaşlatıcı TX1, N, N- dimetilaminoetil metakrilat (DMAEM) ile kopolimerleştirildiğinde polimerik bir fotobaşlatıcı elde edildi. Tüm bu monomerik fotobaşlatıcılar yakın ultraviyole-görünür bölgesinde (390-420 nm; kırmızıya kayma ~10-40 nm) ve tiyokzantona kıyaslanabilir ε değerlerinde absorb ederler. Akrilat polimerizasyonlarını fotobaşlatma etkinlikleri, 385 ve 405 nm'de LED ışık kaynakları ile gerçek zamanlı FTIR spektrometresi kullanılarak ve civa lambası altında foto diferansiyel taramalı kalorimetre kullanılarak incelendi. TX1 ve TX2'nin performansları referans fotobaşlatıcılar olarak kullanılan izopropil tiyokzanton ve TX'e benzerdir. TX3 ve TX4'ün reaktiflikleri çift fonksiyonel gruba sahip olmalarından dolayı daha düşüktür, fakat bu özellik dolayısıyla aynı zamanda çapraz bağlayıcı olarak görev yapabilirler. TX5'in görünür ışık altında fotobaşlatma etkinliği, TX5'in hem fotobaşlatıcı hem de fotoduyarlı gruplar içerdiğini kanıtlar. Fotokimyasal mekanizmalar; elektron döngü rezonansı, durağan durum fotolizi, lazer flaş fotoliz deneyleri ve dönüşümlü voltametri teknikleri ile incelendi.

TABLE OF CONTENTS

LIST OF TABLES

LIST OF FIGURES

LIST OF SYMBOLS

[I]	Concentration of the initiator
k_{diss}	The dissociation rate constant
k_p	The rate constant of the propagation reaction
k_t	The rate constant of the termination reaction
M	The molar mass of the monomer
M_n	The number average molecular weight
N	The number of double bonds per monomer molecule
PI	Photoinitiator
PPI	Polymeric photoinitiator
Q/ s	Heat flow per second
R_i	Rate of initiation
R_{pmax}	The maximum rate of polymerization
R_p	Rate of polymerization
TX1	*tert*-Butyl 2-((9-oxo-9H-thioxanthen-2-yloxy)methyl)acrylate
TX2	2-((9-Oxo-9H-thioxanthen-2-yloxy)methyl)acrylic acid
TX3	*tert*-Butyl 2,2'-(9-oxo-9H-thioxanthene-1,4 diyl)bis(oxy)bis(methylene)diacrylate
TX4	2,2'-((9-Oxo-9H-thioxanthene-1,4-diyl)bis(oxy))bis(methylene))diacrylic acid
TX5	2-(4-(2-Hydroxy-2-methylpropanoyl)phenoxy)ethyl 2-(((9-oxo-9*H*-thioxanthen-2-yl)oxy)methyl)acrylate

ΔH_p	Heat released per mole of double bonds reacted
ε	Extinction coefficient
I_a	Intensity of absorbed light
λ_{max}	The wavelengths for maximum absorption
Φ	Number of propagation chains initiated per light photon absorbed

LIST OF ACRONYMS/ ABBREVIATIONS

AIBN	2,2'-Azobisisobutyronitrile
AA	Acrylamide
AP	Acetophenone
BP	Benzophenone
CO_2Cl_2	Oxalyl chloride
DABCO	1,4-Diazabicyclo[2.2.2]octane
DMAEM	N,N-dimethylaminoethyl methacrylate
DMF	Dimethylformamide
DSC	Differential Scanning Calorimetry
EDB	Ethyl 4-(dimethylamino)benzoate
ESR	Electron Spin Resonance
FT-IR	Fourier Transform Infrared Spectroscopy
GPC	Gel Permeation Chromatography
HDDA	Hexane-1,6-diol diacrylate
IRGACURE 2959	2-Hydroxy-1-[4-(2-hydroxyethoxy)phenyl]-2-methyl-1-Propanone
ITX	2-Isopropylthioxanthone
LFP	Laser Flash Photolysis
MDEA	Methyl diethanolamine
MMA	Methyl methacrylate

NMR	Nuclear Magnetic Resonance spectroscopy
PEG	Poly(ethylene) glycol
PEO	Poly(ethylene) oxide
PVA	Poly(vinyl) alcohol
RHMA	Alkyl α-hydroxymethacrylate
TBBr	*Tert*-butyl α-bromomethacrylate
TBHMA	*Tert*-butyl α-hydroxymethacrylate
TEA	Triethylamine
TEGDMA	Triethyleneglycol dimethacrylate
T_g	Glass transition temperature
THF	Tetrahydrofuran
TFA	Trifluoroacetic acid
TMPTA	Trimethylolpropane triacrylate
TX	Thioxanthone

1. INTRODUCTION: PHOTOPOLYMERIZATION

Photocuring is a growing technology. Its advantages over thermally oriented processes are low energy demand, high production yield, very good price/performance ratio, fast & thorough-curing, low temperature requirements and solvent free formulations (nearly no volatile organic compounds, VOCs). Due to these advantages, photocuring has widespread application in daily life and industry; in areas such as coatings, adhesives, inks, paints, varnishes, microelectronics, optics, printing, production of 3D objects, nanotechnology, and in particular applications in which heating is not acceptable, such as dental fillings and some other medical applications [1-3].

Photopolymerization reactions require a polymerizable medium (a monomer/oligomer matrix), a photoinitiator or a photoinitiating system, and a light source; a strong coherence should be ensured between them. The photoinitiator which has a little mass fraction but a major role in polymerizable formulation, absorbs the energy of the light and forms the reactive species (free radicals or cations) which then converts the monomer or prepolymer into a linear polymer or crosslinked network [4]. Photoinitiators also have an influence on the physical and mechanical properties of the cured network. Depending on the nature of reactive species, the photopolymerization reaction can occur either cationically or free radically [1].

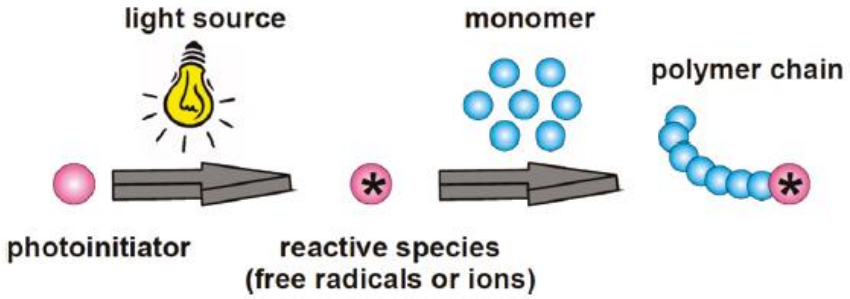

Figure 1.1. Photopolymerization process [3].

1.1. Photoinitiated Free Radical Polymerization

Photoinduced free radical polymerization is widely used in many industrial application areas. Its progress compared to photoinitiated cationic polymerization is due to its applications in a wide range of formulations such as (meth)acrylates, unsaturated polyesters and acrylated polyurethanes. The sustainability of free radical photoinitiators which have absorption in the near-UV and visible range is also another reason why light-induced free radical polymerization is more popular [5].

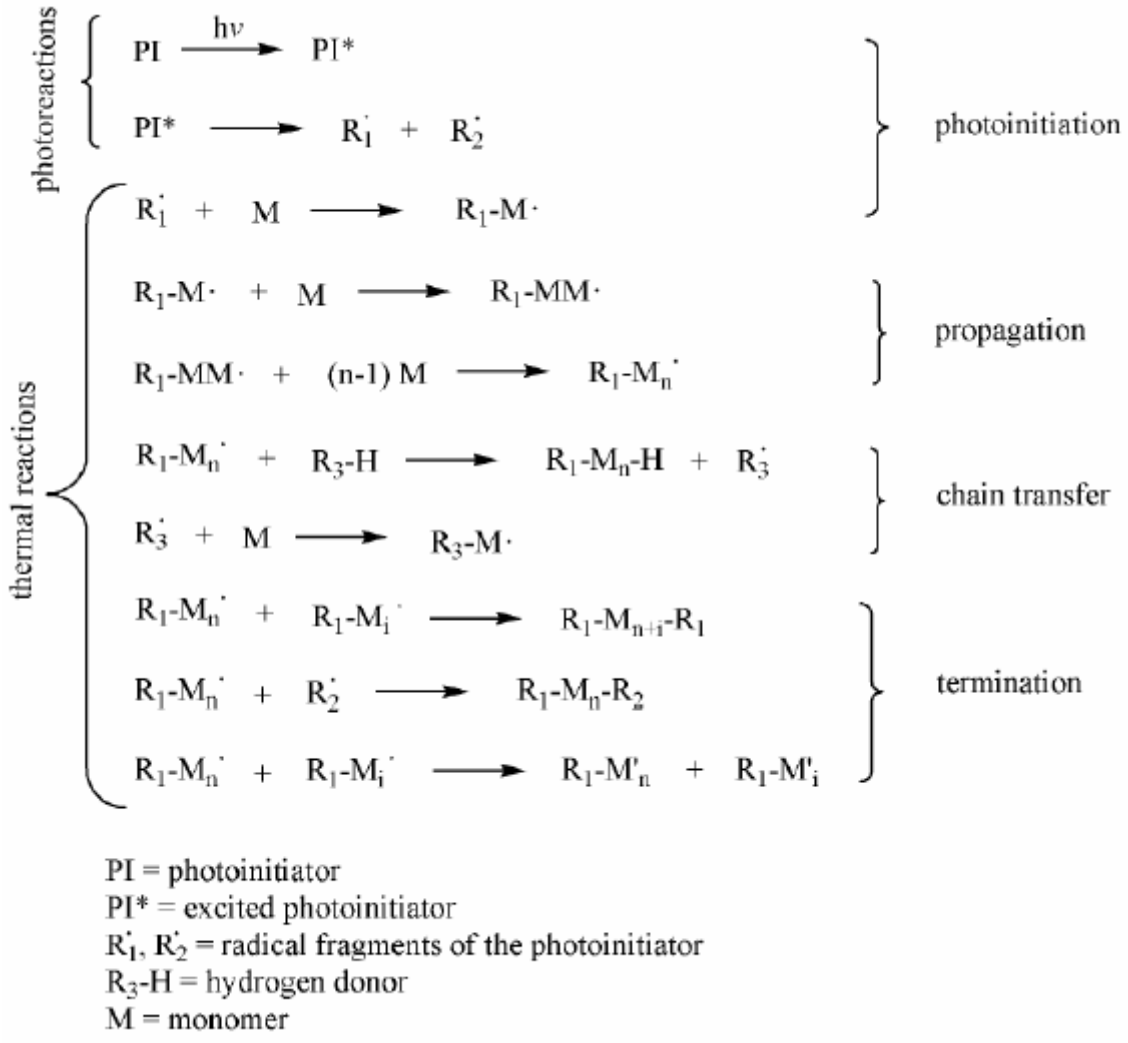

Figure 1.2. Reaction pathway in photoinitiated free radical polymerization.

A free radical polymerization reaction takes place in four steps (Figure 1.2.) which are photoinitiation, propogation, chain transfer and termination [1].

The first step of free radical polymerization, photoinitiation, involves formation of intiating radicals upon light absorption of a photoinitiating system (PIS). A photoinitiating system for light-induced free radical polymerization can be a photoinitiator, a photoinitiator and a co-initiator or a photosensitizer and a photoinitiator [6]. In the second step, the initiating radicals react with monomer and the polymerization reaction propagates. The chain transfer reaction which is called as radical displacement reaction comprises the untimely termination of a growing polymer chain by the transfer of a hydrogen from various species present in the system (e.g. unreacted monomer, initiator or solvent) and formation of new initiating radicals which initiates another polymer chain reaction [7]. The last step is termination reaction which ends the polymerization reaction by consuming the initiating radicals [1].

The rate of initiation (R_i) which determines the rate of radical formation is expressed as

$$R_i = 2\Phi I_a \tag{1.1}$$

where Φ is quantum yield for initiation process which depicts the number of propagating chains initiated per light photon absorbed. The factor of 2 shows that two radicals are formed per molecule which has photolysis. It is not used for the photoinitiating system that generates only one radical. The maximum value of Φ is 1 for all photoinitiating systems. I_a is the symbol for the intensity of absorbed light in moles of light quanta per liter-second. R_i can also be given by

$$R_i = 2\Phi\varepsilon I[\mathrm{PI}]h \tag{1.2}$$

The term Φ indicates the quantum yield for initiation. ε is the molar absorbtivity (extinction coefficient), I is intensity of the incoming light and h is the thickness of reaction system undergoing irradiation.

R_p, the rate of polymerization is expressed as

$$R_p = k_p[M](R_i/2k_t)^{1/2} \quad (1.3)$$

where R_i is the rate of initiation process, k_p is propagation rate constant, [M] is the monomer concentration, k_t is the rate constant for termination.
Combining Equations 1.1 and 1.3 we get

$$R_p = k_p[M](\Phi\varepsilon[I]h/k_t)^{1/2} \quad (1.4)$$

1.2. Free Radical Photoinitiators

Photoinitiators or photoinitiating systems are conjunctives in the photopolymerization formulation between the monomer/oligomer matrix and the light source [8]. The properties that a photoinitiating system must have are; good solubility in the formulation, no odor and toxicity, no darkening due to the migration of residues in the cured film, good storage stability, biocompatibility and low price. Also, superior light absorption, low sensitivity to oxygen and high photochemical reactivity of initiating species are important [1]. The development of novel photoinitiators meeting as many of the above mentioned requirements as possible, is important [4].

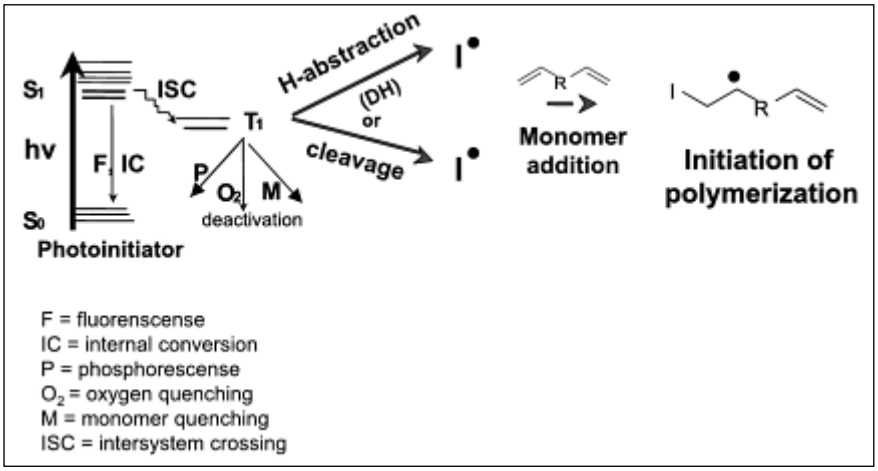

Figure 1.3. Jablonski diagram for light-induced radical photoinitiation [9].

The absorption of light energy and photopolymerization process is illustrated in Figure 1.3. The photopolymerization reaction process starts with absorption of a photon which causes the excitation of an electron from a ground state (singlet state S_0) to an excited state (singlet state S_1, S_2, ...S_n). At higher singlet electronic states, various photophysical processes can occur such as deactivation from these states to S_0 by either nonradiative internal conversion (IC) which removes the excess energy by heat evolution or fluorenscense (photon emission) and transition between a singlet excited state and a triplet excited state by intersystem crossing (ISC). Initiating species (e.g. radicals) are formed at triplet excited state. The active species can react with a monomer to initiatiate a polymerization reaction or turns into the ground state by either quenching of oxygen or monomer or phosphorescence (emission of a photon) [1] [9].

In photopolymerization reactions which proceed in UV-Vis spectrum range, there are two main types of electronic transitions: n-π* or π–π* transitions. n-π* transitions appear generaly in the range of 300-380 nm and have low absorption properties. π–π* transitions are seen usually in the short wavelengths and have high absorption properties (Figure 1.4) [1].

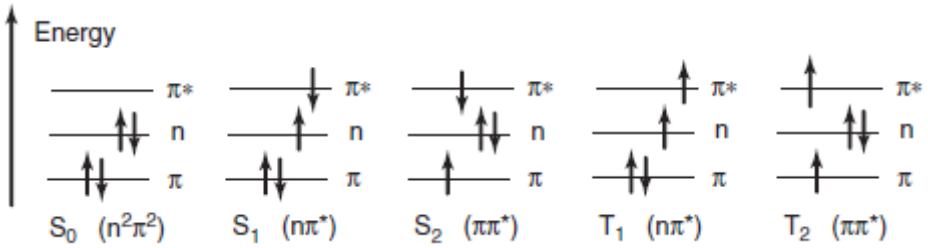

Figure 1.4. Types of electronic transitions of benzoyl-chromophore based PIs [1].

Formation of active species at triplet excited states can occur by either a homolytic cleavage reaction (Type I) or H-abstraction reaction (Type II).

1.2.1. Type I Photoinitiators

In Type I photoinitiation mechanism, two radical species are generated by cleavage from the alpha carbon to the carbonyl upon light exposure. The benzoyl radical has the

major role in the initiation of polymerization, while the other fragment can also take place in the photoinitiation process (Figure 1.5) [10]. Figure 1.6 shows some examples of Type I PIs.

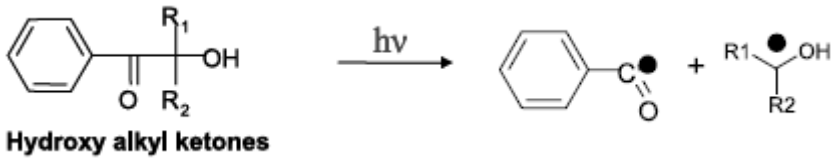

Figure 1.5. Photofragmentation reaction of a Type I PI [9].

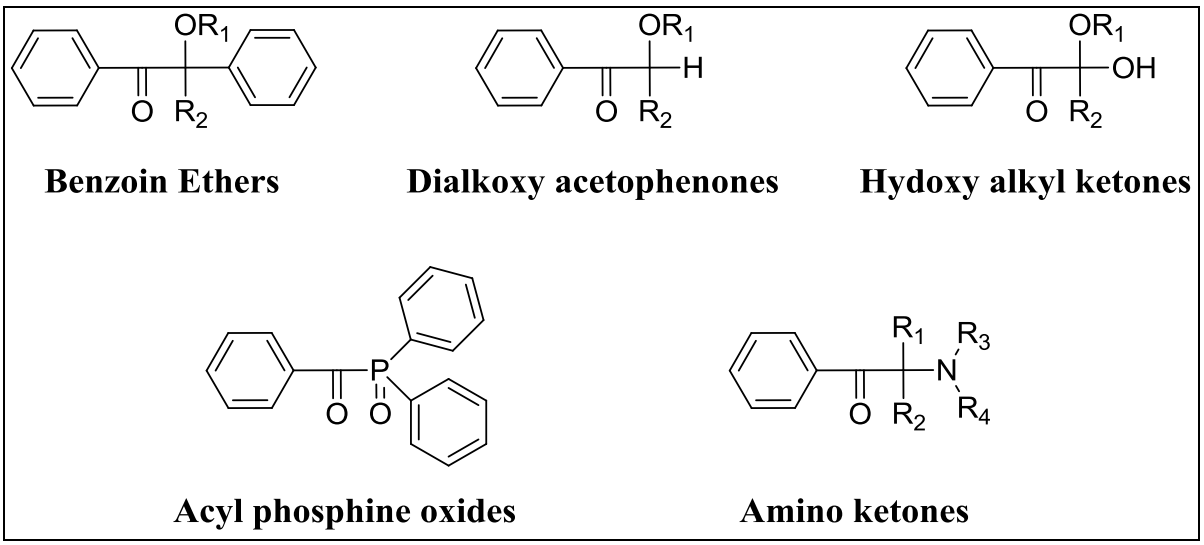

Figure 1.6. Examples of Type I PIs [9].

1.2.2. Type II Photoinitiators

In Type II photoinitiation mechanism, two initiating radical species are formed by a hydrogen abstraction from a H-donor (RH) such as an amine, alcohol or ether upon light exposure. The alkyl radical from the H-donor is the reactive radical in the photopolymerization reaction, whereas the ketyl radical from the carbonyl compound is used in the termination process due to steric hindrance effect [11]. The Type II photoinitiation mechanism of thioxanthone is illustrated in Figure 1.7. Figure 1.8 shows some examples of Type II PIs.

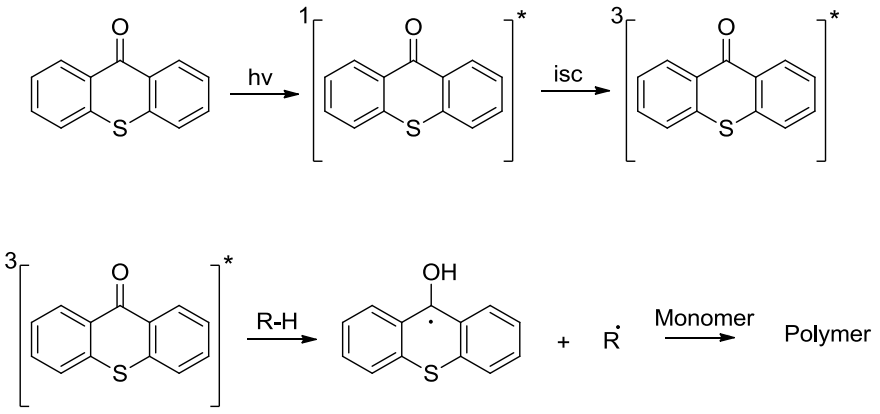

Figure 1.7. H-abstraction reaction of a Type II PI.

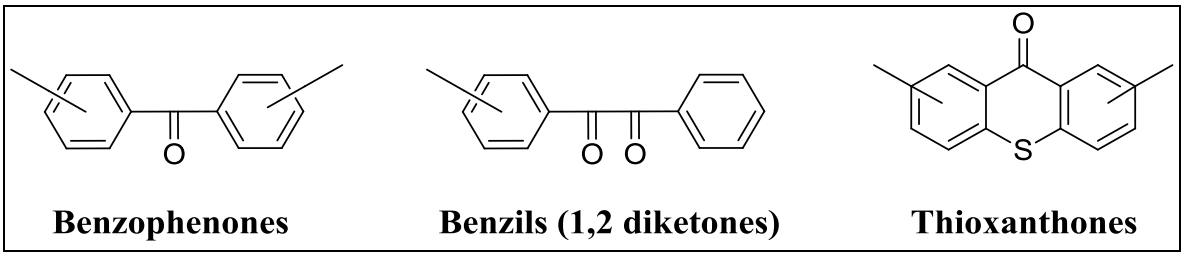

Figure 1.8. Examples of Type II PIs [9].

1.3. Monomeric and Polymeric Photoinitiators

In the beginning of Section 1.2., we listed the properties desired for photoinitiators. Recently, researchers have been investigating polymerizable, polymeric (PPIs), dendritic or hyperbranched radical PIs to better fulfill some of the mentioned requirements, than their corresponding low molecular weight non-monomeric analogues [11-42]. In particular, the larger a molecule is, the less it will migrate, the less toxic it will be, or cause less odor.

Polymeric photoinitiators (PPIs) are macromolecules containing side or main chain photoinitiating groups. They form free radicals by direct fragmentation, hydrogen abstraction or electron transfer upon absorption of light to initiate polymerization. A variety of PPIs containing Type I and Type II free radical photoinitiators were reported in the literature.

Type II photoinitiating systems need a coinitiator, generally a tertiary amine, as already known. However, tertiary amines are toxic and mutagenic, cause yellowing and corrosion in the cured samples. Many photoinitiators have been desired to overcome the mentioned problems by incorporation of coinitiator amines in polymerizable or polymeric PIs.

Benzophenone is a well-known and frequently used Type II photoinitiator. A one component monomeric PI (BDOBPAc) containing benzophenone and the coinitiator sesamol in the same molecule was synthesized [15] (Figure 1.9). According to photopolymerization kinetics, BDOBPAc initiates the photopolymerization of HDDA with a higher R_p and DC than the photoinitiating system benzophenone/ ethyl 4-dimethylamino benzoate (BP/EDAB). BDOBPAc has also reduced migration properties compared to the photoinitiating system BP/EDAB which is advantageous for usage in food packaging and biomedical applications.

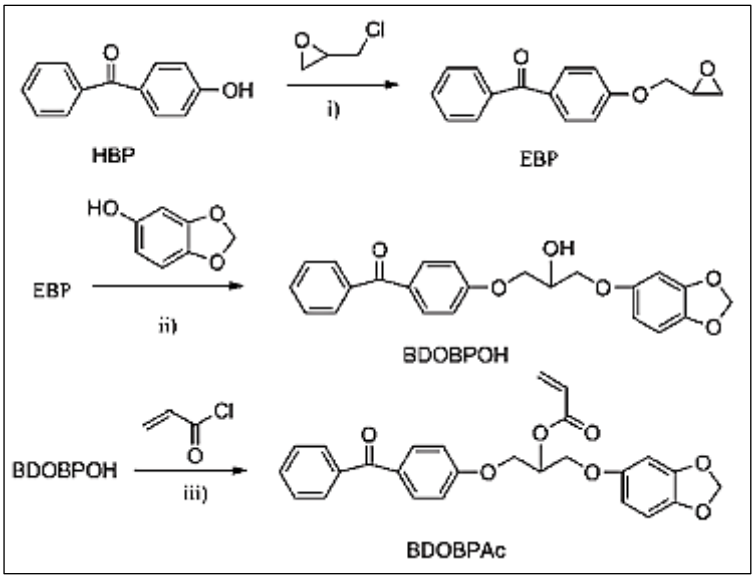

Figure 1.9. The synthesis pathway for BDOBPAc [15].

Water soluble polysiloxane BP based photoinititiators in different amount of silicone were developed [22] (Figure 1.10). The water solubility, triplet state properties, UV absorption characteristics, polymerization kinetics, self-floating abilities and surface morphology of photoinitiators were examined. The polysiloxane benzophenone

photoinitiators have good water solubility. The photoinitiators have longer triplet state life times and smaller rate constants compared to a low molecular weight analogue 4-hydroxybenzophenone. The water soluble polysiloxane benzophenone photoinitiators could find conceivable application areas in the industry of green chemistry [22].

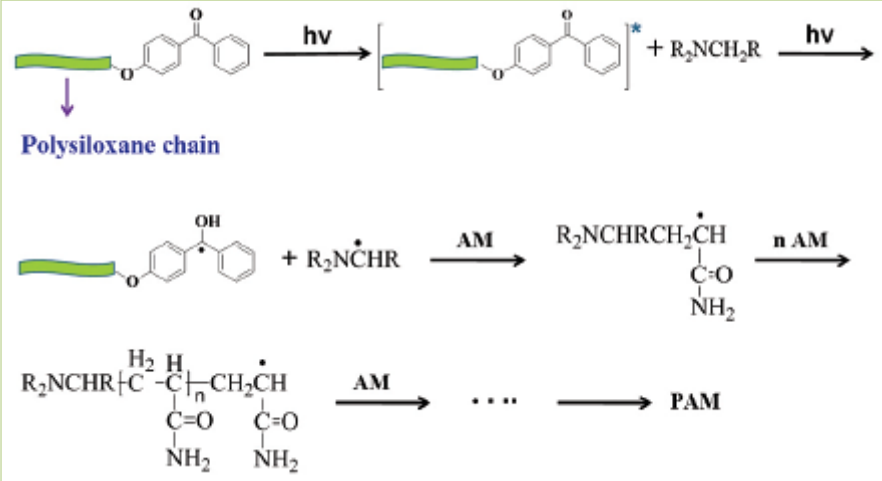

Figure 1.10. Photopolymerization mechanism induced by polysiloxane-based photoinitiators [22].

1.3.1. Monomeric and Polymeric Photoinitiators based on Thioxanthone

Thioxanthone (TX) is a frequently used Type II photoinitator due to its high perfomance in photoinitiation process and absorbance properties at the near-UV range. TX-containing PIs mainly absorb in the UV part of the spectrum, but their absorption curve has a tail extending to 420 nm, hence they can also be used with visible light. Recently visible photoinitiators have attracted more attention because visible light is cheaper and safer. However, TX is hard to dissolve in polymerizable formulations due to its planar structure which causes migration of the photoinitiator out of the cured film surface. Many investigations are in progress to provide better compatibility of thioxanthone with different formulations. Efforts to synthesize PPIs contaning TX is one of the directions taken. [33-42].

An amphipathic polymeric photoinitiator containing light absorbing TX moiety, amino group as coinitiator and a short PEO chain (APTX) was reported (Figure 1.11). APTX shows good solubility in water and also in polar and non-polar solvents. It is

compatible with different multi-functional acrylate monomers. APTX has higher photoinitiation efficiency in aqeous media and in multi-funtional acrylate cross-linkers than its low molecular weight analog TX-PMAC/DHEP which is used as a reference, due to increased compatibility of APTX with the aid of short PEO chain and higher radical formation because of polymeric structure of APTX [36].

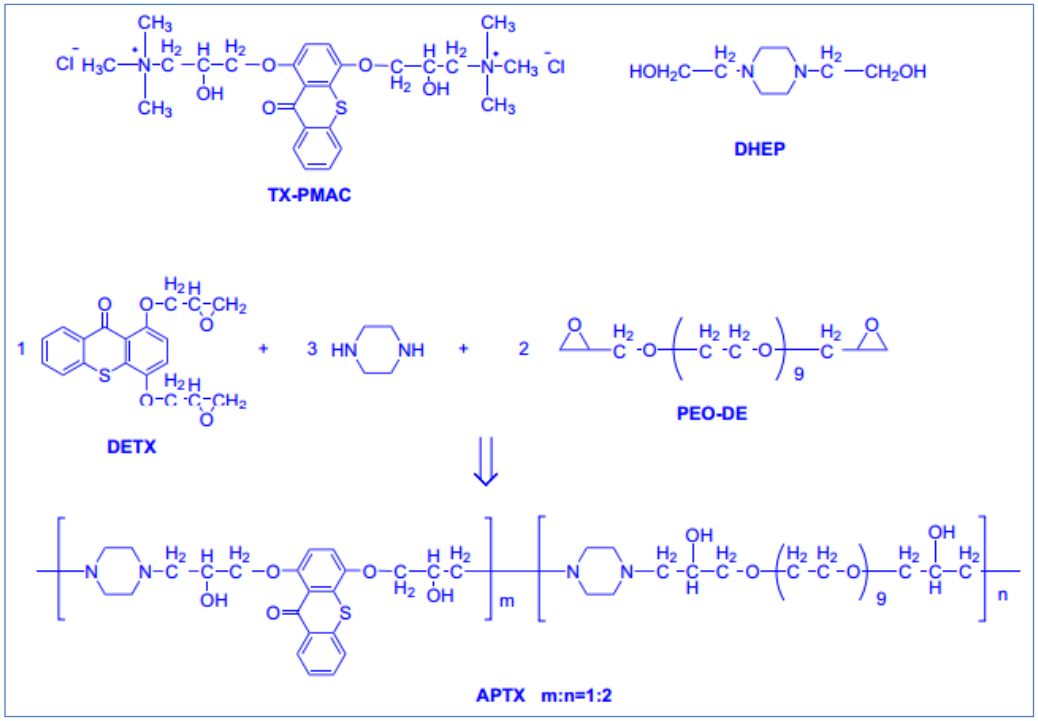

Figure 1.11. Synthesis route of amphipathic polymeric thioxanthone photoiniator [36].

A water soluble one-component macrophotoinitiator (PEG-TX) which possesses TX moiety and PEG unit was synthesized by using Diels-Alder [4 + 2] click chemistry reaction between maleimide end functionalized poly(ethyleneglycol) (PEG-MI) and thioxanthone-anthracene (TX-A) (Figure 1.12). PEG-TX is a one-component photoinitiator, because TX moiety in its photoexcited state abstracts hydrogen from PEG unit. Photophysical characteristics and photopolymerization kinetics of PEG-TX was studied. PEG-TX can initiate photopolymerization of hydrophilic vinyl monomers which increases the range of its use in potential industrial applications [35].

A Type II polymeric photoinitator poly(vinylalcohol)-thioxanthone (PVA-TX) which contains both light absorbing thioxanthone (TX) moiety and hydrogen donating

poly(vinylalcohol) (PVA) in its structure was synthesized by an addition reaction between an aldehyde functionalized TX and PVA (Figure 1.13). Although PVA-TX has higher conversion in the presence of a coinitiator amine in the photopolymerization of methylmethacrylate (MMA) and acrylamide (AA) monomers in an organic and aqeous medium, it can also initiate photopolymerization without a coinitiator [37].

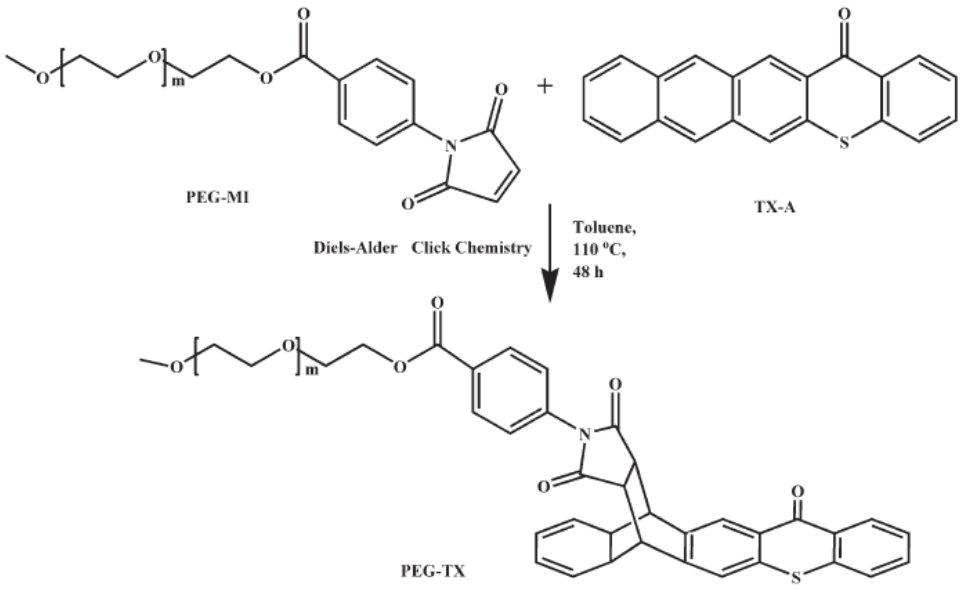

Figure 1.12. Synthesis of one-component macrophotoinitiator (PEG-TX) [35].

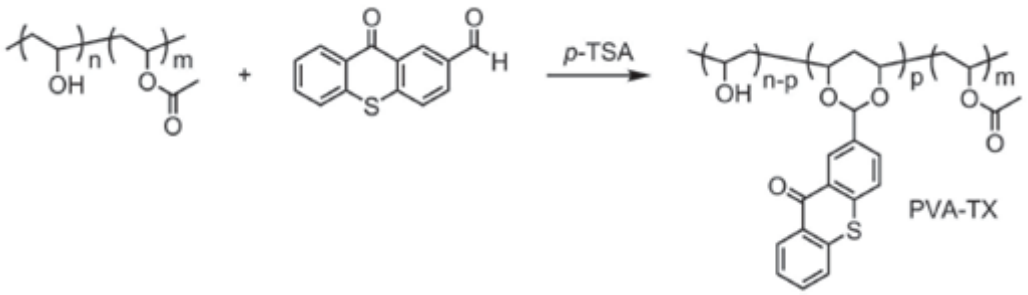

Figure 1.13. Synthesis pathway of one-component polymeric photoinitiator poly(vinylacohol)-thioxanthone (PVA-TX) [37].

2-(11-Mercaptoundecyloxy)thioxanthone (1) was attached at the periphery of silver nanoparticles (Ag NPs) by site exchange reaction (Figure 1.14). Silver-initiator nanoassemblies Ag(0)@1 were prepared as Type II macrophotoinitiator in the

photopolymerization of acrylate monomers to produce Ag(0)-polyacrylate nanocomposite materials. Characterization of the silver nanoassemblies Ag(0)@1 and formed Ag(0)-polyacrylate nanocomposite materials was carried out by fluorescence and UV-Vis spectroscopy, transmission electron microscopy (TEM), X-ray diffraction (XRD), X-ray photoelectron spectroscopy (XPS). Photopolymerization kinetics of Ag(0)@1 and 1 were also tested. Ag(0)@1 macroinitiator has the advantage of having more dispersed and non aggregated polymeric structures at the end of the photopolymerization process [42].

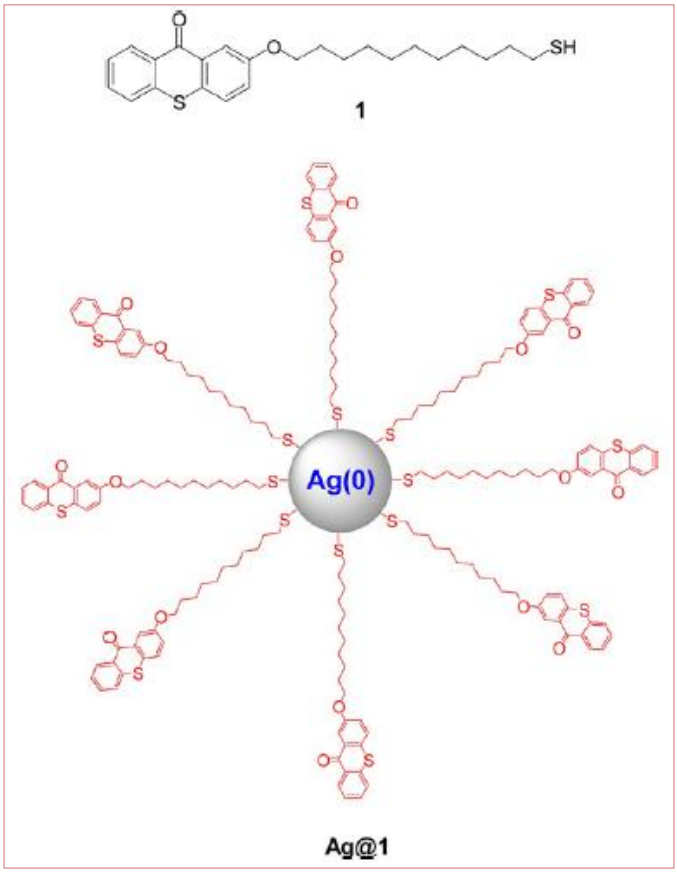

Figure 1.14. Synthesis of silver-initiator assemblies Ag(0)@1 and 2-(11-mercaptoundecyloxy)thioxanthone (1) [42].

Three types of copolymeric dendritic macrophotoinitiators DAB-4-TX-OC, DAB-16-TX-OC, DAB-64-TX-OC were prepared by incorporating thioxanthone (TX) moeity and octene (OC) group onto the surface of dendrimer poly(propylene imine) (PPI) (Figure 1.15). The macrophotoinitiators have many benefits such as no requirement of a low molecular weight coinitiator, good solubility and compatibility in polymerizable formulations, higher cross-linking density [41].

Absorption characteristics, fluorescence emission properties and photopolymerization kinetics were tested. With the increase of PPI's generation, more red shift in the absorption maxima, higher efficiency in the photopolymerization of MMA, shorter triplet state life time were observed due to higher efficiency in quenching of triplet excited state of TX and higher polarity in the surrounding of TX moieties [41].

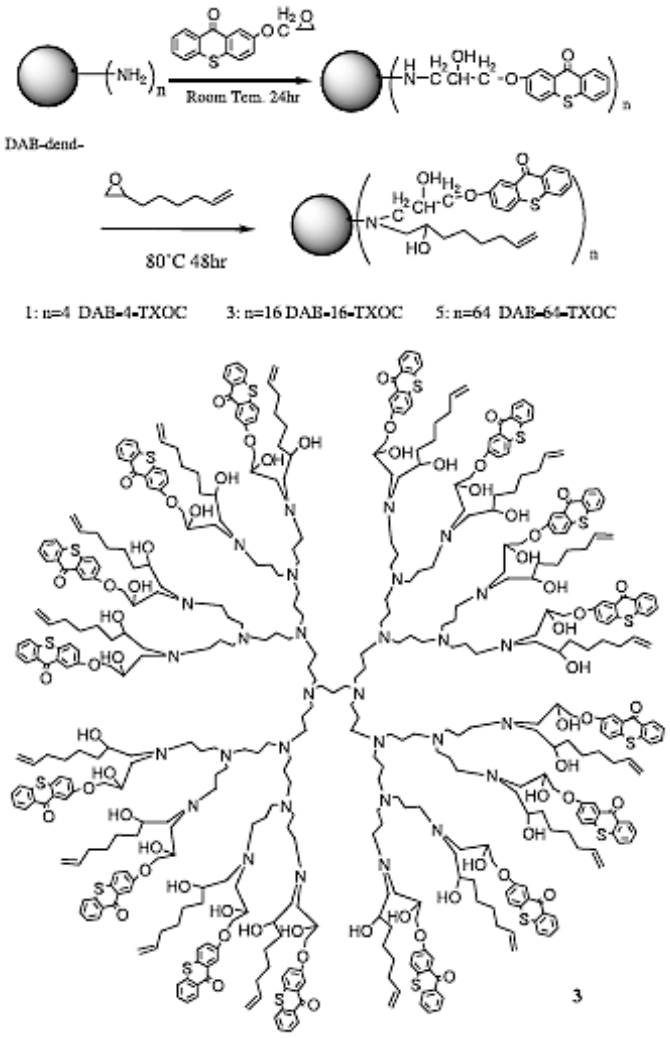

Figure 1.15. Synthesis of copolymeric dendritic macrophotoinitiators [41].

1.4. Monomers

Monomers are one of the essentials in photopolymerization formulations due to their role in adjusting the viscosity and sustaining the final film properties. The basic monomer

types are acrylates, methacrylates, vinyl ethers, unsaturated polyesters, styrene and N-vinyl pyrrolidine [8]. The reasons to prefer one monomer over another are properties of a monomer which are viscosity control, efficiency in rate of polymerization, shrinkage which occurs during photopolymerization, end product properties such as flexibility, hardness, adhesion, cost, shelf life, volatility, odor and toxicity [9].

Acrylates and methacrylates are most frequently used monomers due to their high efficiency in the rate of polymerization, no yellowing property, optical properties, good adhesion, nontacky coatings. However the rate of polymerization depends also on the nature of the photoinitiator [13]. Among acrylates and metharylates, acrylates (Figure 1.16) are more preferable due to their higher rate of polymerization (acrylic > methacrylic > vinylic > allylic) and availability of broad range of functional groups such as monofunctional, difunctional, trifunctional and tetrafunctional [8].

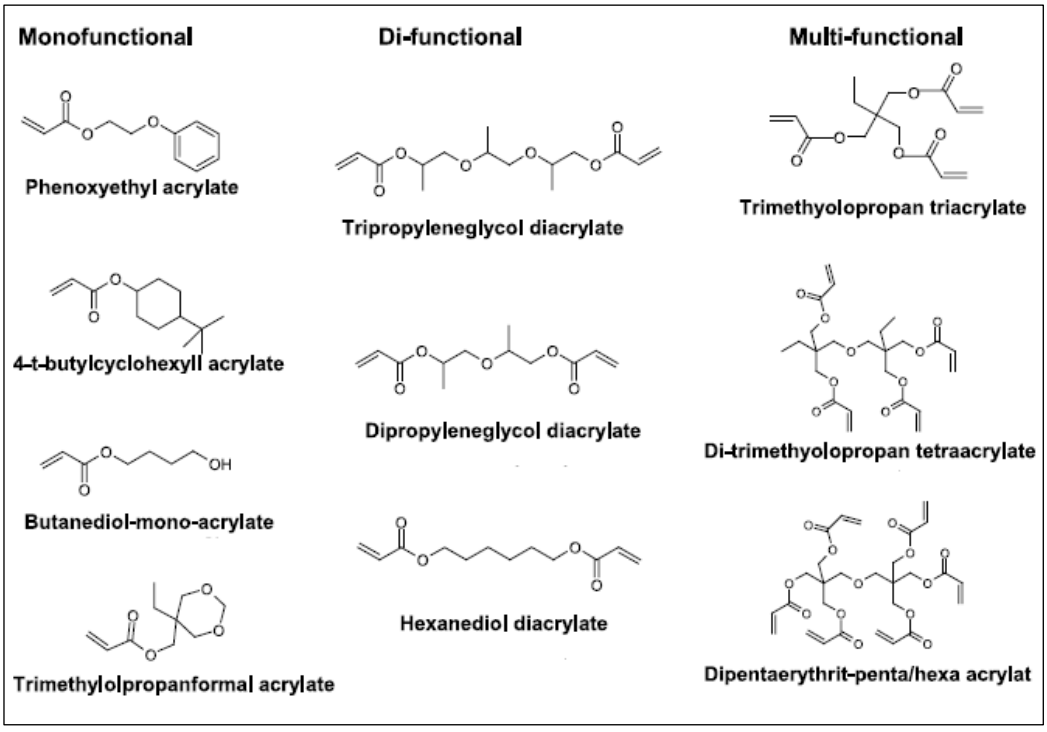

Figure 1.16. Structure of basic acrylate based monomers [9].

Multifunctional monomers can generate local crosslinked structures immediately due to their high reactivity which leads to local viscosity increment and early gelation process.

Therefore, rate of polymerization starts to increase sharply even at the beginning of the polymerization which is known as autoaccelaration "Trommsdorff Effect" [13].

1.5. Light Sources

A wide range of light sources is used to initiate the photopolymerization reaction: xenon lamps, mercury arc lamps, light-emitting diodes (LEDs) and laser sources.

Xenon (Xe) lamps have high electrical power needs and release a lot of heat but emit a high light intensity over a wide spectral range. Mercury arc lamps also emit photons in a broad range of the electromagnetic spectrum (blue bars) as shown in Figure 1.17 [1]. Characteristic narrow transitions occur between some of the excited atomic energy levels and ground state. A set of particular wavelengths is thus emitted: 254, 313, 366, 405, 435, 546 and 579 nm [9].

LEDs emit energy in the form of photons at specific wavelength range centered at 365 nm (345-385 nm) or 395 nm (380-420 nm) with an intensity about a few 10-100 mW cm^{-2}. The main benefits of LEDs are (i) low heat generation (no IR light); (ii) low energy consumption; (iii) low operating costs, less maintenance, a ~50000 h life and portability; and (iv) a possible incorporation in programmed robots that can move the lamps to improve the curing of shadow areas [1].

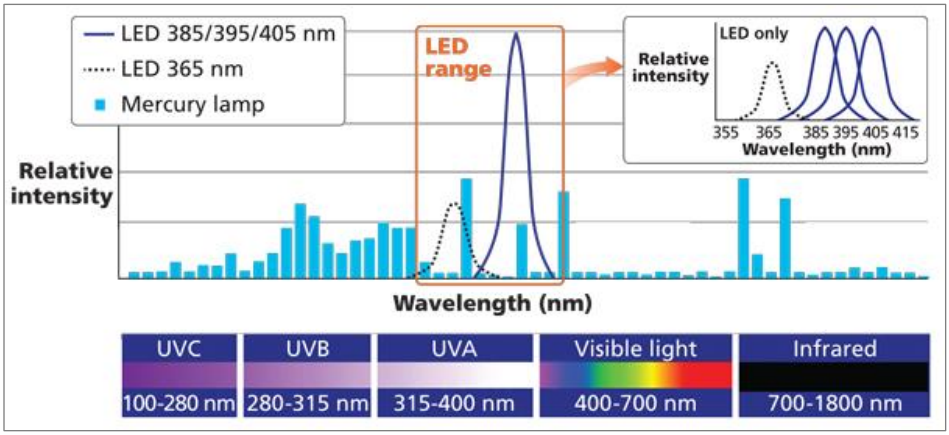

Figure 1.17. Emission spectra of mercury arc lamp and UV LEDs.

Lasers also emit energy in the form of photons at specific wavelengths. As in conventional sources, many lasers deliver the light continuously as a function of time. Some lasers can also emit the light as a (very) short pulse.

2. OBJECTIVES

The goal of the study is to design and synthesize new monomeric and polymeric photoinitiators usable in the visible light range. Five novel monomeric photoiniators based on alkyl α-hydroxymethacrylate (RHMA) and containing photoinitiating TX moiety are prepared and characterized. The features of monomeric PIs are i) one or two double bonds leading to linear or crosslinked polymer structures; ii) adhesion-promoting carboxylic acid groups; iii) both Type I (Irgacure 2959) and Type II (TX) PI groups, which may lead to improved range of absorption of light and elimination of the need for hydrogen donor compounds (particularly amines) with their problems of odor, toxicity and migration. Copolymerization of one of the monomers with an amine monomer gives novel polymeric photoinitiators. The photophysical and photochemical properties of the synthesized PIs are investigated.

,

3. EXPERIMENTAL WORK

3.1. Materials and Characterization

3.1.1. Materials

2-Hydroxy thioxanthone [43], 1,4-dihydroxy thioxanthone [44] and *tert*-butyl α-bromomethacrylate (TBBr) [45-46] were prepared according to literature procedures.

The following analytical-grade chemicals were obtained from commercial sources and used without further purification: 1,6-hexanediol diacrylate (HDDA), trimethylolpropane triacrylate (TMPTA), thiosalicylic acid, potassium carbonate (K_2CO_3), trifluoroacetic acid (TFA), oxalyl chloride (CO_2Cl_2), pyridine, Irgacure 2959, 2,2'-azobis(isobutyronitrile) (AIBN), dimethylaminoethyl methacrylate (DMAEM), ethyl 4-(dimethylamino)benzoate (EDB), methyl diethanolamine (MDEA), *tert*-butyl acrylate, 2-isopropylthioxanthone (ITX) and thioxanthone (TX), 1,4-Diazabicyclo[2.2.2]octane (DABCO), and all other reagents and solvents were obtained from Aldrich Chemical Co.; phenol from Panreac; hydroquinone, paraformaldehyde, sodium sulfate, sulfuric acid (H_2SO_4) (95-98%) from Merck. Dichloromethane (DCM) (Merck) and dimethylformamide (DMF) (Merck) were dried over activated molecular sieves.

3.1.2. Characterization

^{1}H and ^{13}C-NMR spectra were obtained on a Varian Gemini (400 MHz) spectrometer. Photopolymerizations were performed using a TA Instruments Q100 differential photocalorimeter (DPC) and FTIR spectroscopy (JASCO FTIR 4100). The glass transition temperatures were also obtained using TA Instruments Q100 differential photocalorimeter, under nitrogen atmosphere at a heating rate of 10 °C/min. The UV-Vis spectra were obtained by using a Shimadzu UV-2450 spectrophotometer. A Nicolet 6700 FT-IR spectrophotometer was used for recording IR spectra. A Q-switched nanosecond Nd/YAG laser was used for LFP experiments. Voltalab 6 Radiometer was used for cyclic

voltametry experiments. Bruker EMX-plus spectrometer (X-band) was used for ESR-Spin Trapping experiments.

3.2. Synthesis of Monomeric Photoinitiators

3.2.1 Synthesis of TX1

To a mixture of 2-hydroxythioxanthone (1.13 g, 4.96 mmol) and K_2CO_3 (7.11 g, 51.46 mmol) in acetone (10 mL) under nitrogen, TBBr (1.18 g, 5.32 mmol) was added dropwise at room temperature. After stirring at 60 °C for 48 h, the solvent was removed under reduced pressure. Dichloromethane (5 mL) was added and the solution was extracted with water (3 x 5 mL). And then, the organic phase was extracted with %1 NaOH (2 x 2 mL) to remove phenol. The organic phase was dried over anhydrous sodium sulfate, filtered and the solvent was evaporated under reduced pressure. The residue was purified by recrystallization from methanol to give the pure product as a yellow-orange solid in 53% yield (mp 106-107 °C).

^{1}H-NMR ($CDCl_3$, 400 MHz, δ): 1.46 (s, 9H, CH_3), 4.78 (s, 2H, CH_2-O), 5.86 (s, 1H, CH_2=C), 6.27 (s, 1H, CH_2=C), 7.23 (s, 1H, Ar-CH), 7.25 (s, 1H, Ar-CH), 7.43 (t, 2H, Ar-CH), 7.52 (d, 1H, Ar-CH), 8.06 (s, 1H, Ar-CH), 8.56 (d, 1H, Ar-CH) ppm.

^{13}C-NMR ($CDCl_3$, 400 MHz, δ): 27.35 (CH_3), 65.86 (CH_2-O), 80.72 (C-O), 110.79 (Ar-CH), 121.70 (Ar-CH), 124.69 (*C*H_2=C), 124.88 (Ar-CH), 125.05 (Ar-CH), 126.26 (Ar-C), 127.51 (Ar-C), 128.38 (Ar-CH), 128.81(Ar-C), 129.12 (Ar-CH), 130.95 (Ar-CH), 136.00 (Ar-C), 136.35 (*C*=CH_2), 156.14 (Ar-C), 163.44 (C=O ester), 178.53 (C=O ketone) ppm.

FTIR (ATR, cm^{-1}): 2974 (C-H), 1707 (C=O ester), 1633 (C=O ketone), 1145 (C-O).

3.2.2 Synthesis of TX2

TFA (0.36 mL, 4.75 mmol) was added dropwise to TX1 (0.5 g, 1.36 mmol) in an ice bath under nitrogen. The mixture was stirred at room temperature for 24 h. After removal of excess TFA, the crude product was recrystallized from methanol to give the pure product

as a yellow solid in 50-60 % yield. Melting point could not be detected due to degradation of the sample.

^{1}H-NMR (DMSO, 400 MHz, δ): 4.36 (s, 2H, CH_2-O), 5.99 (s, 1H, CH_2=C), 6.30 (s, 1H, CH_2=C), 7.17 (d, 1H, Ar-CH), 7.57 (t, 1H, Ar-CH), 7.78 (m, 3H, Ar-CH), 7.93 (d, 1H, Ar-CH), 8.46 (d, 1H, Ar-CH) ppm.

^{13}C-NMR (DMSO, 400 MHz, δ): 66.42 (CH_2-O), 109.51 (Ar-CH), 111.51 (Ar-CH), 122.79 (Ar-CH), 126.53 (Ar-CH), 126.60 (*C*H_2=C), 126.70 (Ar-C), 127.68 (Ar-C), 128.19 (Ar-CH), 128.61 (Ar-C), 129.06 (Ar-CH), 129.42 (Ar-CH), 132.78 (Ar-C), 136.73 (*C*=CH_2), 156.85 (Ar-C), 166.42 (C=O acid), 178.40 (C=O ketone) ppm.

FTIR (ATR, cm^{-1}): 3202 (O-H), 1720 (C=O ester), 1680 (C=O ketone), 1145 (C-O).

3.2.3. Synthesis of TX3

To a mixture of 1,4-dihydroxy thioxanthone (0.24 g, 1 mmol) and K_2CO_3 (1.42 g, 10.29 mmol) in acetone (2 mL) under nitrogen, TBBr (4.86 g, 22 mmol) was added dropwise at room temperature. After stirring at 60 °C for 48 h, the solvent was removed under reduced pressure. Dichloromethane (5 mL) was added and the solution was extracted with water (3 x 2 mL) and 1 wt % NaOH (1 x 2 mL). The organic phase was dried over anhydrous sodium sulfate, filtered and the solvent was evaporated under reduced pressure. The residue was purified by recrystallization from methanol to give the pure product as an orange solid in 60% yield (mp 156-157 °C).

^{1}H-NMR ($CDCl_3$, 400 MHz, δ): 1.44 (s, 18H, CH_3), 4.80 (d, 2H, CH_2-O), 5.99 (s, 1H, CH_2=C), 6.30 (s, 1H, CH_2=C), 6.34 (s, 1H, CH_2=C), 6.40 (s, 1H, CH_2=C), 6.83 (d, 1H, Ar-CH), 7.03 (d, 1H, Ar-CH), 7.35 (m, 1H, Ar-CH), 7.48 (d, 1H, Ar-CH), 8.37 (t, 1H, Ar-CH), 8.39 (t, 1H, Ar-CH) ppm.

^{13}C-NMR ($CDCl_3$, 400 MHz, δ): 28.07 (CH_3), 68.08 (C-O), 76.70 (C-O), 81.60 (C-O), 110.69 (Ar-CH), 115.13 (Ar-CH), 120.74 (Ar-C), 125.81 (*C*H_2=C), 126.06 (Ar-CH), 126.26 (Ar-CH), 129.43 (Ar-C), 130.12 (Ar-C), 131.63 (Ar-CH), 135.52 (Ar-CH), 135.52

(Ar-C), 136.73 (*C*=CH_2), 146.90 (Ar-C-O), 155.18 (Ar-C-O), 164.94 (C=O ester), 182.0 (C=O ketone) ppm.

FTIR (ATR, cm^{-1}): 2974 (C-H), 1735 (C=O ester), 1636 (C=O ketone), 1140 (C-O).

3.2.4. Synthesis of TX4

TFA (0.51 mL, 6.67 mmol) was added dropwise to TX3 (1 g, 2 mmol) in an ice bath under nitrogen. The mixture was stirred at room temperature for 24 h. After removal of excess TFA, the crude product was recrystallized from methanol to give the pure product as an orange solid 50-55 % yield.

^{1}H-NMR (DMSO, 400 MHz, δ): 4.80 (s, 2H, CH_2-O), 4.92 (s, 2H, CH_2-O), 6.09 (s, 1H, CH_2=C), 6.35 (s, 2H, CH_2=C), 6.46 (s, 1H, CH_2=C), 7.12 (d, 1H, Ar-CH), 7.45 (d, 1H, Ar-CH), 7.54 (t, 1H, Ar-CH), 7.70 (t, 1H, Ar-CH), 7.81 (d, 1H, Ar-CH), 8.30 (d, 1H, Ar-CH) ppm.

^{13}C NMR (DMF, 400 MHz, δ): 67.84 (C-O), 68.17 (C-O), 111.15 (CH_2=C), 116.07 (CH_2=C), 120.01 (Ar-C), 125.40 (Ar-CH), 126.10 (Ar-CH), 126.39 (Ar-C), 128.82 (Ar-CH), 129.04 (Ar-CH), 131.33 (Ar-C), 132.20 (Ar-CH), 135.17 (Ar-CH), 137.10 (Ar-C), 146.89 (C=CH_2), 154.88 (Ar-C-O), 166.50 (Ar-C-O), 179.44 (C=O acid), 205.99 (C=O ketone) ppm.

FTIR (ATR, cm^{-1}): 3047 (O-H), 2899 (C-H), 1695 (C=O acid), 1634 (C=O ketone), 1160 (C-O).

3.2.5. Synthesis of TX5

TX2 (0.33 g, 1.072 mmol) was purged with nitrogen for 15 minutes. Dry CH_2Cl_2 (1.28 mL) was added. Then the mixture of oxalyl chloride (0.74 g, 0.5 mL) in dry CH_2Cl_2 (1.88 mL) was added dropwise under ice bath and nitrogen. Ten drops of solution (1 mL of CH_2Cl_2 and 0.2 mL of dimethylformamide) was added and the reaction mixture was stirred for half an hour under ice bath and nitrogen. After half an hour, ice bath was removed and the

reaction was stirred for another three and half an hour at room temperature. The solvent and extra oxalyl chloride were evaporated with nitrogen and the remaining acid chloride were used in the next step.

To a solution of acid chloride (0.35 g, 1.072 mmol) and Irgacure 2959 (0.27 g, 1.18 mmol) in 2.70 mL of dry dichloromethane, pyridine (0.095 mL (0.094 g), 1.18 mmol) in 2.15 mL of dry dichoromethane was added dropwise in an ice bath under N_2. After stirring 2.5 h at room temperature, 30 mL of dichloromethane was added, and the solution was extracted with distilled water (2 x 9 mL) and 5 wt% $NaHCO_3$ (2 x 9 mL). The organic phase was dried over anhydrous sodium sulfate, filtered and the solvent was evaporated under reduced pressure. The crude product was washed with ether and purified by recrystallization from methanol to give TX5 as a brown solid in 15-20% yield (no mp was observed).

^{1}H-NMR ($CDCl_3$, 400 MHz, δ): 1.60 (s, 9H, CH_3), 4.31 (s, 2H, CH_2-O), 4.59 (s, 2H, CH_2-O), 4.88 (s, 2H, CH_2-O), 6.07 (s, 1H, CH_2=C), 6.48 (s, 1H, CH_2=C), 6.92 (d, 1H, Ar-CH), 6.96 (d, 1H, Ar-CH), 7.28 (d, 1H, Ar-CH), 7.47 (d, 1H, Ar-CH), 7.49 (d, 1H, Ar-CH), 7.58 (t, 1H, Ar-CH), 7.61 (d, 1H, Ar-CH), 8.01 (d, 1H, Ar-CH), 8.04 (d, 1H, Ar-CH), 8.09 (d, 1H, Ar-CH), 8.6 (d, 1H, Ar-CH) ppm.

^{13}C-NMR ($CDCl_3$, 400 MHz, *δ*): 28.61 (CH_3), 30.90 (CH_3), 62,97 (CH_2-O), 65,88 (CH_2-O), 66.45 (CH_2-O), 75.79 (C-C=O), 111.72 (Ar-CH), 114.18 (Ar-CH), 122.85 (*C*H_2=C), 125.97 (Ar-CH), 126.15 (Ar-C), 126.27 (Ar-CH), 127.40 (Ar-CH), 127.96 (Ar-C), 128.49 (Ar-C), 129.68 (Ar-CH), 129.82 (Ar-CH), 130.18 (Ar-C), 132.11 (Ar-CH), 132.36 (Ar-CH), 135.11 (Ar-C), 137.40 (*C*=CH_2), 156.97 (Ar-C), 162.21 (Ar-C), 165.08 (C=O ester), 179.55 (C=O ketone), 202.51 (C=O ketone) ppm.

FTIR (ATR, cm^{-1}): 3409 (O-H), 2927 (C-H), 1708 (C=O ester), 1644 (C=O ketone), 1620 (C=O ketone), 1155 (C-O).

3.3. Synthesis of Polymeric Photoinitiators

Copolymerizations of TX1 with DMAEM were carried out in THF at 60-70 °C using AIBN as thermal initiator with standard freeze-evacuate-thaw procedures. The polymers were purified by precipitation into petroleum ether, filtered, dried under vacuum and stored in the dark.

3.4. Laser Flash Photolysis

Nanosecond Laser flash photolysis (LFP) experiments were carried out using a Q-switched nanosecond Nd/YAG laser (λexc = 355 nm (9 ns pulses; energy reduced down to 10 mJ; minilite Continuum) and the analyzing system (for absorption measurements) consisted of a ceramic xenon lamp, a monochromator, a fast photomultiplier and a transient digitizer (Luzchem LFP 212) [47].

3.5. Redox Potentials

The oxidation potentials (E_{ox} vs SCE) of the studied PI derivatives were measured in acetonitrile by cyclic voltammetry with tetrabutylammonium hexafluorophosphate (0.1 M) as a supporting electrolyte (Voltalab 6 Radiometer). The working electrode was a platinum disk and the reference electrode was a saturated calomel electrode (SCE). Ferrocene was used as a standard, and the potentials were determined from the half-peak potentials. The free energy change ΔG for an electron transfer between the studied PIs and MDEA can be calculated from the classical Rehm Weller equation (equation 3.1, where E_{ox}, E_{red}, E_S (or E_T), and C are the reduction potential of the studied PIs, the oxidation potential of MDEA, the excited singlet (or triplet) state energy of the studied PIs, and the electrostatic interaction energy for the initially formed ion pair, generally considered as negligible in polar solvents) [48]:

$$\Delta G = E_{ox} - E_{red} - E_S \text{ (or } E_T) + C \quad (3.1)$$

3.6. ESR Spin Trapping (ESR-ST) Experiments

ESR-ST experiments were carried out using a Bruker EMX-plus spectrometer (X-band). The radicals were generated at RT upon LED at 385 nm exposure under N_2. The radicals generated were trapped by phenyl-N-*tert*-butylnitrone (PBN) according to a procedure [49] described in detail. The ESR spectra simulations were carried out using the WINSIM software.

3.7. Photopolymerization Experiments

Photopolymerizations were conducted by real time FTIR spectroscopy (JASCO FTIR 4100) [50-51]. The photosensitive formulations were deposited on a BaF_2 pellet under air or in laminate (25 μm thick) for irradiation with different lights. Two different visible lights were used for the irradiation of samples: LEDs at 385 nm (ML385-L2, ThorLabs,∼35 mW cm^{-2}), LEDs at 405 nm (M405-L2, Thorlabs; ∼110 mW cm^{-2}). The evolution of the double bond content (at about 1630 cm^{-1}) of TMPTA was followed continuously.

Photopolymerization kinetics of the synthesized photoinitiators was also determined by photo-DSC. HDDA and TMPTA samples (3-4 mg) containing 1 mol% of TX1, TX2, TX3, TX4, TX5**,** TX with 3 mol % of DMAEM or poly-DMAEM and polymeric photoinitiators were irradiated at 40 °C under nitrogen with a mercury lamp (light intensity of 20 mW/cm^2). Rates of polymerization were calculated according to the formula;

$$Rate = \frac{\left({}^{Q}/_{s}\right)M}{n(\Delta Hp)m}$$

where Q/s is the heat flow per second, M the molar mass of the monomer, n the number of double bonds per monomer molecule, ΔH_p the heat released per mole of double bonds reacted and m the mass of monomer in the sample. The theoretical value used for ΔH_p was 13.1 kcal/mol for methacrylate double bonds [52].

3.8. Computational Procedure

All calculations were carried out with the Gaussian 09 series of programs [53]. Geometry optimizations were done with density functional theory at B3LYP/6-31G(d) level after detailed corformational search for all photoinitiators. The electronic absorption spectra of the compounds were calculated with the time-dependant density functional theory at the B3LYP/6-31G(d) level on their most stable conformation in chloroform.

The triplet state energy levels (E_T) of the different thioxanthone derivatives were calculated as the energy difference between the fully optimized triplet state and the ground state.

4. RESULTS AND DISCUSSION

4.1. Monomeric Photoinitiators

4.1.1. Synthesis and Characterization of Photoinitiators

Synthesis of the novel series of photoinitiators involved nucleophilic substitution reactions of *tert*-butyl α-bromomethacrylate (TBBr) with 2-hydroxy thioxanthone and 1,4-dihydroxy thioxanthone to give monomers TX1 and TX3; and conversion of monomer TX1 and monomer TX3 to monomer TX2 and monomer TX4 by cleavage of *tert*-butyl ester groups with TFA (Figure 4.1).

Synthesis of the monomer with two side-chain photoinitiating groups, TX5, involved conversion of TX2 to the corresponding acid chloride on treatment with oxalyl chloride, followed by the reaction of this intermediate with Irgacure 2959 in the presence of pyridine in dichloromethane (Figure 4.1). Monomers were obtained as yellow to orange solids in 20-60% yield after purification by recrystallization from methanol. Table 4.1 summarizes the solubility of monomeric PIs in selected solvents and their good compatibility with the commercial HDDA and TMPTA acrylate monomers.

The structures of the monomeric PIs were examined by FTIR, ^{1}H and ^{13}C NMR spectra. ^{1}H NMR spectrum of TX1 showed characteristic peaks for methylene protons at 4.78 ppm, double bond protons at 5.86 and 6.27 ppm and aromatic protons between 7.23 and 8.56 ppm (Figure 4.2). In the ^{1}H NMR spectrum of TX2 and TX4, the absence of *tert*-butyl peak at 1.46 and 1.44 ppm can be considered as evidence of successful cleavage. Moreover, we observed two different peaks for methylene protons of TX2 and TX4, indicating special conformations provided by the rigid structure of these molecules. ^{1}H NMR spectrum of TX5 also indicates two triplets at 4.31 and 4.59 ppm corresponding to methylene units of Irgacure 2959. Also, for all monomers, IR peaks due to both the ester and ketone/carboxylic acid C=O groups were observed (Figure 4.3).

Table 4.1. Solubilities of the synthesized photoinitiators in selected solvents.

Monomer	H_2O	Methanol	Ether	CH_2Cl_2	THF	DMF
TX	-	+	-	+	+	+
TX1	-	+	±	±	±	+
TX2	-	+	±	±	±	+
TX3	-	-	-	+	+	+
TX4	-	+	-	-	+	+
TX5	-	+	-	+	+	+

4.1.2. UV-Vis Spectral Characterization

UV-vis absorption spectra of the synthesized photoinitiators in DMF are shown in Figure 4.4, as well as TX itself. The wavelengths for maximum absorption (λ_{max}) and the values of molar extinction coefficient at λ_{max} are given in Table 4.2. TX shows a strong $\pi \rightarrow \pi^*$ absorption at 266 nm (ε = 23830 L mol^{-1} cm^{-1}), and weaker absorption at 380 nm (ε = 5890 L mol^{-1} cm^{-1}). The monomeric PIs showed $\pi \rightarrow \pi^*$ absorptions similar to TX (λ_{max} = 266-272 nm, ε = 15240-32700 L mol^{-1} cm^{-1}) but a clear bathochromic shift is observed for the lowest energy transition (λ_{max} = 390-420 nm, ε = 2670-6910 L mol^{-1} cm^{-1}) compared to TX, which may be due to the effect of oxygen attached to TX. Therefore, these monomeric PIs allow larger and more efficient coverage of the emission spectra of visible light sources and can be better for the use of LED@385 nm, 395 nm or even 405nm. In addition, we observed another absorption at 318 and 324 nm for TX3 and TX4 with higher extinction coefficient than the lowest energy transition.

Figure 4.5 shows the spectra of TX5 and the reference PIs Irgacure 2959 and TX. Liska et al. said that the extinction coefficient in a two-component system is usually additive, as long as there is no interaction between the two components. It was observed that TX5 has a higher extinction coefficient in comparison with TX and Irgacure 2959 in the region of the $\pi \rightarrow \pi^*$ transition. Actually, the extinction coefficients of both components were approximately additive, confirming the above mentioned behaviour.

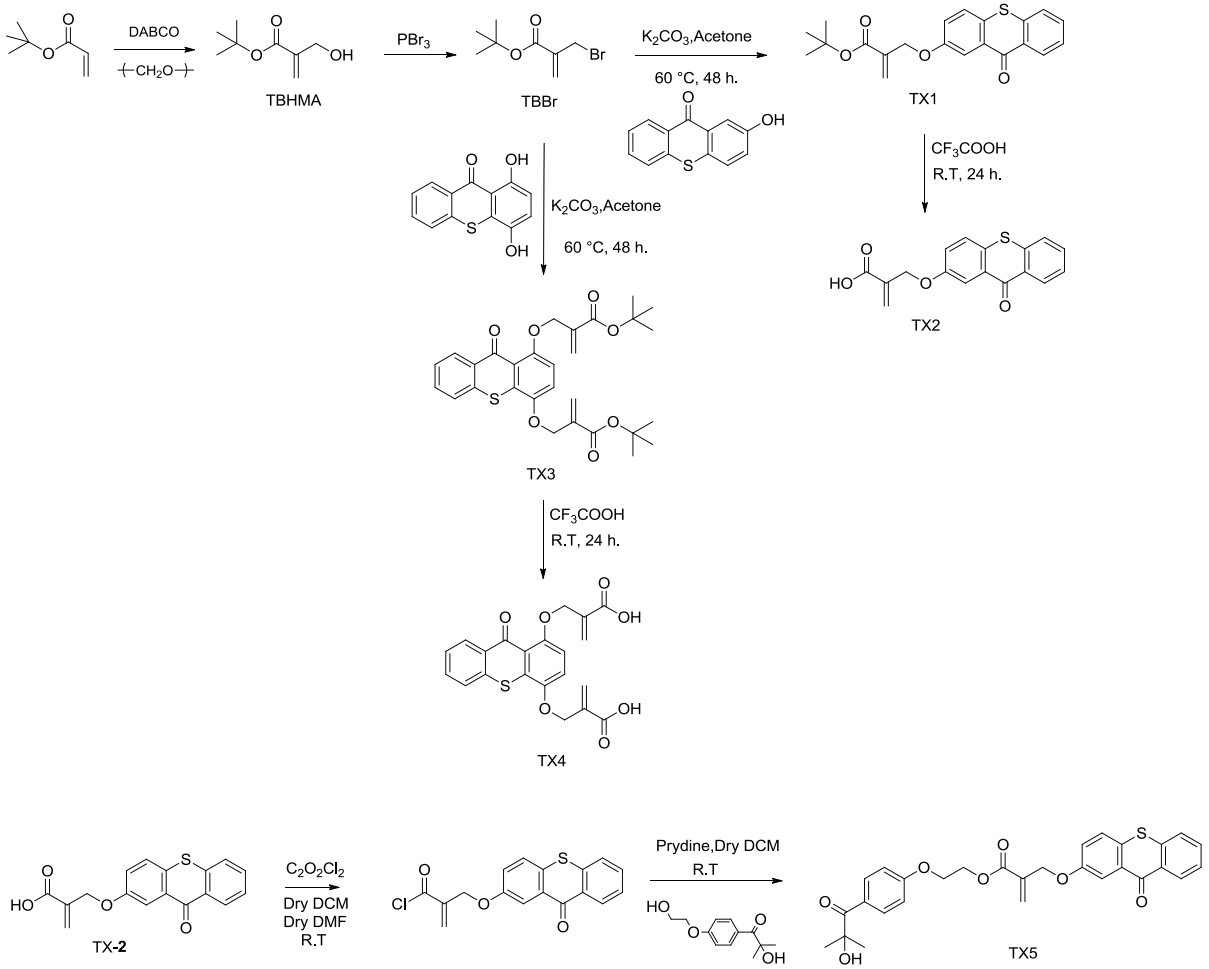

Figure 4.1. Synthesis of monomeric PIs.

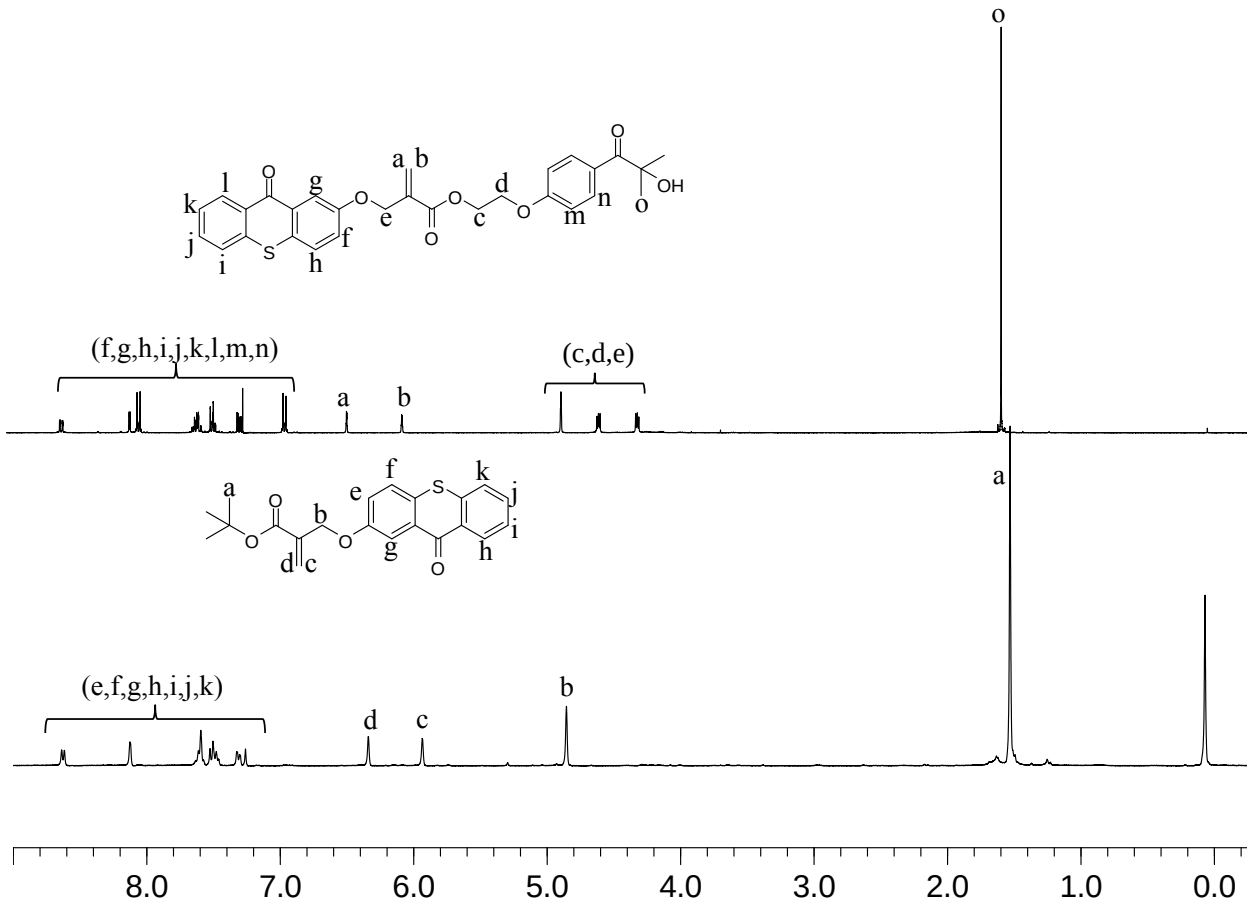

Figure 4.2. ^{1}H NMR spectra of TX1 and TX5.

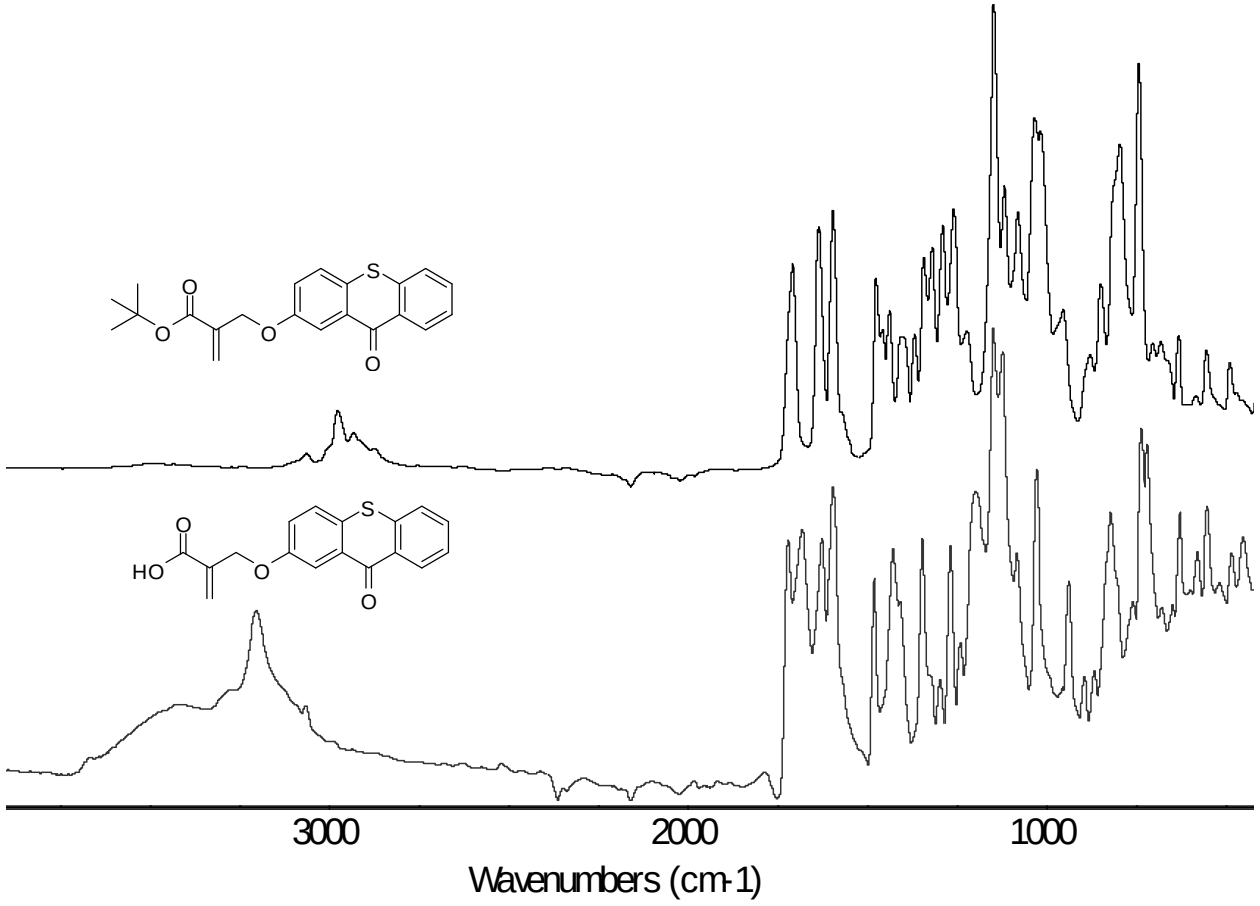

Figure 4.3. FTIR spectra of TX1 and TX2.

Table 4.2. Absorption properties of the synthesized photoinitiators compared with TX and Irgacure 2959 in dimethylformamide solution.

PI	λ_{max} (nm)	λ_{max} (nm)	λ_{max} (nm)	ε (L mol^{-1} cm^{-1})[a]	ε (L mol^{-1} cm^{-1})[a]	ε (L mol^{-1} cm^{-1})[a]
TX	266	-	380	23827	-	5885
TX1	266	-	400	31893	-	6913
TX2	272	-	400	19665	-	2666
TX3	266	318	390	20810	9963	5423
TX4	266	324	420	15243	10586	2993
TX5	272	-	400	32700	-	4721
Irgacure 2959	272	-	-	14407	-	-

[a] in terms of photoinitiating repeating units

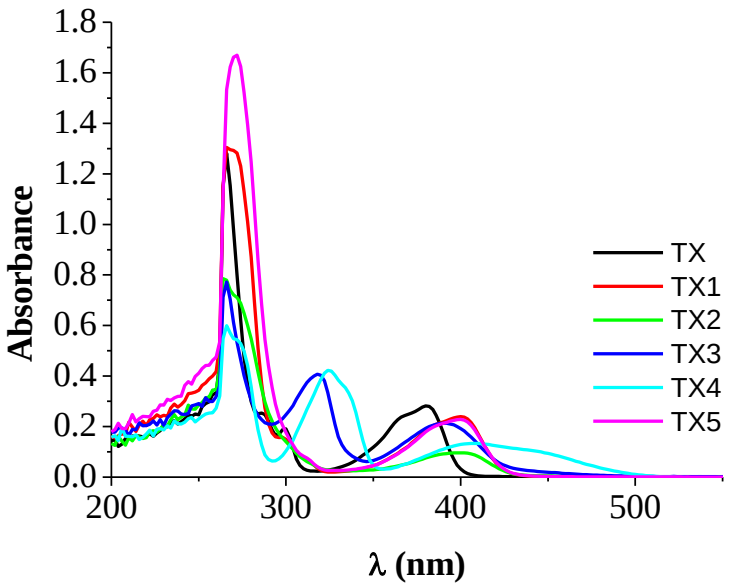

Figure 4.4. UV-Vis absorption spectra of TX, TX1, TX2, TX3, TX4 and TX5 in dimethylformamide ($4x10^{-5}$ M) solution.

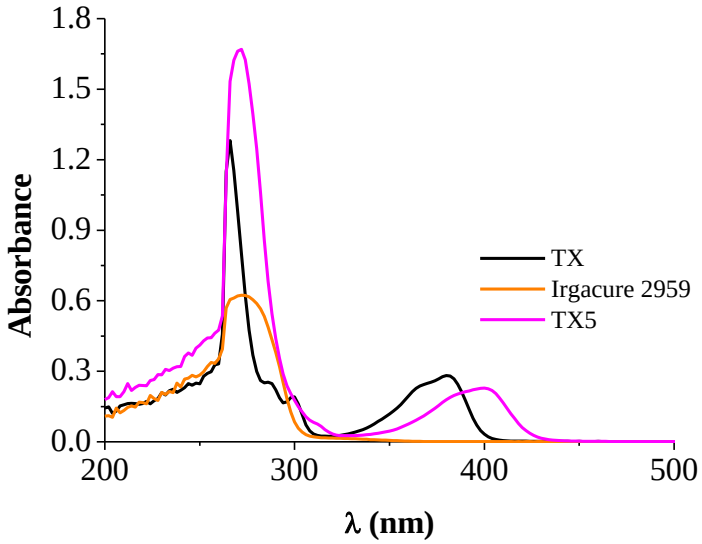

Figure 4.5. UV-Vis absorption spectra of TX, TX5 and Irgacure 2959 in dimethylformamide ($4x10^{-5}$ M) solution.

4.1.3. Molecular Modeling

Molecular orbital calculations using TDDFT have been used to understand the role of substituents in altering the electronic spectrum of the starting TX compound. The spectra show that the lowest energy transition involves strongly delocalized HOMO and LUMO for all the compounds ($\pi \rightarrow \pi^*$ character). In all the compounds the delocalization develops on the aromatic rings adjacent to the central TX ring. In general in this work, as substituents are introduced to the compound TX the calculated lowest energy transitions are shifted to longer wavelengths (Figure 4.6 and Figure 4.7). This is in full agreement with the experimental findings i.e. TX1-TX5 exhibit a bathochromic shift of about 20nm compared to the neat TX. The energy gaps between the frontier orbitals ($\Delta E_{HOMO-LUMO}$) reveal the fact that the substituents added to TX based monomeric PIs improve its properties as a photoinitiator by decreasing the gap between the LUMO and the HOMO, TX1, TX2 and TX5 having lower band gaps than the others.

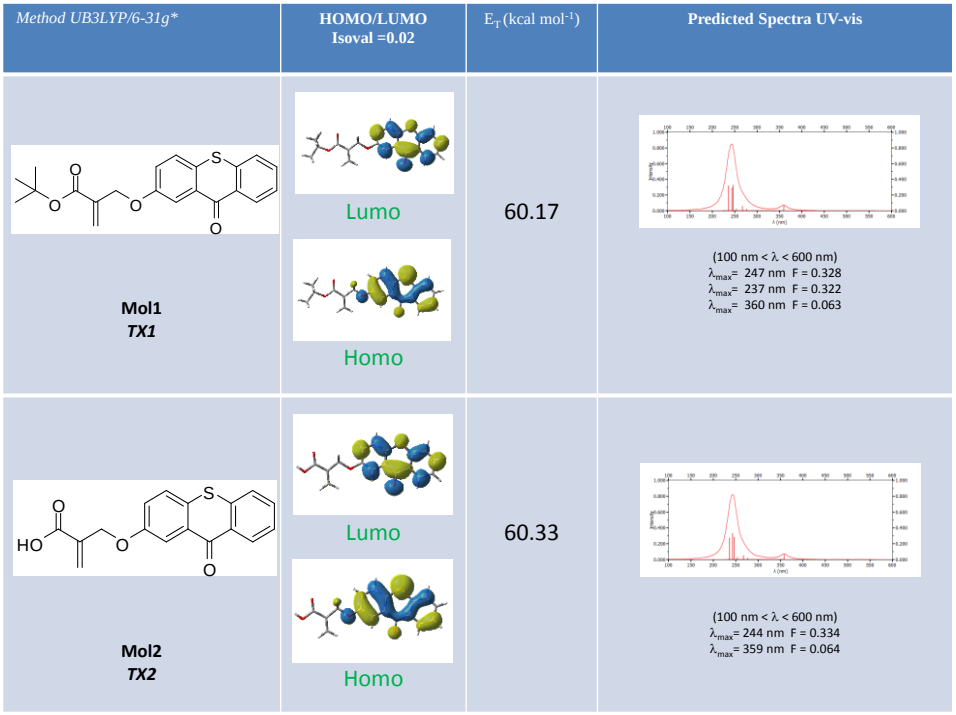

Figure 4.6. Molecular modeling results for TX1 and TX2.

In TX the main transition has contributions from the HOMO-4 to the LUMO, the HOMO-3 to the LUMO+1, the HOMO-2 to the LUMO and the HOMO to the LUMO+1. These transitions have $\pi \rightarrow \pi^*$ as well as $n \rightarrow \pi^*$ character. In TX1 the main transition can be attributed to transitions from the HOMO-4,-3,-1 to the LUMO and the HOMO to the LUMO+2,+3,+4 respectively, these transitions have the same character as the ones in TX, there is a minor contribution that can be characterized as charge transfer from the ethylenic double bond of the side chain to the ring, electrons on the side-chain playing no role. TX2 resembles TX1 in terms of the HOMO-LUMO energy gap as well as the distribution of frontier orbitals. Notice that the acidic/esteric terminal groups don't play a major role in the photo activation of these species.

*Method UB3LYP/6-31g**	**HOMO/LUMO Isoval =0.02**	E_T (kcal mol^{-1})	**Predicted Spectra UV-vis**
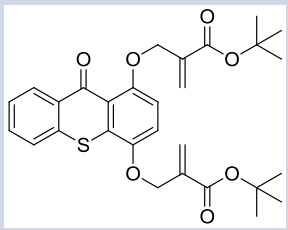 **Mol3** ***TX3***	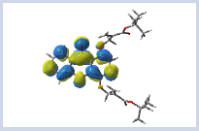 Lumo 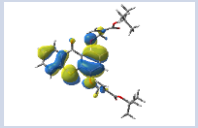 Homo	63.89	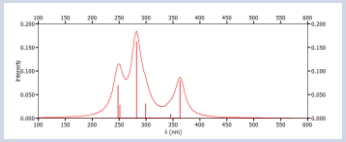 (100 nm < λ < 600 nm) λ_{max}= 282 nm F= 0.163 λ_{max}= 363 nm F= 0.080 λ_{max}= 248 nm F= 0.070
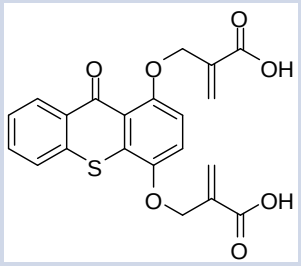 **Mol4** ***TX4***	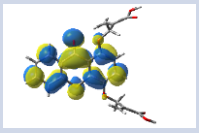 Lumo 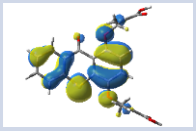 Homo	61.03	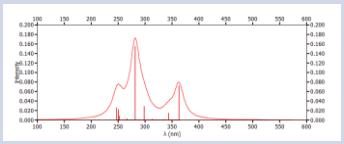 (200 nm < λ < 600 nm) λ_{max}= 282 nm F= 0.155 λ_{max}= 363 nm F= 0.072 λ_{max}= 248 nm F= 0.026
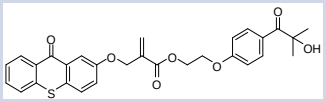 **Mol5** ***TX5***	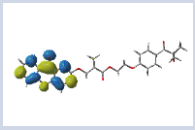 Lumo 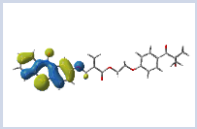 Homo	60.34	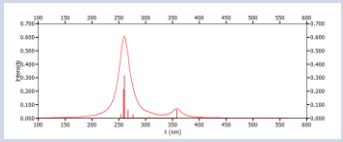 (100 nm < λ < 600 nm) λ_{max}= 261 nm F= 0.317 λ_{max}= 359 nm F= 0.064

Figure 4.7. Molecular modeling results for TX3, TX4 and TX5.

TX3 and TX4 which have two acrylate moieties on the same aromatic ring display similarities regarding the HOMO-LUMO energy gap. These substitions at the ortho-position of the central ring do not seem to improve the photoelectronic properties of TX as in the case of the single meta substitution in the case of TX1 and TX2. In TX5 where there is mainly $\pi \rightarrow \pi^*$ transition, the peaks in the UV region are more intense due to the presence of an extra aromatic ring.

4.1.4. Photoinitiating Activity

The photoinitiating activities of the monomeric PIs were tested using TMPTA or HDDA monomer through real time FTIR and photo-DSC. First series of experiments were carried out with real time FTIR. The photopolymerizations of TMPTA in the presence of TX1-TX5 PIs in laminated conditions were carried out using two different irradiation sources, low intensity LED@385 nm or LED@405 nm. The plots of conversion versus irradiation time are shown in Figures 4.8 and 4.10 and the final conversions are summarized in Table 4.3. All the polymerizations were found to be more efficient at 405 nm irradiation in agreement with the highest light intensity of this LED (110 mW/cm² @405 nm vs. 35 mw/cm² @ 385 nm). TX1/MDEA and TX2/MDEA systems lead to similar conversions (59 and 64 %) at 405 nm and (61 and 59%) at 385 nm in laminated conditions. These values are comparable with those obtained with the commercial photoinitiator: 2-isopropylthioxanthone (ITX) (Conversions = 62% at 405 nm and 58% at 385 nm). However, the final conversions when using TX3/MDEA and TX4/MDEA systems are relatively low (46 and 30% at 405 nm) due to higher crosslinking density at the beginning of polymerization which limits the extent of conversion. These PIs can also serve as a crosslinker and systems containing monofunctional monomers do not need an additional crosslinking agent. The lowest conversion obtained for TX4, the presence of the additional carboxylic acid groups in its structure which may also contribute to an increased rigidity of the system by hydrogen bonding.

The photopolymerization of TMPTA in the presence of TX1-TX5 PIs under air was carried out at 405 nm. As can be seen in Figure 4.9 and Table 4.4, the polymerization rate and final conversion of TMPTA except in the case of TX4 were both lower under air than those in laminated conditions due to the oxygen inhibition effect. For TX4/MDEA, the oxygen inhibition is slightly lower than for the other compounds (conversions were quite similar under air vs. laminate) despite a lower polymerization rate under air. The photopolymerization of TMPTA in the presence of monomeric PIs were also investigated by using LED @ 385 nm, as can be seen in Appendix B, in Figure B.1.

In the literature, several benzophenone- and TX-based photosensitizers (PSs) were covalently bonded to hydroxyalkylphenone- and aminoalkylphenone-based PIs to

investigate the effect on the excitation transfer when PI and PS are in close contact. In general, the triplet-energy levels of PS should be higher than PI for an effective excitation energy transfer. Liska et al. was found that with selective excitation of the PS, the energy transfer was improved in covalently bonded photoinitiators in comparision with the physical mixtures, despite the above mentioned requirement did not seem to be fulfilled for the TX-based PS (TX5) (E_T = 264 kJ/mol) covalently bonded to Irgacure 2959-based PI (E_T = 295 kJ/mol). These results were explained with the closeness of triplet energy levels of the PI and PS enough for sufficient energy transfer and literature values depend on method of determination and solvent. When TX5 was irradiated at 405 and 385 nm to ensure the selective excitation of TX, conversions of 44 and 34% were obtained in laminated conditions. A similar conversion was found for the physical mixture of TX and Irgacure 2959 but Irgacure 2959 by itself cannot initiate the polymerization under these conditions (Figure 4.10). Therefore, the successful photoinitiating by TX5 could be explained either by an efficient energy transfer between triplet energy levels of the PS and PI (albeit not highly favorable - see above) or a hydrogen abstraction through intra-molecular reaction in TX5 or intermolecular reaction (abstraction from the monomer unit). The addition of MDEA to TX5 significantly enhanced both the rate of polymerization and conversion (57% at 405 nm and 53% at 385 nm). To the best of our knowledge, TX5 is the first monomeric PI containing both PS and PI groups on the same monomer.

The photopolymerizations of HDDA and TMPTA in the presence of TX1, TX2, TX3 and TX5 PIs under nitrogen were also carried out using photo-DSC with a mercury arc lamp. The dimethyl aminoethyl methacrylate (DMAEM) was used as coinitiator. The maximum rate of polymerizations followed the order: TX5 > TX2 > TX~TX1 > TX3. The final conversion values for TX2/DMAEM and TX5/DMAEM are similar with TX/DMAEM in the polymerization of HDDA (Figure 4.11). However, TX3 has lower final conversion compared to commercial TX/MDEA due to having higher crosslinking density at the beginning of polymerization (Figure 4.11). In the polymerization of TMPTA, TX1/DMAEM, TX2/DMAEM and TX5/DMAEM have similar final conversion values, as can be seen in Figure 4.12.

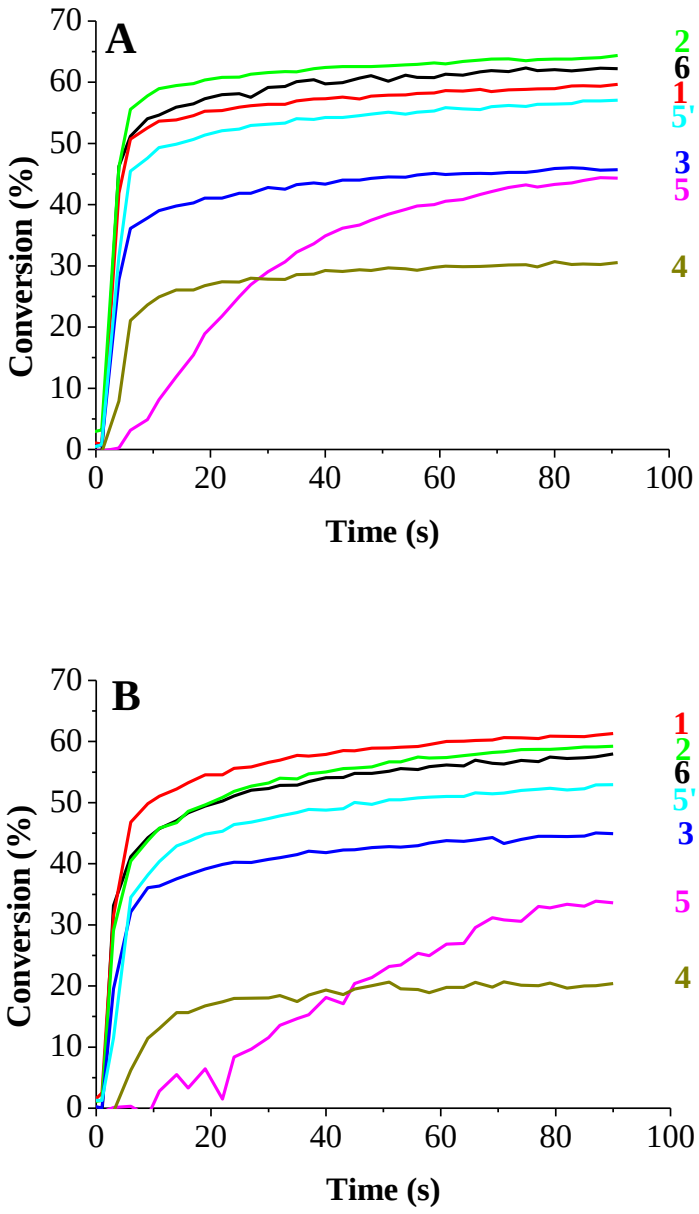

Figure 4.8. Photopolymerization profiles of TMPTA in laminate in the presence of TX1/MDEA (1), TX2/MDEA (2), TX3/MDEA (3), TX4/MDEA (4), TX5 alone (5), TX5/MDEA (5'), ITX/MDEA (6) upon exposure to (A) LED@405 nm; (B) LED@385 nm.

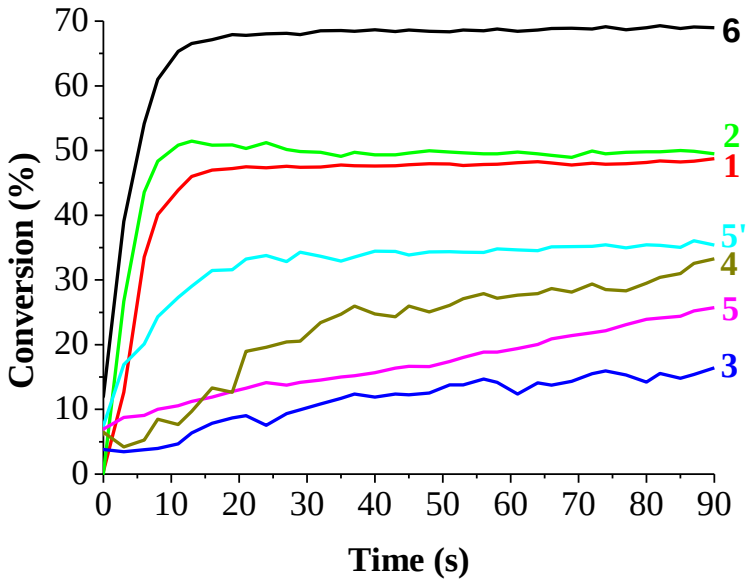

Figure 4.9. Photopolymerization profiles of TMPTA under air in the presence of TX1/MDEA (1), TX2/MDEA (2), TX3/MDEA (3), TX4/MDEA (4), TX5 alone (5), TX5/MDEA (5'), ITX/MDEA (6) upon exposure to LED@405 nm.

Table 4.3. TMPTA conversions obtained in laminate upon exposure to different LED sources for 90 s in the presence of TX1/MDEA (1/3%, w/w), TX2/MDEA (1/3%, w/w), TX3/MDEA (1/3%, w/w), TX4/MDEA (1/3%, w/w), TX5/MDEA (1/3%, w/w), TX5 (1%, w).

PI	LED (405 nm)	LED (385 nm)
ITX/MDEA	62 %	58 %
TX1/MDEA	59 %	61 %
TX2/MDEA	64 %	59 %
TX3/MDEA	46 %	45 %
TX4/MDEA	30 %	20 %
TX5/MDEA	57 %	53 %
TX5	44 %	34 %

Table 4.4. TMPTA conversions obtained under air upon exposure to LED (405 nm) for 90 s in the presence of TX1/MDEA (1/3%, w/w), TX2/MDEA (1/3%, w/w), TX3/MDEA (1/3%, w/w), TX4/MDEA (1/3%, w/w), TX5/MDEA (1/3%, w/w), TX5 (1%, w).

PI	LED (405 nm)
ITX/MDEA	69 %
TX1/MDEA	49 %
TX2/MDEA	49 %
TX3/MDEA	16 %
TX4/MDEA	33 %
TX5/MDEA	35 %
TX5	25 %

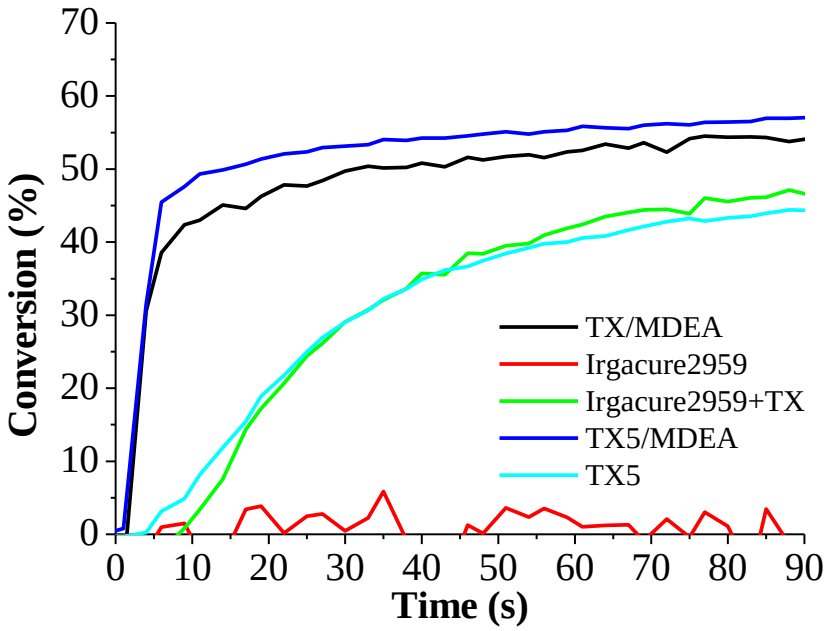

Figure 4.10. Photopolymerization profiles of TMPTA in laminate upon LED@405 nm exposure.

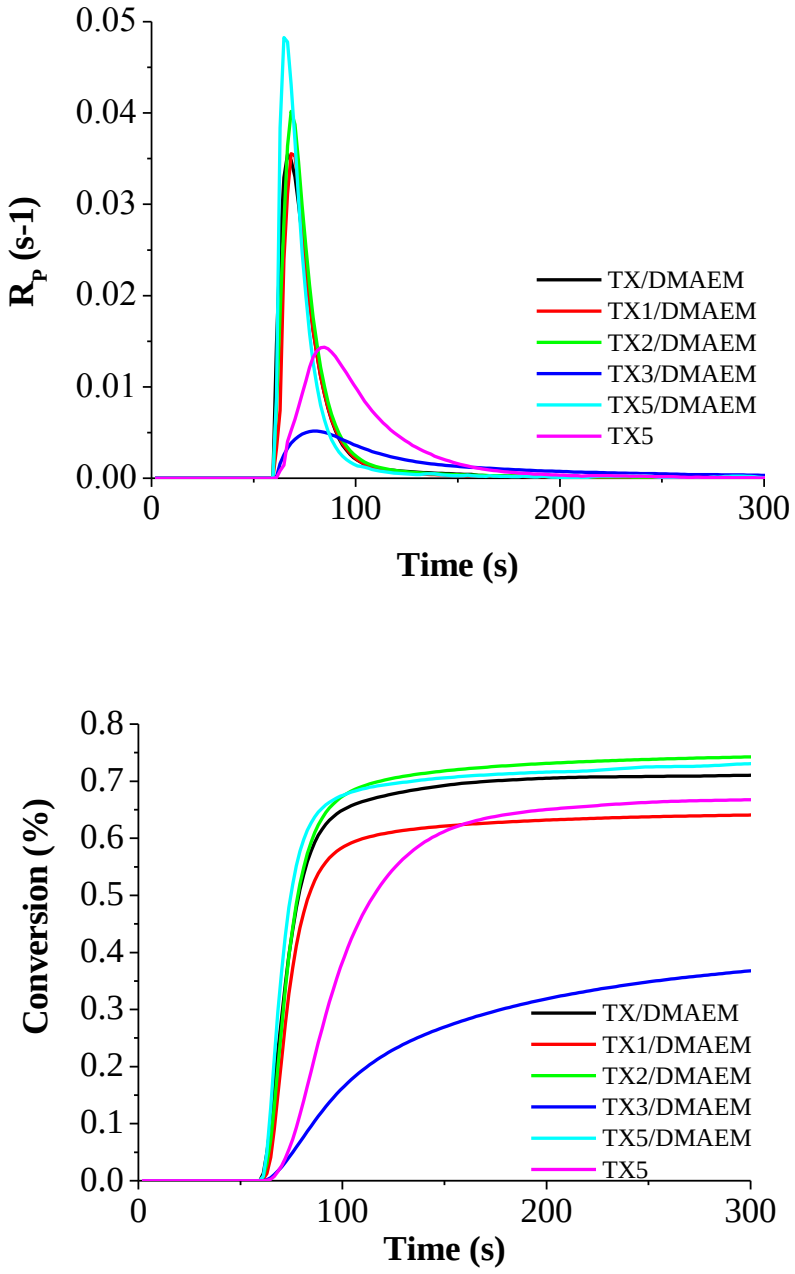

Figure 4.11. Rate-time and conversion-time plots for the photopolymerization of HDDA initiated by TX1/DMAEM, TX2/DMAEM, TX3/DMAEM, TX5/DMAEM, TX5. TX5 concentration in monomer is 0.5 mole %. PI and amine concentration in monomer are 1 and 3 mol% for TX1/DMAEM, TX2/DMAEM, TX3/DMAEM, TX5/DMAEM.

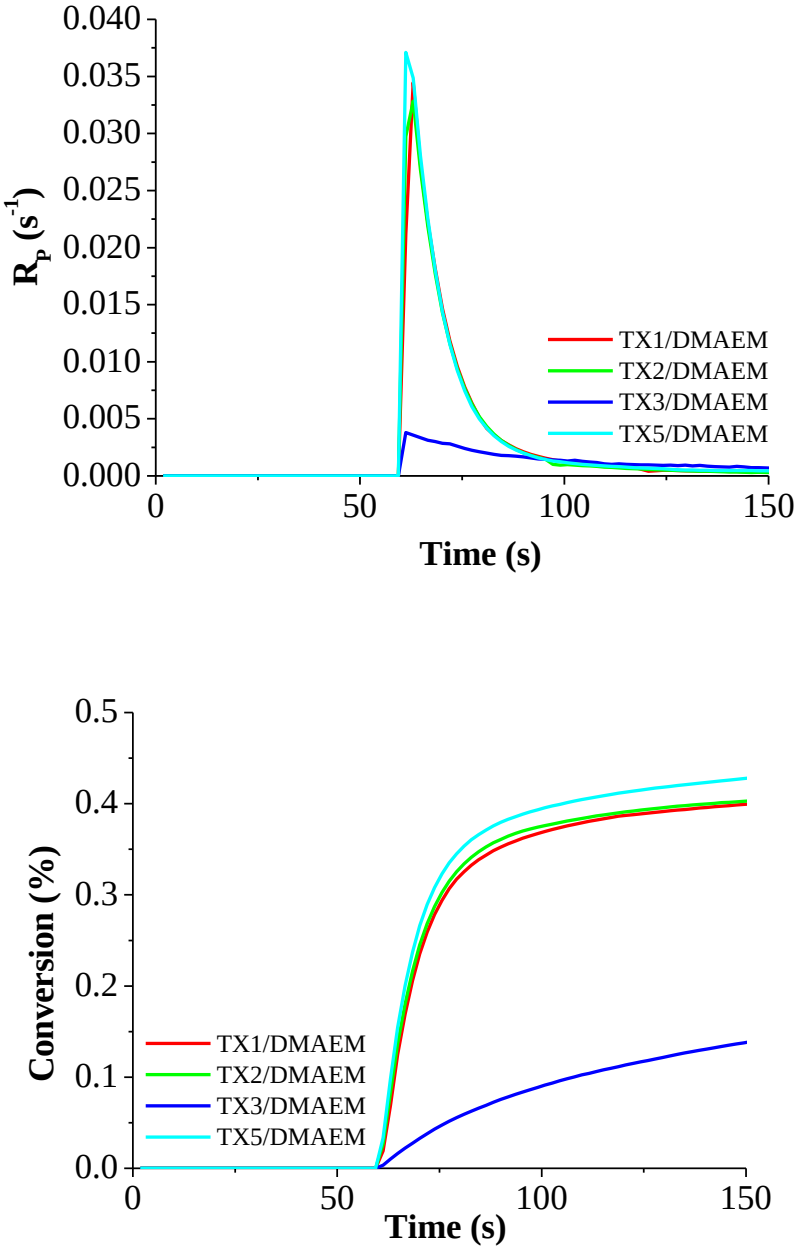

Figure 4.12. Rate-time and conversion-time plots for the photopolymerization of TMPTA initiated by TX1/DMAEM, TX2/DMAEM, TX3/DMAEM, TX5/DMAEM. Photoinitiator and amine concentration in monomer are 1 and 3 mol%.

4.1.5. ESR Analysis

In ESR spin trapping experiments, radicals were trapped by PBN according to the following reaction (Figure 4.13). The hyperfine a_N and a_H coupling constants were extracted from the ESR simulated spectra (Figure 4.14). These values were found to be a_N = 14.4 G; a_H = 2.4 G and indicated the formation of aminoalkyl radicals ($amine_{(-H)}^{\bullet}$) from TX1/amine (e.g. EDB) and TX2/amine solutions in agreement with reference values [54] (Reaction 4.1).

$$^{3}TX1 + EDB \rightarrow TX1\text{-}H^{\bullet} + EDB_{(-H)}^{\bullet} \quad (4.1)$$

ESR spin trapping experiments were also carried out for TX5/MDEA and TX5 solutions, as we can see in Appendix C, in Figure C.1.

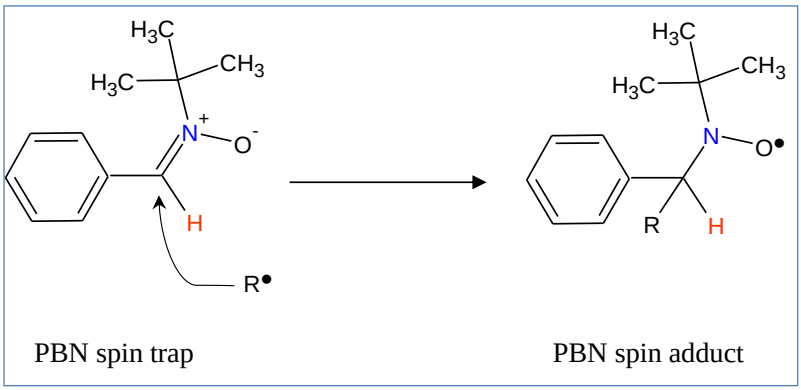

Figure 4.13. Principle of ESR-ST experiments.

4.1.6. Redox Potentials

The redox properties of the proposed photoinitiators were also investigated using cyclic voltammetry (Figure 4.15, Figure D.1, Figure D.2 and Table 4.5). The reduction potentials are slightly more favorable for ITX (-1.57 V; Table 4.5); this is ascribed to the electron donating effect of the oxygen substituent in the new proposed TX1-TX5.

And remarkably, the free energy change for the electron transfer reaction evaluated through the Rehm-Weller equation (Equation 3.1) (see Table 4.6) is favourable ($\Delta G < 0$). Therefore, the hydrogen transfer reaction (Reaction 4.1) corresponds to an electron followed by proton transfer process.

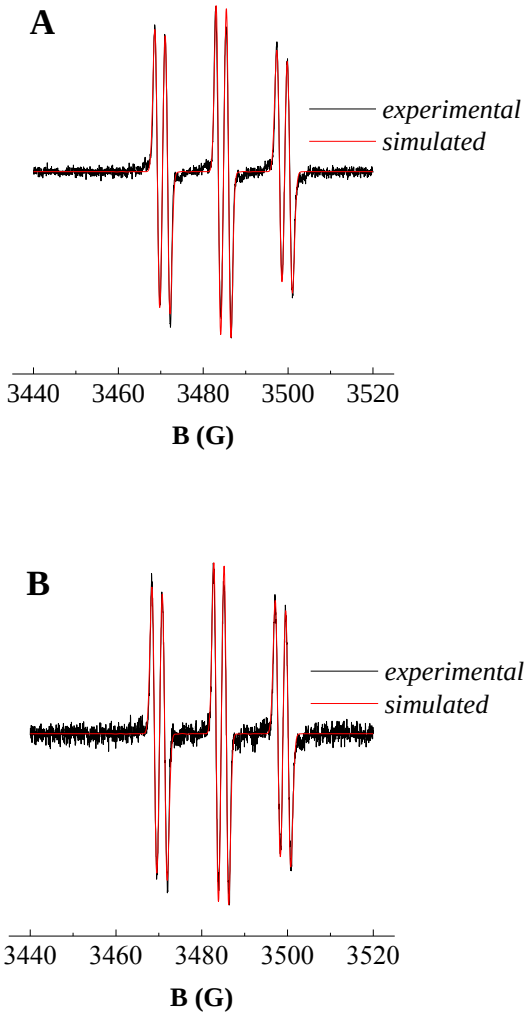

Figure 4.14. ESR spectra of the radicals generated in (A) TX1/EDB, (B) TX2/EDB upon the LED@385 nm exposure and trapped by PBN in *tert*-butylbenzene. PBN/aminoalkyl radical adducts obtained in TX1/EDB and TX2/EDB: a_N = 14.4 G, a_H = 2.4 G, a_N = 14.4 G, a_H = 2.4 G, respectively; reference values [54].

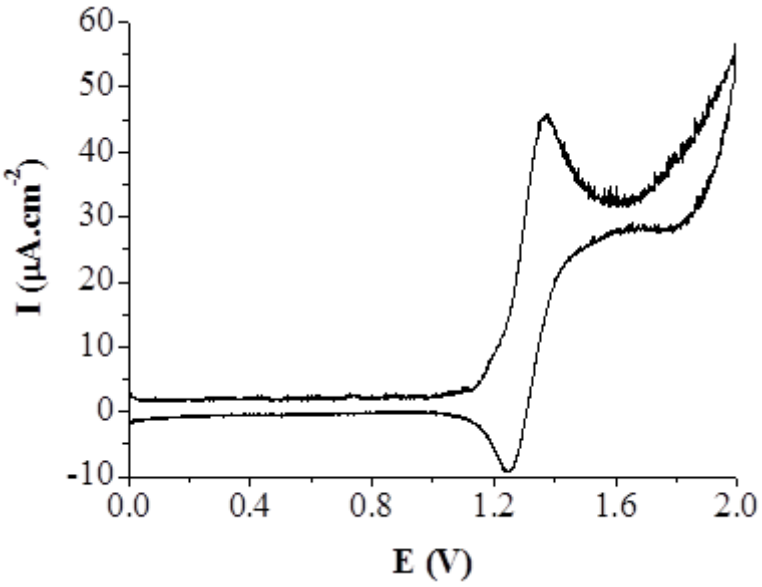

Figure 4.15. Cyclic voltammogram of TX3 in acetonitrile.

Table 4.5. Redox Potentials for some of the monomeric PIs and ITX.

PI	E_{ox} (eV)[a]	E_{red} (eV)[a]
TX1	1.4	-1.7
TX2	1.4	-1.7
TX3	1.3	-1.8
ITX		-1.57

[a] E_{ox} and E_{red} values: measured by cyclic voltammetry for TX1, TX2 and TX3.

4.1.7. Laser Flash Photolysis Experiments

The transient absorption spectra following the laser excitation of TX1 and TX2 at 355 nm in acetonitrile are given in Figure 4.16, Figure 4.17 and Figure 4.18. The triplet states of these compounds are easily observed at 600 nm, as for ITX, in agreement with an excited triplet state centered on the TX moiety. Very high rate constants of quenching between their triplet state and amine were found (Table 4.6; > 10^8 $M^{-1}s^{-1}$) showing a very favourable process.

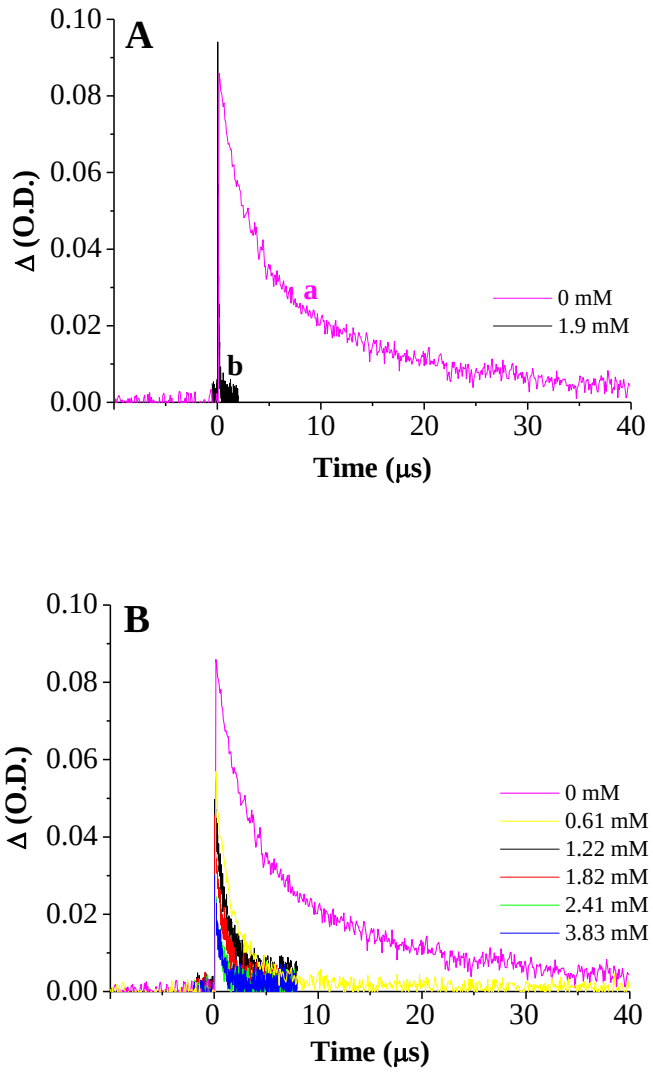

Figure 4.16. Triplet state decay traces observed after laser excitation of TX1 in acetonitrile at 355 nm, kinetic traces recorded at 600 nm: (A) (a) under N_2, (b) under air; (B) in different MDEA concentrations under N_2.

The triplet state energy levels are weakly affected in ITX vs. TX1-TX5 and accordingly, the ΔG for the reduction by MDEA is slightly more favorable for ITX compared to TX1-TX5. The triplet state lifetimes are also rather similar for TX1-TX5 compared to ITX (Table 4.6; 7-10 μs).

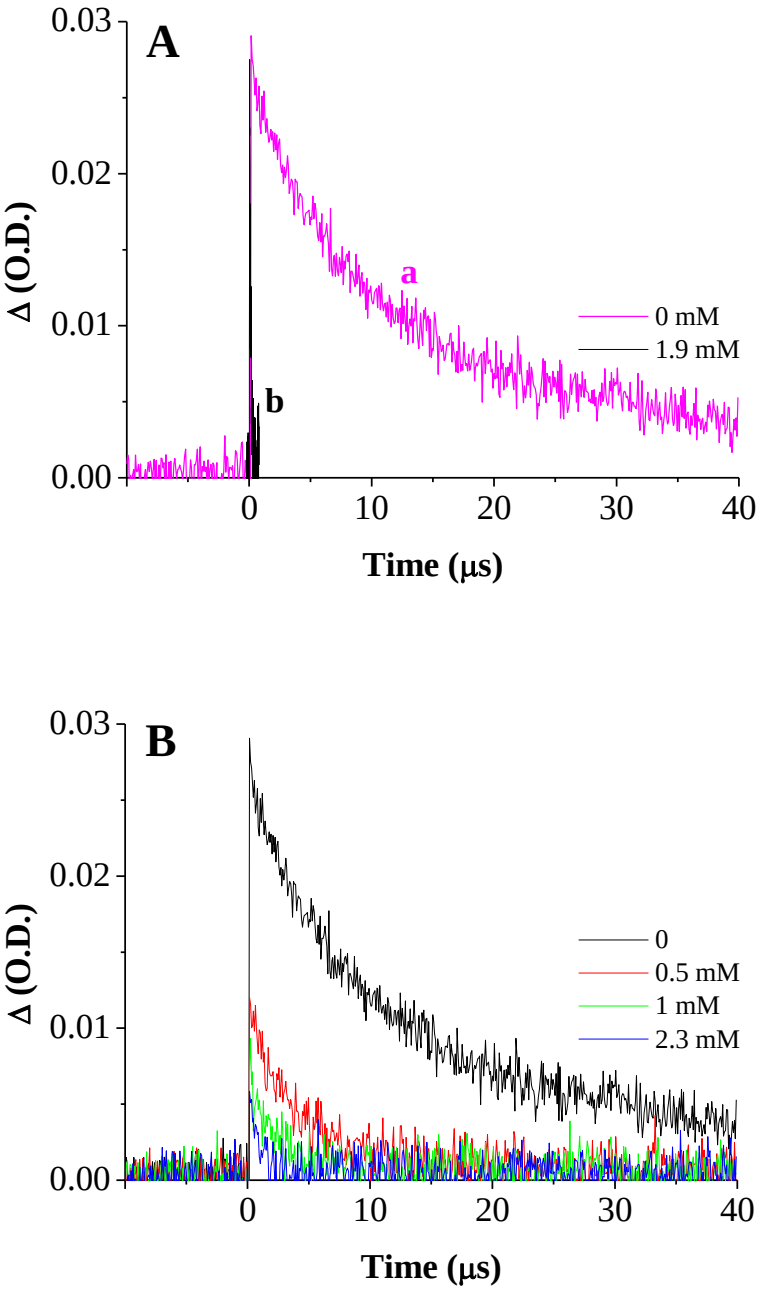

Figure 4.17. Triplet state decay traces observed after laser excitation of TX2 in acetonitrile at 355 nm, kinetic traces recorded at 600 nm: (A) (a) under N_2, (b) under air; (B) in different MDEA concentrations under N_2.

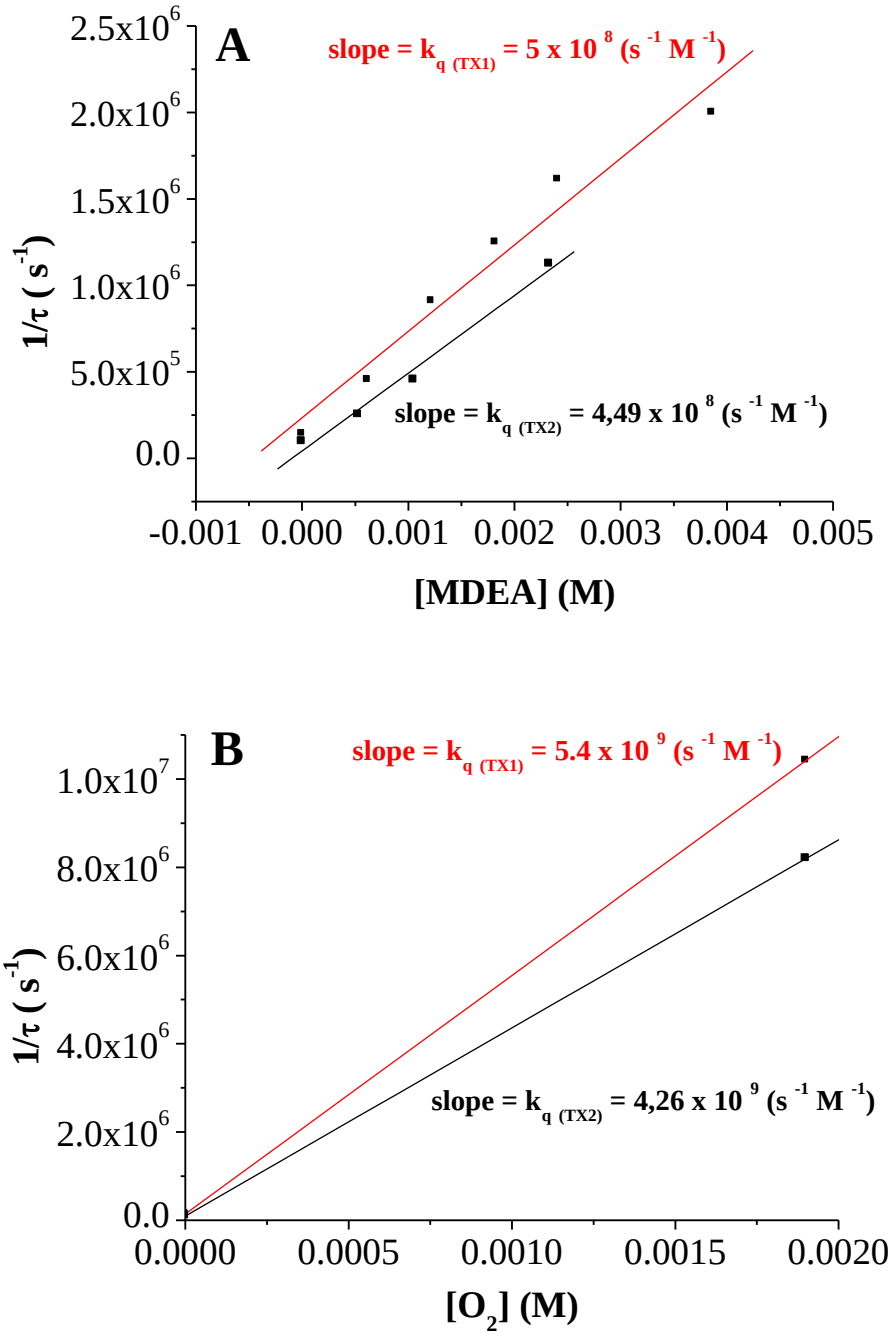

Figure 4.18. Stern–Volmer plot for the quenching of; (A) ^{3}TX1 (red line) and ^{3}TX2 (black line) by MDEA. (B) ^{3}TX1 (red line) and ^{3}TX2 (black line) by O_2. λ_{exc} = 355 nm.

Table 4.6. Parameters characterizing the reactivity of PIs: redox potentials (Eox, Ered), free energy changes (ΔG), triplet state energies (ET), PIs/additive interaction rate constants (kq) and lifetimes (τ).

PI	E_{ox} (eV)[a]	E_{red} (eV)[a]	$\Delta G_{T\ (MDEA)}$ (eV)[b]	E_T (eV)[d]	$k_{q\ (MDEA)}$ ($M^{-1}s^{-1}$)[c]	$k_{q\ (O2)}$ ($M^{-1}s^{-1}$)[c]	$\tau_{\ (N2)}$ (μs)	$\tau_{\ (O2)}$ (μs)
TX1	1.4	-1.7	-0.11	2.61	$5x10^8$	$5.4x10^9$	7	0.096
TX2	1.4	-1.7	-0.12	2.62	$4.49x10^8$	$4.26x10^9$	10.3	0.122
TX3	1.3	-1.8	-0.17	2.77				
ITX		-1.57	-0.38	2.75			7	

[a] E_{ox} and E_{red} values: measured by cyclic voltammetry for TX1, TX2 and TX3.

[b] ΔG_T = free energy change for the triplet state interaction of TX1 and TX2 with MDEA. E_{ox} = 0.8 V for MDEA [55].

[c] kq = TX1/MDEA (or O_2) and TX2/MDEA (or O_2) interaction rate contants measured by laser flash photolysis experiments.

[d] E_T = E_T values were calculated by molecular modeling.

4.1.8. Steady State Photolysis Experiments

The steady state photolysis of ITX, TX1 and TX1/MDEA in acetonitrile at 395 nm under air is given in Figure 4.19 and Figure 4.20. A fast bleaching of TX1/MDEA solution indicated high photoreactivity of TX1 (Figure 4.20.B). There was almost no bleaching in TX1 and ITX in the absence of amine (Figure 4.20.A and Figure 4.19) showing the importance of the amine for an efficient process.

From all these data, the aminoalkyl radicals generated in (Reaction 4.1) are the polymerization initiating structures. The oxygen inhibition is ascribed to the conversion of the initiating radicals (or propagating radicals) to stable peroxyls (Reaction 4.2; $ROO^{\bullet}$) that are quite stable and can not initiate the polymerization process. But also to the quenching of the triplet state by O_2 (shown very high for the investigated derivatives – Table 4.6 and Figure 4.16, Figure 4.17 and Figure 4.18) that is in competition with the reaction of the excited triplet state with amine (Reaction 4.1) reducing the yield in initiating aminoalkyl radicals.

$$R^{\bullet} + O2 \rightarrow ROO^{\bullet} \qquad (4.2)$$

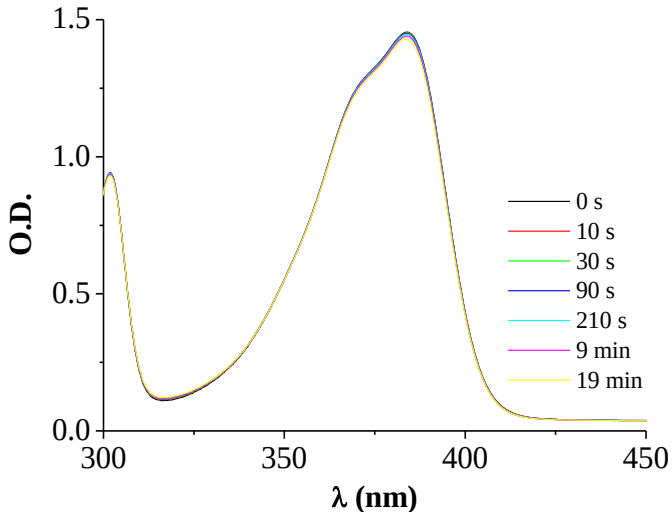

Figure 4.19. Steady state photolysis of ITX in acetonitrile upon LED@395 nm exposure; UV–vis spectra recorded at different irradiation time.

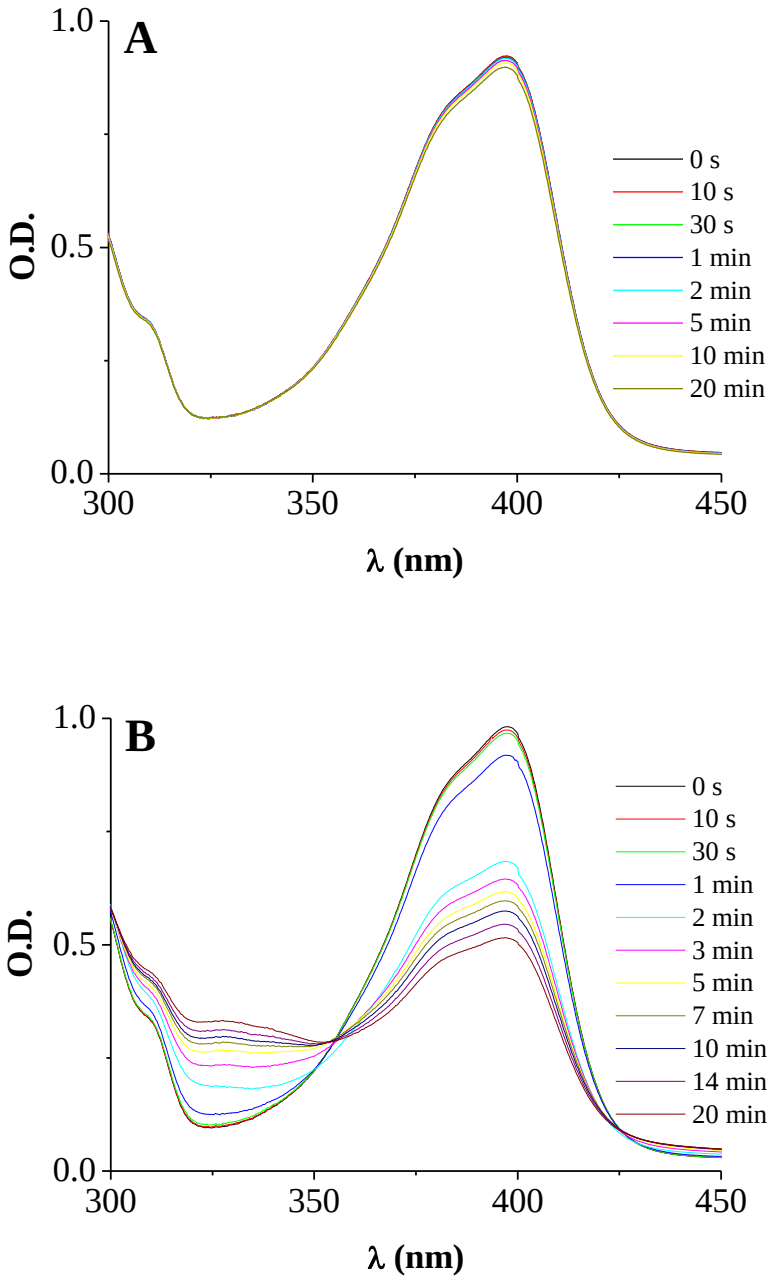

Figure 4.20. Steady state photolysis of (a) TX1, (b) TX1/MDEA ([MDEA] = 13 M) in acetonitrile upon the LED@395 nm exposure; UV–vis spectra recorded at different irradiation time.

4.4. Polymeric Photoinitiators

4.2.1 Synthesis and Characterization of Polymeric Photoinitiators

Two polymeric photoinitiators PPI(TX1-*co*-DMAEM) (15:85 mol %) and PPI(TX1-*co*-DMAEM) (7.5:92.5 mol %) were synthesized through copolymerization of monomeric photoinitiator TX1 with N, N-dimethylaminoethyl methacrylate (DMAEM) (Figure 4.21). Data concerning synthesis and properties of the polymers are reported in Table 4.7. Monomer concentration (TX1) was low in mol % compared to DMAEM to increase their solubility.

The polymeric photoinitiators are soluble in some of the common organic solvents such as methanol, dichloromethane and THF, partially soluble in ether but insoluble in petroleum ether and water (Table 4.8). They are also compatible with the cross-linker monomers such as HDDA and TMPTA.

^{1}H NMR and FTIR spectra verified the structure of the photoinitiators. ^{1}H NMR spectra show the disappearance of double bond peaks (Figure 4.22). FTIR spectra indicate shift of carbonyl peak due to removal of conjugation in polymeric photoinitiators (Figure 4.22). Figure 4.22 illustrates ^{1}H NMR spectra of PPI(TX1-*co*-DMAEM) (15:85 mol %), poly-DMAEM and TX1. The peaks at around 7-9 ppm show the aromatic protons of TX unit, whereas the peaks at around 2 ppm depicts methyl and methylene protons of DMAEM attached to nitrogen in the copolymer spectrum. The peak at 4 ppm belong to the oxymethylene protons of both TX and DMAEM. Copolymers' composition was calculated using ^{1}H NMR spectra, by comparing the integration of aromatic protons of TX group with respect to oxymethylene protons of both TX1 and DMAEM. The copolymer compositions are similar to the feed ratios as shown in Table 4.7 which may be due to the high conversion yields obtained through copolymerization process (>50 %). The reactivity ratios of the monomers could not be estimated because of the same reason. The number average molecular weight (M_n) and polydispersity index (PDI) values of the copolymers are demonstrated in the last column of the Table 4.7. The M_n values of the copolymers increase with the increase of mol ratio of DMAEM in the formulation.

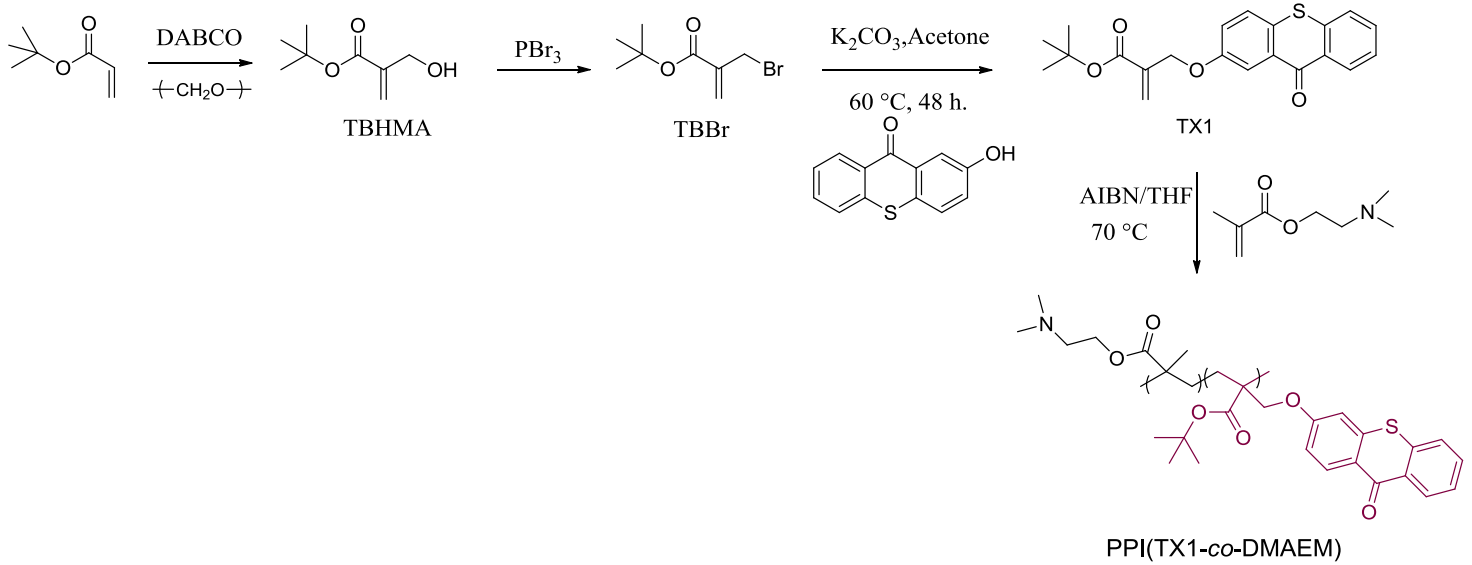

Figure 4.21. Synthesis of PPIs.

Table 4.7. Synthesis and characterization data for PPIs.

	PI in feed (mol %)	**PI in copolymer (mol %)**	**[M]**	**[AIBN] x 10^{-2}**	**Temp. (˚C)**	**Time (h)**	**Yield (%)**	**M_n/PDI**
PPI(TX1-*co*-DMAEM)	20.0	15.0	8.60	14	70	3.5	52	133160/1.0
PPI(TX1-*co*-DMAEM)	12.5	7.5	8.66	14	70	3.5	73	164050/1.1

Table 4.8. Solubilities of the synthesized PIs in selected solvents.

Polymer	H_2O	Methanol	Ether	Petroleum Ether	CH_2Cl_2	THF
PPI(TX1-*co*-DMAEM) (15:85 mol %)	-	+	±	-	+	+
PPI(TX1-*co*-DMAEM) (7.5:92.5 mol %)	-	+	±	-	+	+
TX1	-	+	±	±	±	±
TX	-	+	-	-	+	+

Thermal characteristics of the copolymeric photoinitiators were evaluated by DSC. As it could be seen in Figure 4.24, PPI(TX1-*co*-DMAEM) (15:85 mol %) and PPI(TX1-*co*-DMAEM) (7.5:92.5 mol %) has T_g values of 50 ℃ and 40 ˚C, respectively. DMAEM which has more flexibility compared to TX takes role in the decrease of T_g values.

4.4.1. UV-Vis Spectral Characterization of Photoinitiators

UV-Vis absorption spectra of PPIs were performed in DMF solution (Figure 4.25). The λ_{max} and ε values are given in Table 4.9.

Figure 4.25 shows that TX1 and PPIs have strong $\pi \rightarrow \pi^*$ absorption at nearly the same λ_{max} values with TX, but they have red-shifted $n \rightarrow \pi^*$ absorption which may be due to electron donating ability of oxygen attached to TX. The red-shift $n \rightarrow \pi^*$ absorption makes these photoinitators more efficient in visible light.

When we compare the absorption characteristics of TX1 with the copolymeric photoinitiators, we can see that there is no difference in their λ_{max} values which shows that polymeric structure does not have any explicit effect in the absorption properties of the photoinitiators. However, the extinction coefficients of polymeric photoinitiators are higher than TX1 and commercial TX.

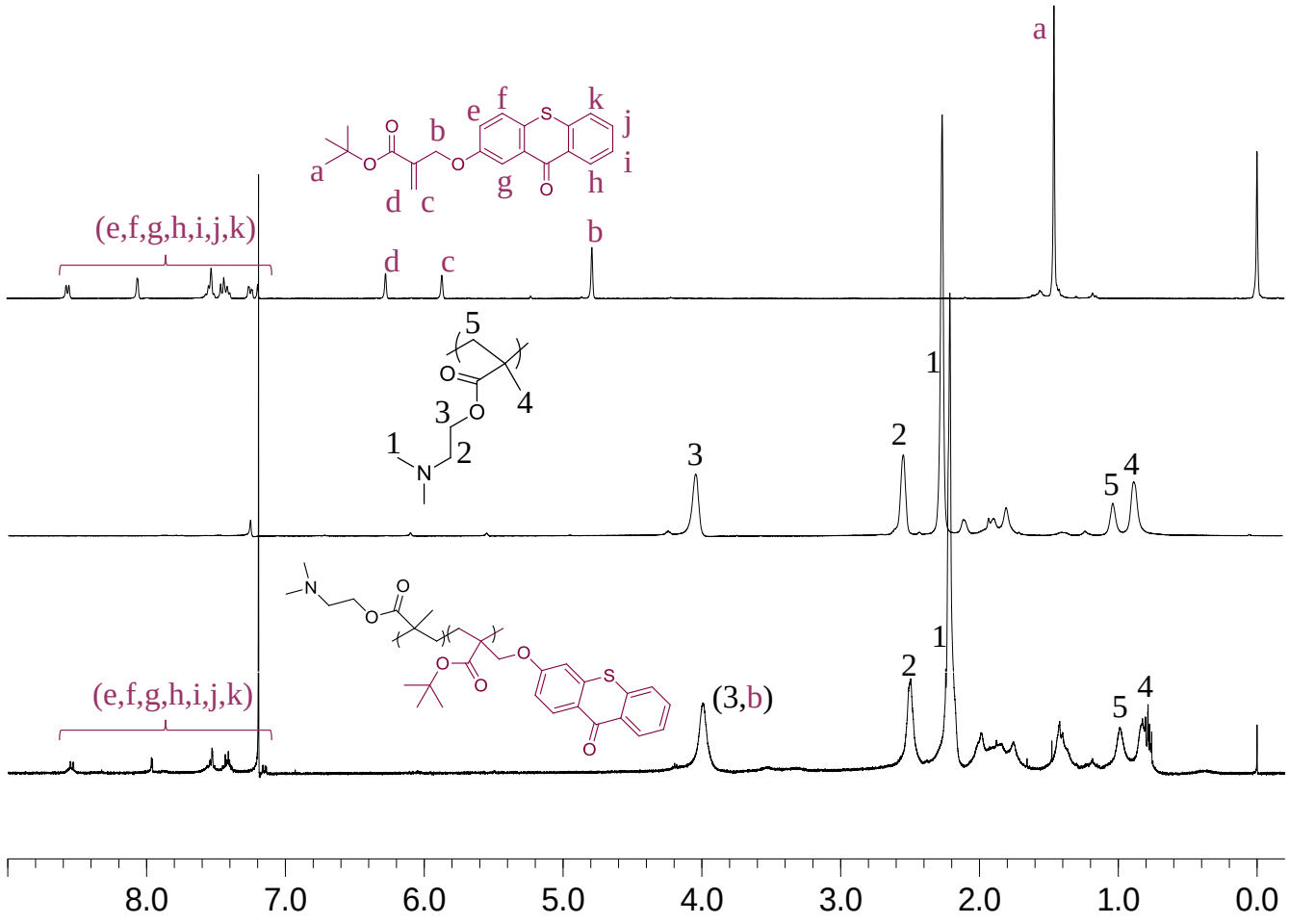

Figure 4.22. ^{1}H NMR spectra of TX1, PPI(TX1-*co*-DMAEM) (15:85 mol%) and poly-DMAEM.

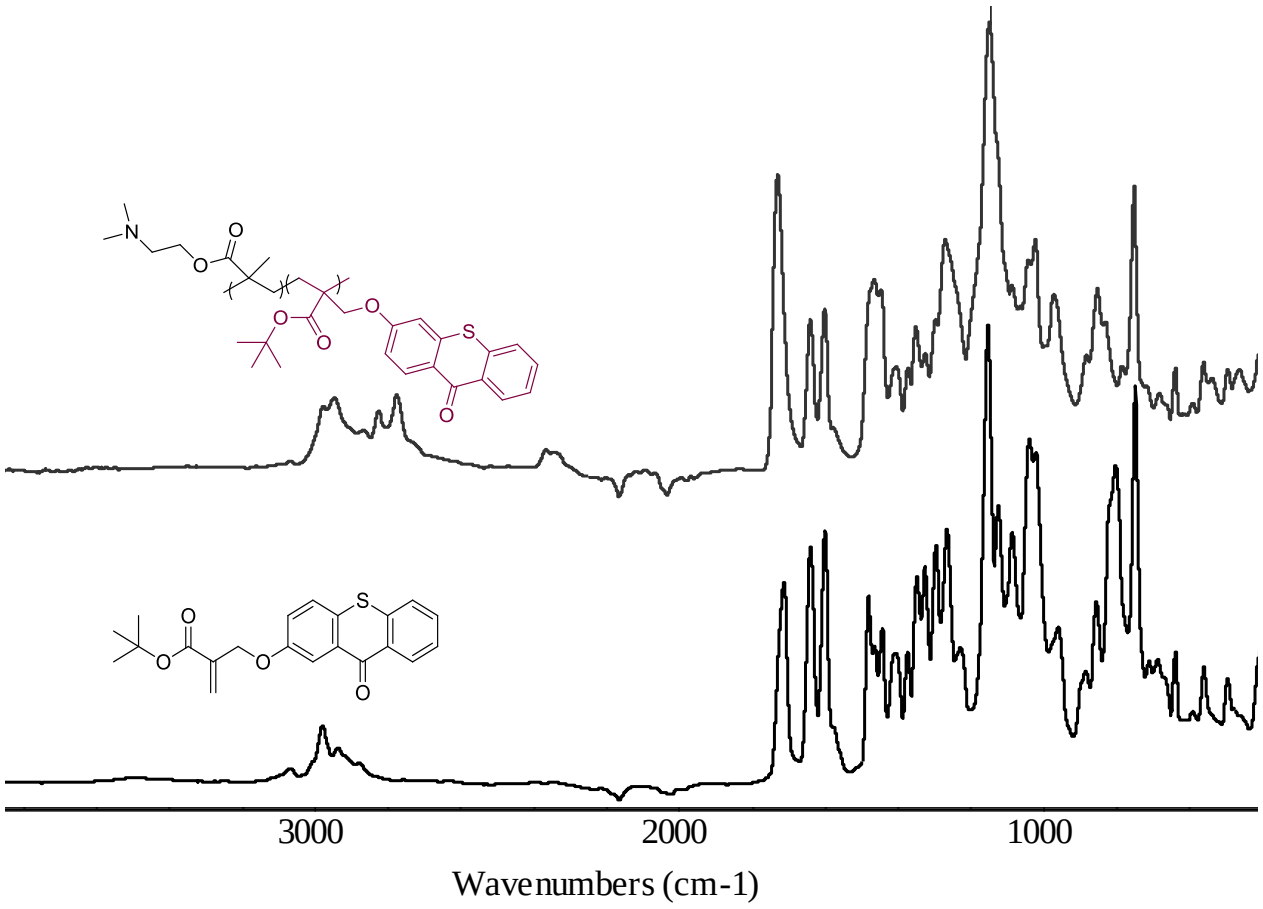

Figure 4.23. FTIR spectra of PPI(TX1-*co*-DMAEM) (15:85 mol %) and TX1.

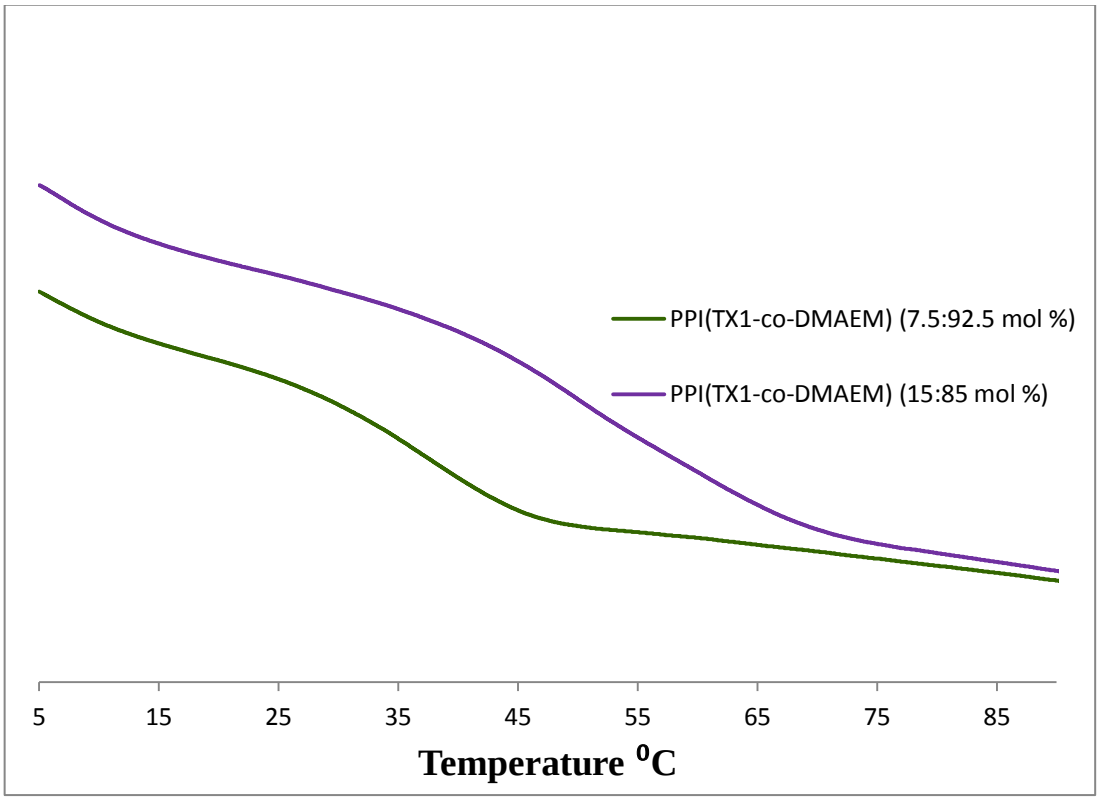

Figure 4.24. T_g analysis of polymeric photoinitiators.

Table 4.9. Absorption properties of the synthesized photoinitiators in dimethylformamide solution.

PI	λ_{max} (nm)	λ_{max} (nm)	ε (L mol^{-1} cm^{-1})[a]	ε (L mol^{-1} cm^{-1})[a]
TX	266	380	23830	5890
TX1	266	400	31890	6910
PPI(TX1-*co*-DMAEM) (15:85 mol %)	272	400	34660	7230
PPI(TX1-*co*-DMAEM) (7.5:92.5 mol %)	272	400	40190	8040

[a] in terms of photoinitiating repeating units

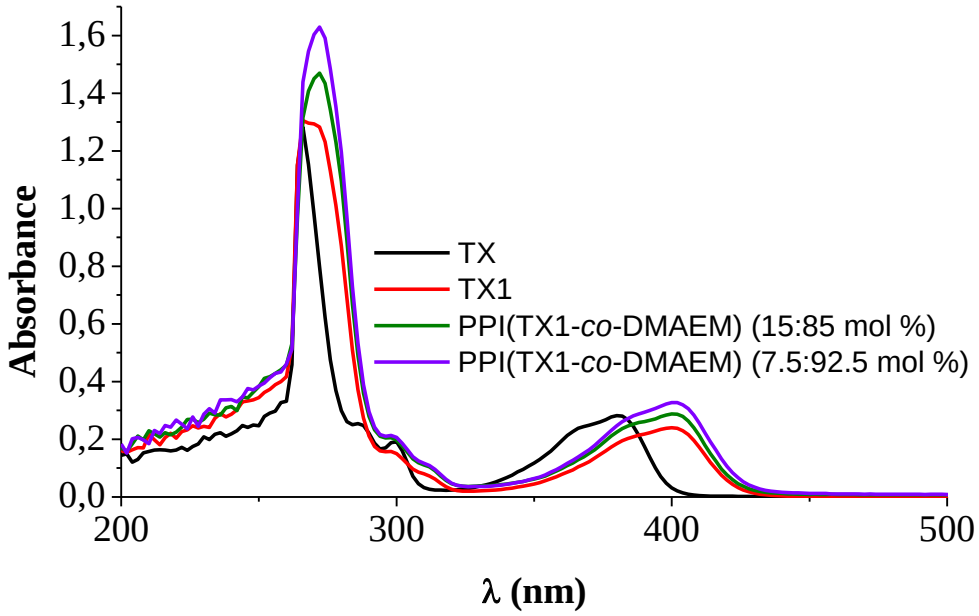

Figure 4.25. UV-Vis absorption spectra of TX, TX1, PPI(TX1-*co*-DMAEM) (15:85 mol %) and PPI(TX1-*co*-DMAEM) (7.5:92.5 mol %) in dimethylformamide ($4x10^{-5}$ M) solution.

4.4.2. Photoinitiating Activity

The phoinitiating activity measurements of the copolymeric photoinitiators, PPI(TX1-*co*-DMAEM) (15:85 mol %) and PPI(TX1-*co*-DMAEM) (7.5:92.55 mol %), were tested toward TMPTA monomer using real time FTIR instrument and photo-DSC.

First, the photopolymerizations of TMPTA were performed using real time FTIR in laminated conditions by using two different light sources, low intensity LED@385 nm or LED@405 nm. The commercial PI TX and monomeric counterpart TX1 were also studied under the same conditions for comparison. The polymerization profiles (Figure 4.26) shows the conversion versus irradiation time. The exact values of the final conversions were also shown in Table 4.10. The conversion values of the copolymeric photoinitiators, TX1 and commercial TX are more or less similar both at LED@385 nm and LED@405 nm.

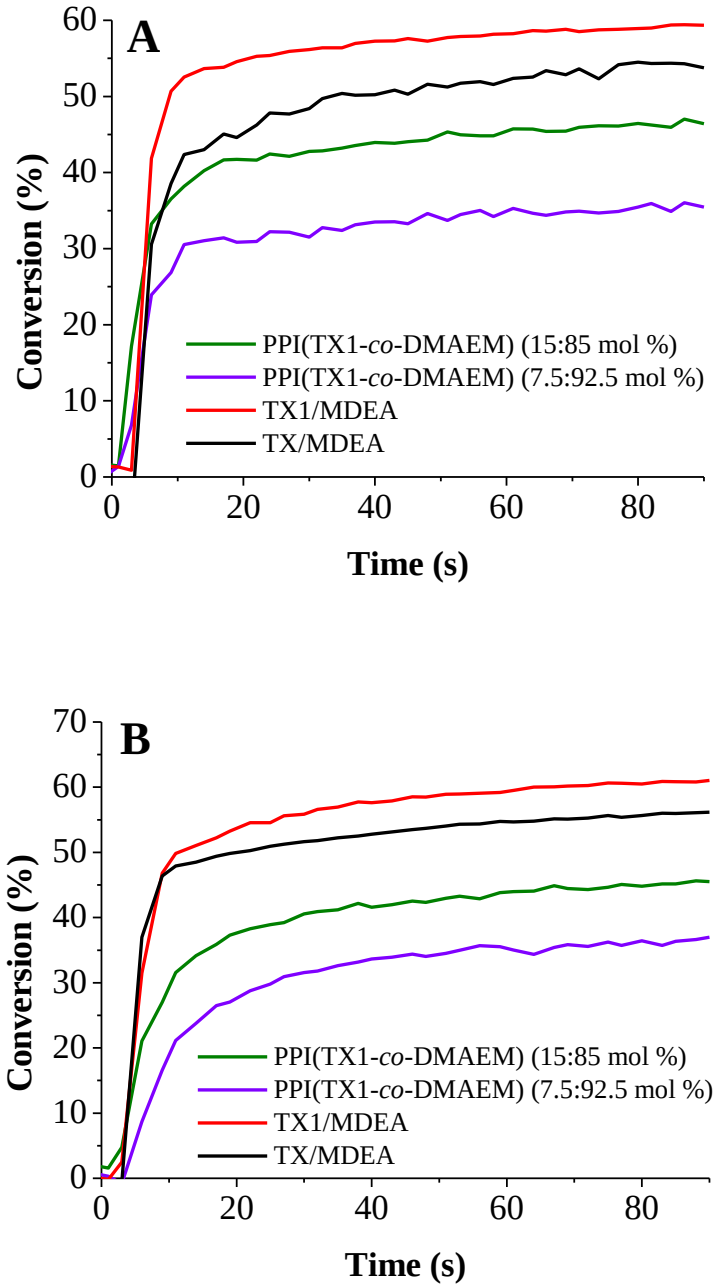

Figure 4.26. Photopolymerization profiles of TMPTA in laminate in the presence of (A) upon the LED@405 nm; (B) upon the LED@385 nm exposure.

Table 4.10. TMPTA conversions obtained in laminate upon exposure to different LED sources for 90 s in the presence of ITX/MDEA (1/3%, w/w), TX1/MDEA (1/3%, w/w), PPI(TX1-*co*-DMAEM) (15:85 mol %) (1%,w) (TX1/DMAEM (0.3/0.7%, w/w), PPI(TX1-*co*-DMAEM) (7.5:92.5 mol %) (1%,w) (TX1/DMAEM (0.2/0.8%, w/w).

	LED (405 nm)	LED (385 nm)
TX/MDEA	54 %	56 %
TX1/MDEA	59 %	61 %
PPI(TX1-*co*-DMAEM) (15:85 mol %)	46 %	46 %
PPI(TX1-*co*-DMAEM) (7.5:92.5 mol %)	36 %	37 %

However, rate of polymerization of the photoinitiators are higher at LED@405 nm compared to LED@385 nm as it can be deduced from the slope of the conversion versus induction time plots. TX/MDEA and TX1/MDEA have similar conversion values (54% and 59%) at 405 nm LED and (56% and 61%) at LED@385 nm in laminated conditions show similar final conversions. However, final conversions of the copolymeric photoinitiators PPI(TX1-*co*-DMAEM) (15:85 mol %) (46% at LED@405 and LED@385 nm) and PPI(TX1-*co*-DMAEM) (7.5:92.55 mol %) (36% at LED@405 and 37% at LED@385 nm) are relatively low. These results may stem from the fact that the reactive radical located in the polymeric chain restricts the movement towards the monomers which makes the hydrogen transfer between the excited state of TX1 and DMAEM difficult. The copolymeric photoinitiators do not need any additional hydrogen donor compound, because they already have amine (DMAEM) unit as coinitiator in their structure.

The photopolymerization kinetics were evaluated in the polymerization of HDDA by also using Photo-DSC instrument with a mercury arc lamp. And also, TX1/DMAEM in 15:85 mol % was subjected to photopolymerization experiments as a reference for PPI(TX1-*co*-DMAEM) (15:85 mol %) using the same conditions. As shown in Figure 4.27, TX1/DMAEM (15:85 mol %) has higher R_p and conversion values compared to PPI(TX1-*co*-DMAEM) (15:85 mol %) which may arise from the easier mobility of the aminoalkyl radical than polymeric amine radical. PPI(TX1-*co*-DMAEM) (15:85 mol %)

and PPI(TX1-*co*-DMAEM) (7.5:92.55 mol %) has similar final conversions but PPI(TX1-*co*-DMAEM) (15:85 mol %) has higher R_p due to its higher TX1 content than the other.

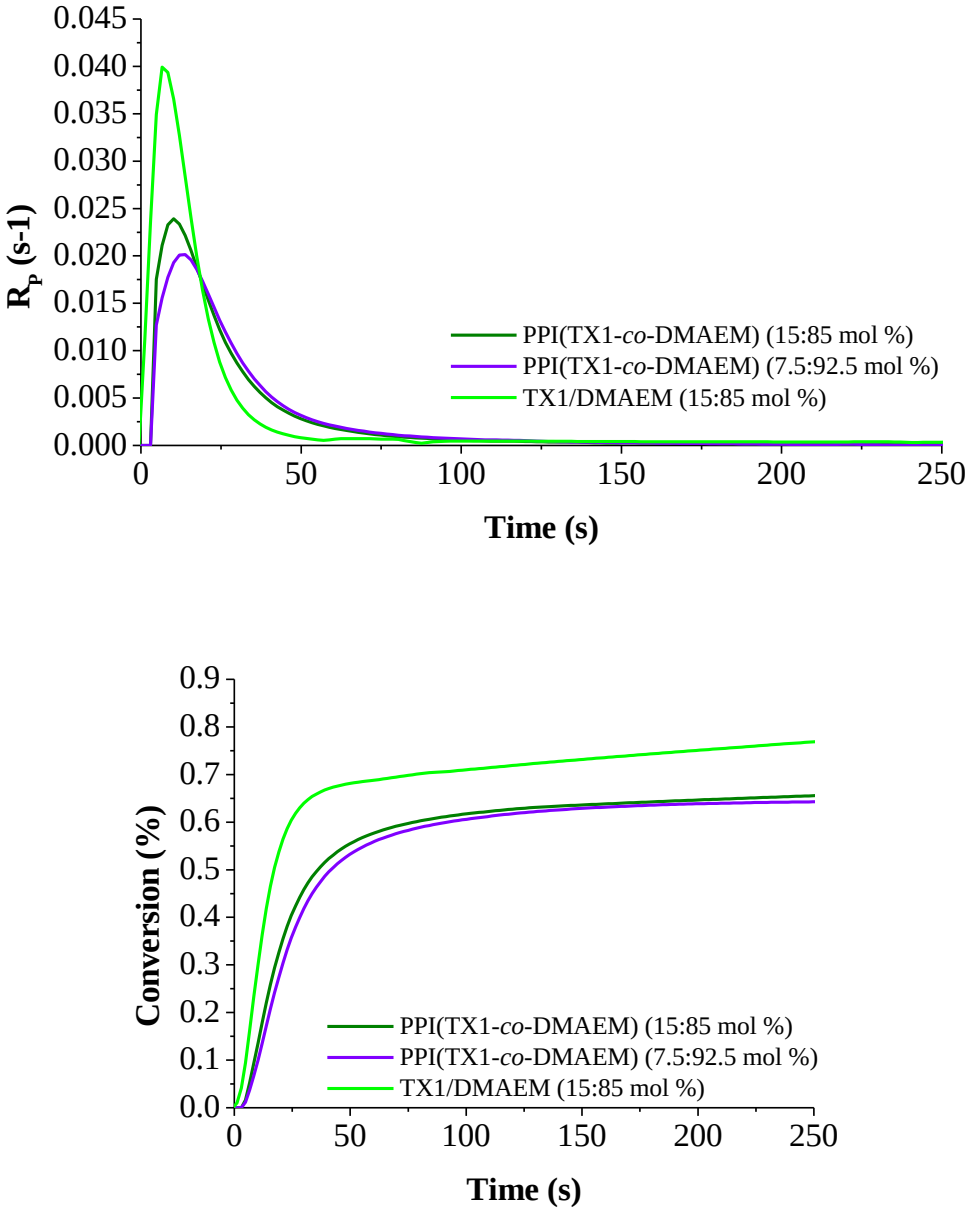

Figure 4.27. Rate-time and conversion-time plots for the photopolymerization of TMPTA initiated by PPI(TX1-co-DMAEM) (15:85 mol %), PPI(TX1-co-DMAEM) (7.5:92.5 mol %), TX1/DMAEM (15:85 mol %).

4.4.3. ESR Analysis

A *tert*-butylbenzene solution of both PPI(TX1-*co*-DMAEM) (15:85 mol %) and PPI(TX1-*co*-DMAEM) (7.5:92.5 mol%) with PBN was irradiated under LED@385 nm in non-aerated medium during 1 minute and then monitored by ESR spectrometer. The presecence of a two different carbon-centered radicals which may be generated from the methylene and methyl groups next to nitrogen from PPI(TX1-*co*-DMAEM) (15:85 mol %) and PPI(TX1-*co*-DMAEM) (7.5:92.5 mol%) solutions are confirmed by ESR spin trapping experiments (Figure 4.28 and Figure 4.29).

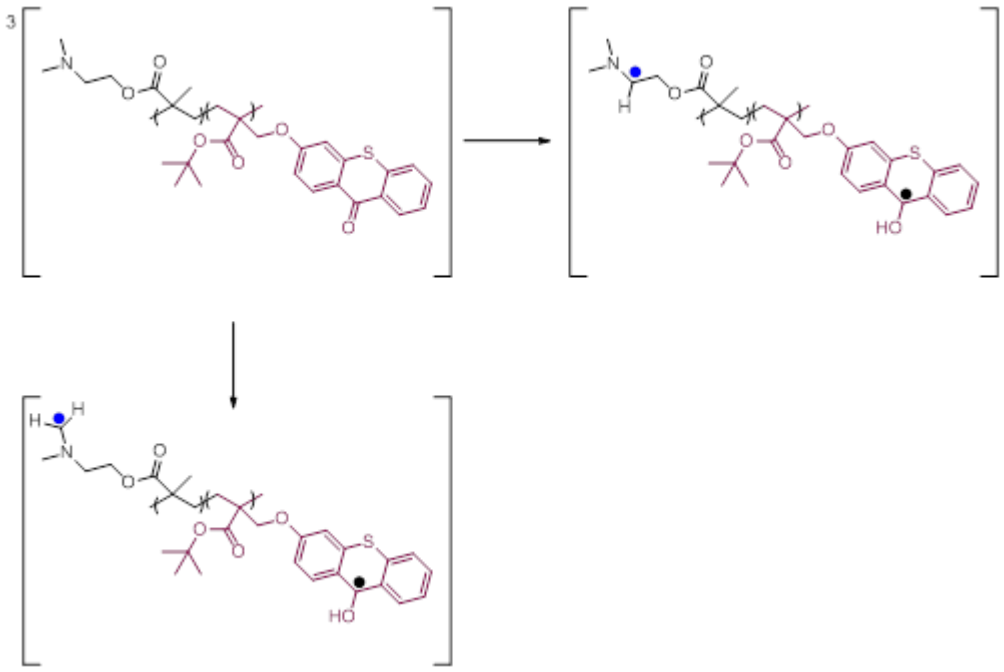

Figure 4.28. Photoinitiation mechanism of PPI(TX1-*co*-DMAEM) (15:85 mol %) and PPI(TX1-*co*-DMAEM) (7.5:92.5 mol%).

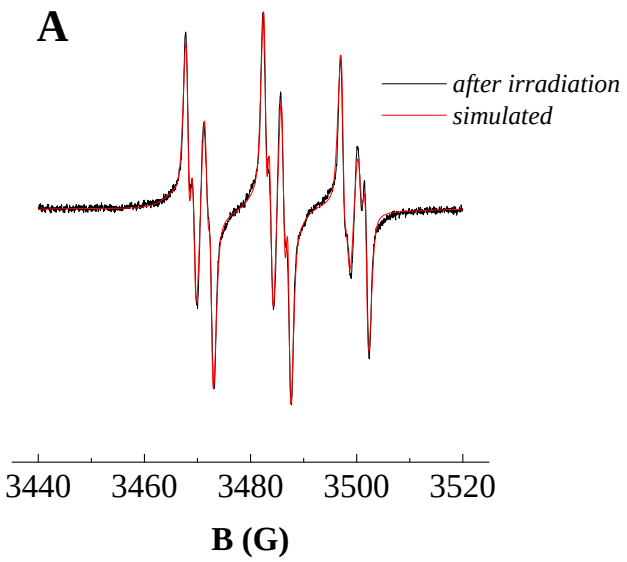

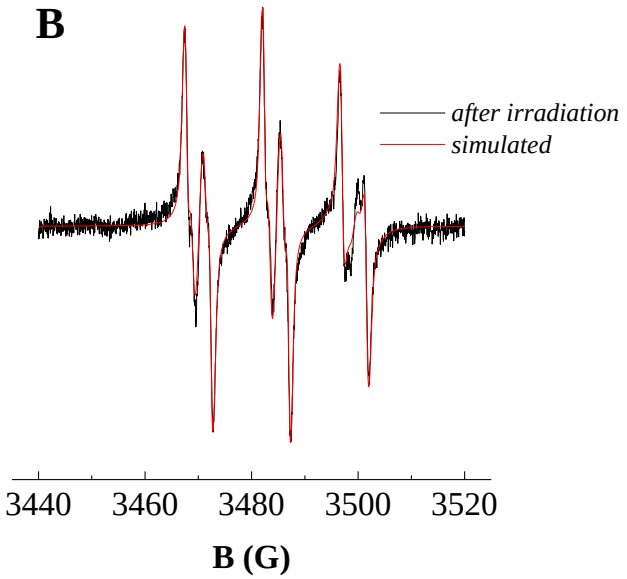

Figure 4.29. ESR spectra of the radicals generated in (A) PPI(TX1-*co*-DMAEM) (15:85 mol %), (B) PPI(TX1-*co*-DMAEM) (7.5:92.5 mol%) upon the LED@385 nm exposure and trapped by PBN in *tert*-butylbenzene.

4.4.4. Redox Potentials

The redox properties of the copolymeric photoinitiators were investigated (Figure 4.30 and Table 4.11). The free energy changes ΔG for electron transfer reaction determined through the Rehm-Weller equation are negative which is favorable (ΔG = -0.21 eV for both of the copolymeric PIs, using the following paramaters: oxidation potential E_{ox} for DMAEM = 0.7 eV, reduction potentials E_{red} = -1.7 eV for both of the copolymeric PIs, as calculated by cyclic voltammetry and triplet excited state energy E_T of TX1 = 2.61 eV, as determined by the method UB3LYP/6-31G*), as can be seen in Table 4.12. The free energy changes ΔG for electron transfer reaction between copolymeric PIs (PPI(TX1-*co*-DMAEM) (15:85 mol %) and PPI(TX1-*co*-DMAEM) (7.5:92.5 mol %)) and MDEA are also negative which is favorable (ΔG = -0.11 eV for both of them, using the following paramaters: oxidation potential E_{ox} for MDEA = 0.8 eV, reduction potentials E_{red} = -1.7 eV for both of them, as calculated by cyclic voltammetry and triplet excited state energy E_T of TX1 = 2.61 eV, as determined by the method UB3LYP/6-31G*), as can be seen in Table 4.12.

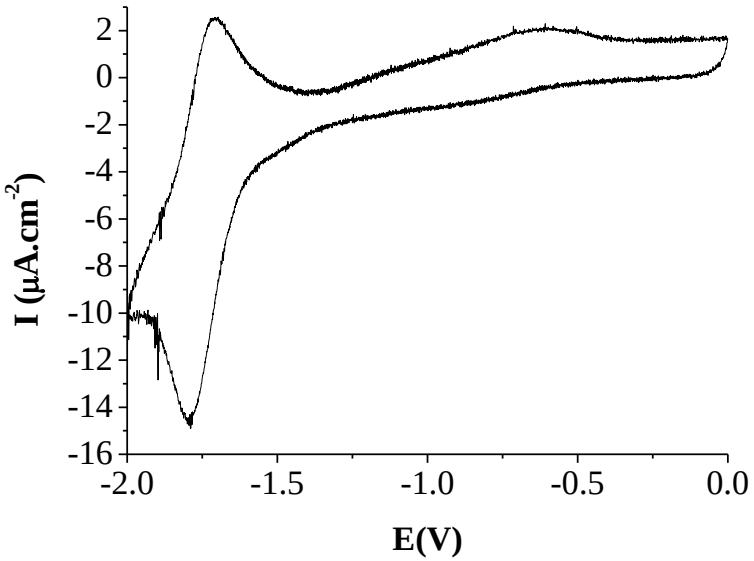

Figure 4.30. Cyclic voltammogram of PPI(TX1-*co*-DMAEM) (7.5:92.5 mol %) in acetonitrile.

Table 4.11. Redox Potentials for PPIs.

Photoinitiator	E_{ox} (eV)[a]	E_{ox} (DMAEM) (eV)[a]	E_{red} (eV)[a]
PPI(TX1-*co*-DMAEM) (15:85 mol %)	1.5	0.7	-1.7
PPI(TX1-*co*-DMAEM) (7.5:92.5 mol %)	1.4	0.7	-1.7

[a] E_{ox} and E_{red} values: measured by cyclic voltammetry for PPI(TX1-*co*-DMAEM) (15:85 mol %) and PPI(TX1-*co*-DMAEM) (7.5:92.5 mol %).

The reduction potentials are slightly more favorable for ITX (-1.57 V; Table 4.10); this is ascribed to the electron donating effect of the oxygen substituent in copolymeric PIs.

4.4.5. Laser Flash Photolysis Experiments

The transient absorption spectra following the laser excitation of PPI(TX1-*co*-DMAEM) (15:85 mol %) and PPI(TX1-*co*-DMAEM) (7.5:92.5 mol %) at 355 nm in acetonitrile are given in Figure 4.31, Figure 4.32 and Figure 4.33. The triplet states of these compounds are observed at 600 nm, as for ITX, in agreement with an excited triplet state centered on the TX moiety. Very high rate constants of quenching between their triplet state and amine (MDEA) were found (Table 4.10; $> 10^9$ $M^{-1}s^{-1}$) showing a very favourable process.

The triplet state lifetimes of PPI(TX1-*co*-DMAEM) (15:85 mol %) and PPI(TX1-*co*-DMAEM) (7.5:92.5 mol %) are smaller compared to TX1 and ITX, as we can see in Table 4.5 and Table 4.10, which may stem from the intramolecular hydogen abstraction reaction mechanism of the copolymeric photoinitiators (Figure 4.28).

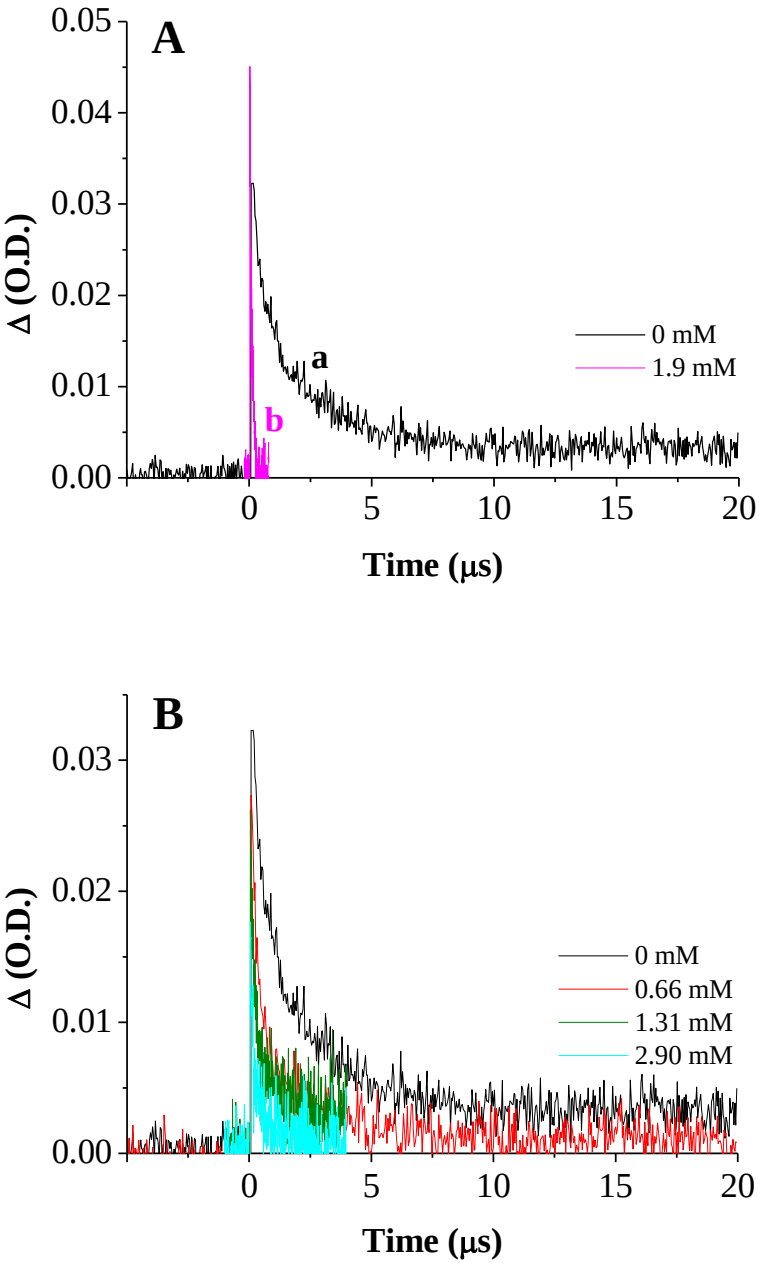

Figure 4.31. Triplet state decay traces observed after laser excitation of PPI(TX1-*co*-DMAEM) (15:85 mol %) in acetonitrile at 355 nm, kinetic traces recorded at 600 nm: (A) (a) under N_2 (black curve, $[O_2] = 0$), (b) under air (pink curve, $[O_2] = 1.9$ mM); (B) in different MDEA concentrations under N_2.

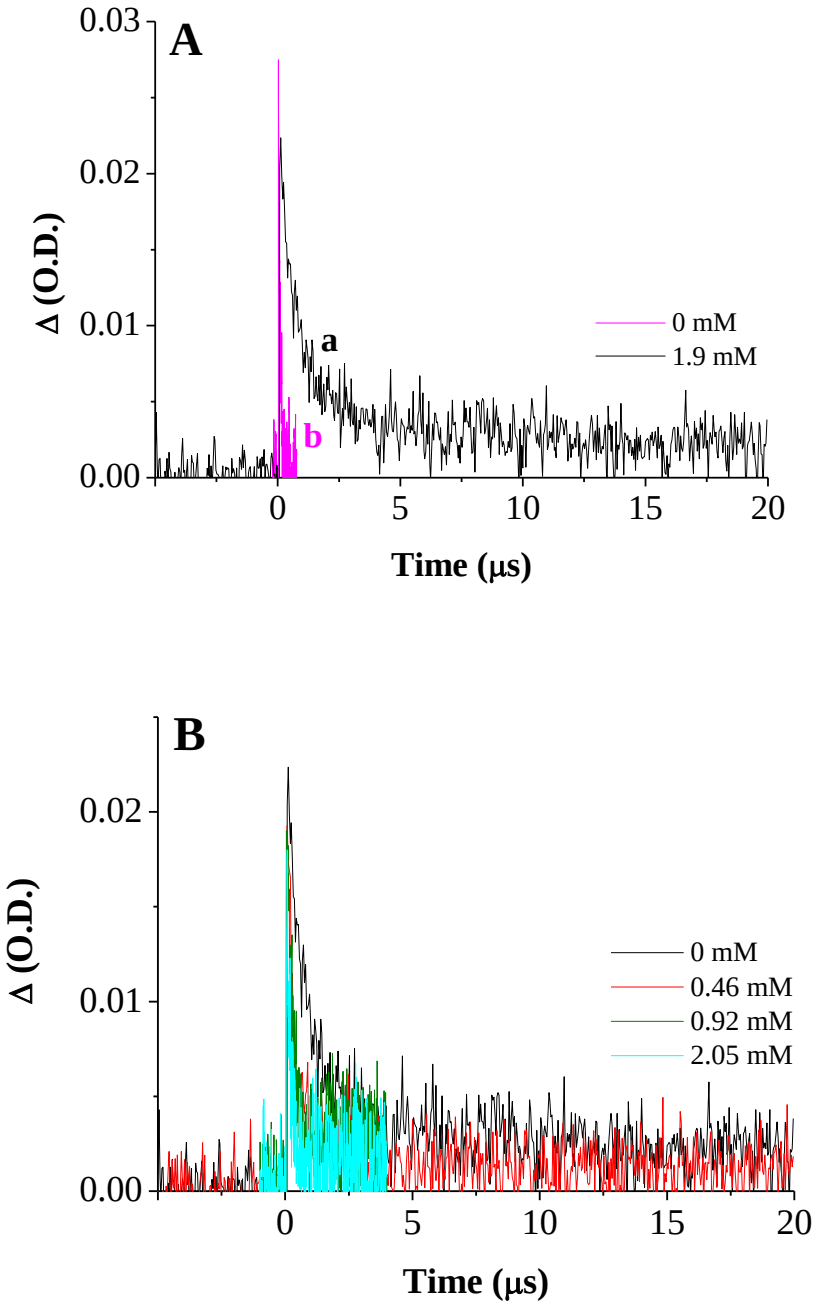

Figure 4.32. Triplet state decay traces observed after laser excitation of PPI(TX1-*co*-DMAEM) (7.5:92.5 mol %) in acetonitrile at 355 nm, kinetic traces recorded at 600 nm: (A) (a) under N_2 (black curve, $[O_2] = 0$), (b) under air (pink curve, $[O_2] = 1.9$ mM); (B) in different MDEA concentrations under N_2.

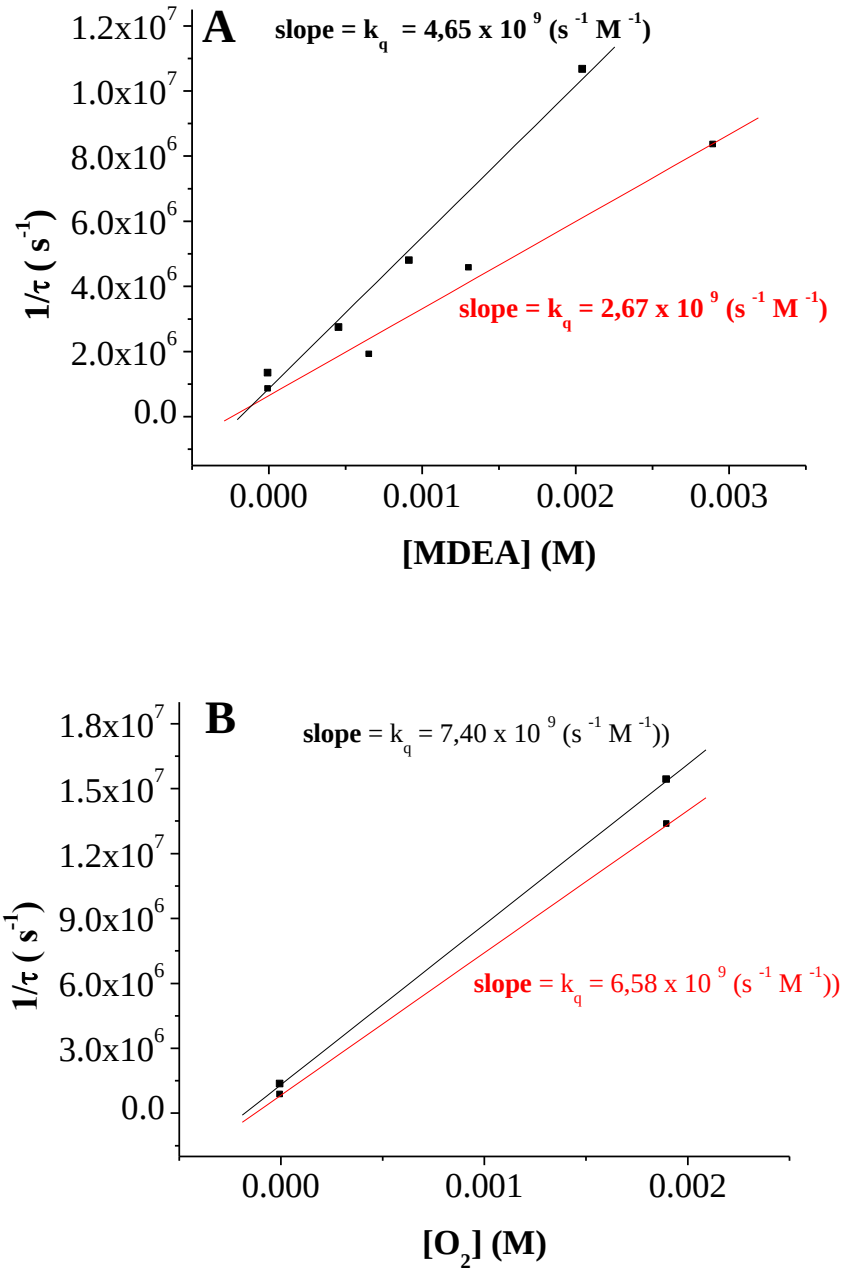

Figure 4.33. Stern–Volmer plot for the quenching of; (A) ^{3}PPI(TX1-*co*-DMAEM) (15:85 mol %) (red line) and ^{3}PPI(TX1-*co*-DMAEM) (7.5:92.5 mol %) (black line). (B) ^{3}PPI(TX1-*co*-DMAEM) (15:85 mol %) (red line) and ^{3}TX1*co*DMAEM (7.5:92.5 mol %) (black line) by O_2. λ_{exc} = 355 nm.

Table 4.12. Parameters characterizing the reactivity of PIs: redox potentials (Eox, Ered), free energy changes (ΔG), PIs/additive interaction rate constants (kq) and lifetimes (τ).

						O_2	DMAEM	MDEA	
Photoinitiator	E_{ox} (eV)[a]	E_{ox} (DMAEM) (eV)[a]	E_{red} (eV)[a]	$\tau_{(N2)}$ (μs)	$\tau_{(O2)}$ (μs)	k_q ($M^{-1}s^{-1}$)[d]	ΔG_T (eV)[c]	ΔG_T (eV)[b]	k_q ($M^{-1}s^{-1}$)[d]
PPI(TX1-*co*-DMAEM) (15:85 mol %)	1.5	0.7	-1.7	1.21	0.076	$6.58x10^9$	-0.21	-0.11	$2.67x10^9$
PPI(TX1-*co*-DMAEM) (7.5:92.5 mol %)	1.4	0.7	-1.7	0.765	0.065	$7.40x10^9$	-0.21	-0.11	$4.65x10^9$

[a] E_{ox} and E_{red} values: measured by cyclic voltammetry for PPI(TX1-*co*-DMAEM) (15:85 mol %) and PPI(TX1-*co*-DMAEM) (7.5:92.5 mol %).

[b] ΔG_T = free energy change for the triplet state interaction of PPI(TX1-*co*-DMAEM) (15:85 mol %) and PPI(TX1-*co*-DMAEM) (7.5:92.5 mol %) with MDEA. E_{ox} = 0.8 V for MDEA [55].

[c] ΔG_T = free energy change for the triplet state interaction of PPI(TX1-*co*-DMAEM) (15:85 mol %) and PPI(TX1-*co*-DMAEM) (7.5:92.5 mol %) with DMAEM.

[d] kq = PPI(TX1-*co*-DMAEM) (15:85 mol %) (with MDEA or O_2) and PPI(TX1-*co*-DMAEM) (7.5:92.5 mol %) (with MDEA or O_2) interaction rate contants measured by laser flash photolysis experiments.

4.4.6. Steady State Photolysis Experiments

The steady state photolysis of PPI(TX1-*co*-DMAEM) (15:85 mol %) in acetonitrile at 395 nm under air is given in Figure 4.34. A fast bleaching of PPI(TX1-*co*-DMAEM) (15:85 mol %) solution indicated its high photoreactivity without using any additional hydrogen donor compound.

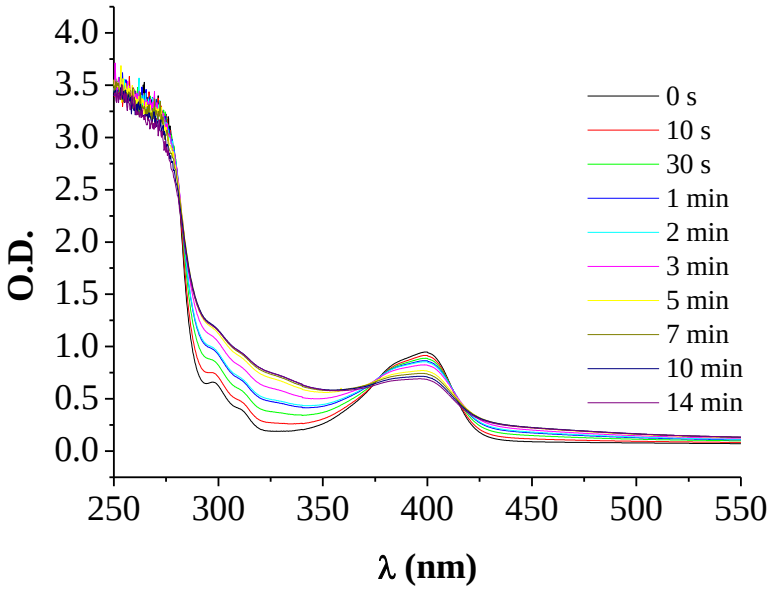

Figure 4.34. Steady state photolysis of PPI(TX1-*co*-DMAEM) (15:85 mol %) in acetonitrile upon LED@395 nm exposure; UV–vis spectra recorded at different irradiation time.

5. CONCLUSION

A new series of monomeric photoinitiators (TX1, TX2, TX3, TX4 and TX5) based on TX and usable under violet LED exposure were designed and synthesized. Their absorption properties are rather close to those of TX. Their photoinitiating performance, both in laminate or under air, is more or less similar to that of the 2-isopropylthioxanthone ITX/amine system reference (according to the considered systems and the irradiation conditions). The excited state processes of the thioxanthone moiety are close to that of ITX. These monomeric PIs are incorporated into the photocurable matrix, thereby decreasing e.g. their migration.

One of the monomeric PIs, TX1, was used to make polymeric PIs, PPI(TX1-*co*-DMAEM). These photoinitiators have lower triplet state life times than monomeric PIs (TX1 and TX2) in both N_2 and O_2 due to their one-component structure which does not require any additional hydrogen donor.

APPENDIX A: H^1 NMR, ^{13}C NMR and FTIR SPECTRA

^1H NMR spectrum of TX3, ^{13}C NMR spectra of TX1 and TX5 and FTIR spectrum of TX3 were also included.

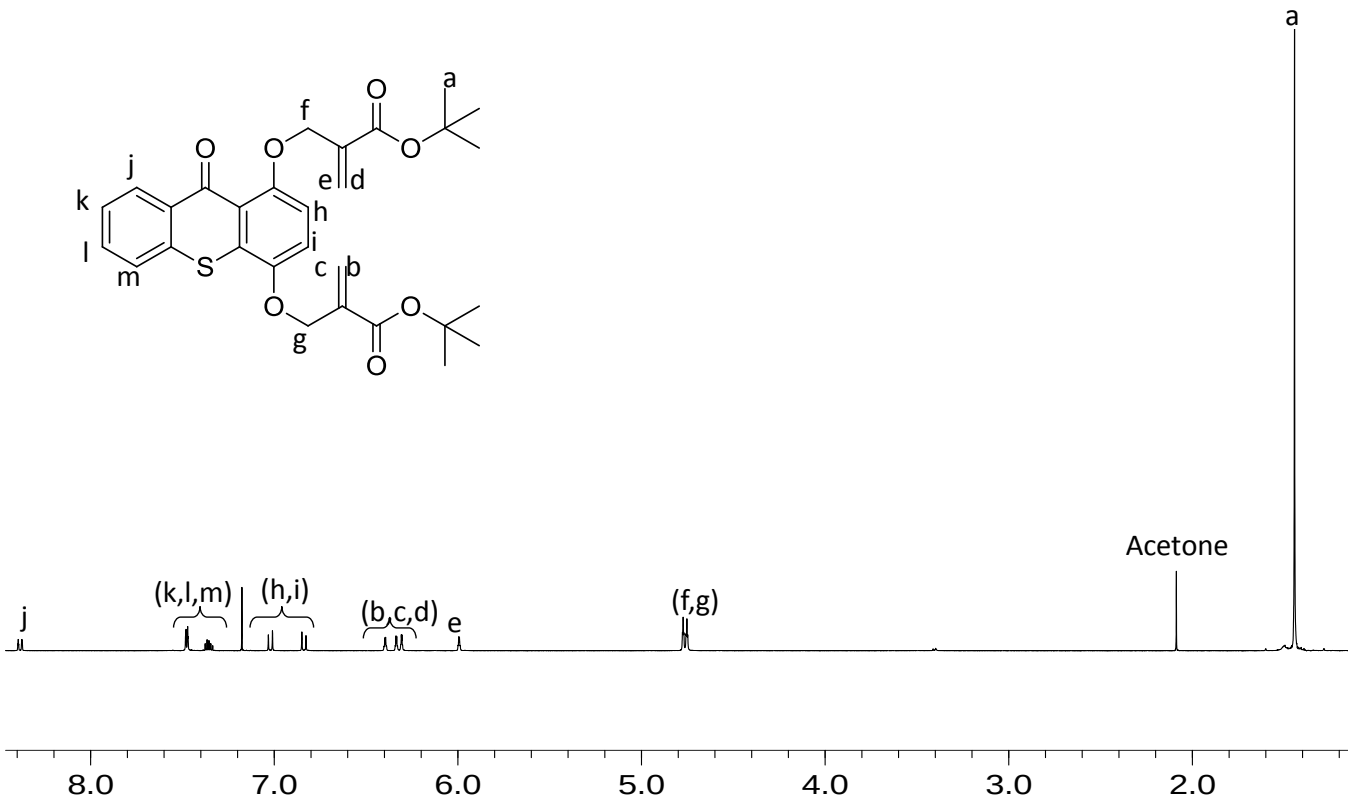

Figure A.1. ^{1}H NMR spectrum of TX3.

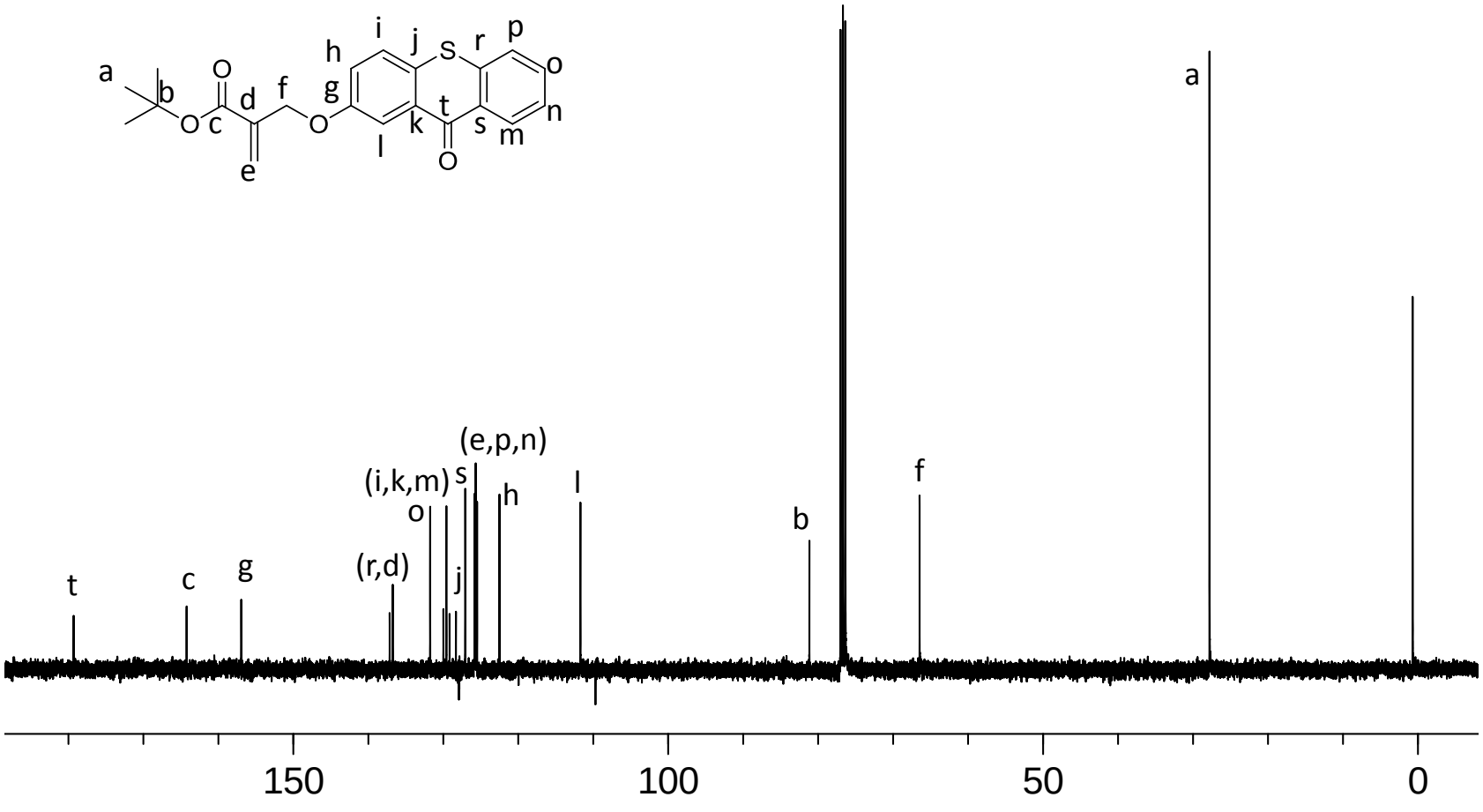

Figure A.2. ^{13}C NMR spectrum of TX1.

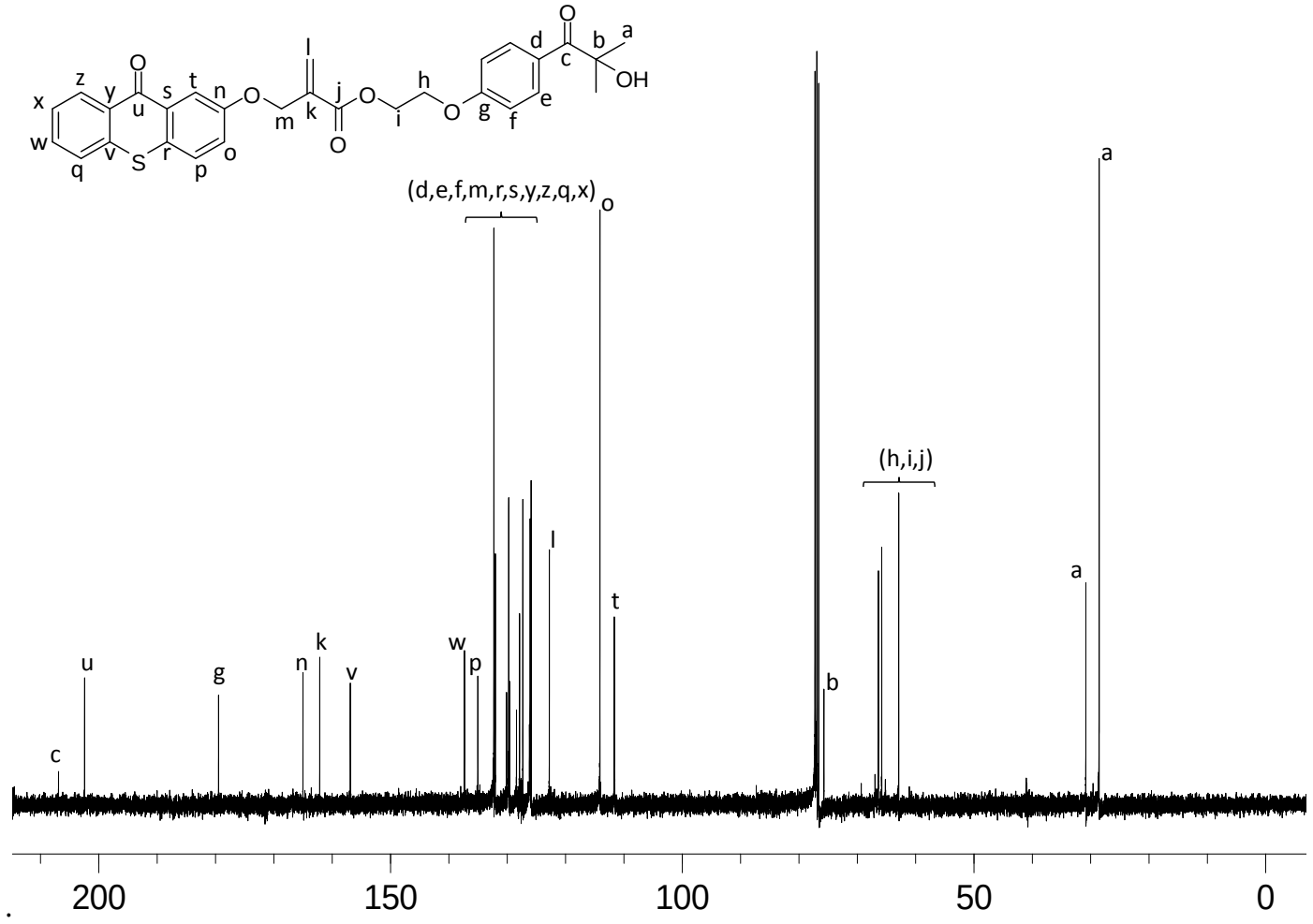

Figure A.3. ^{13}C NMR spectrum of TX5.

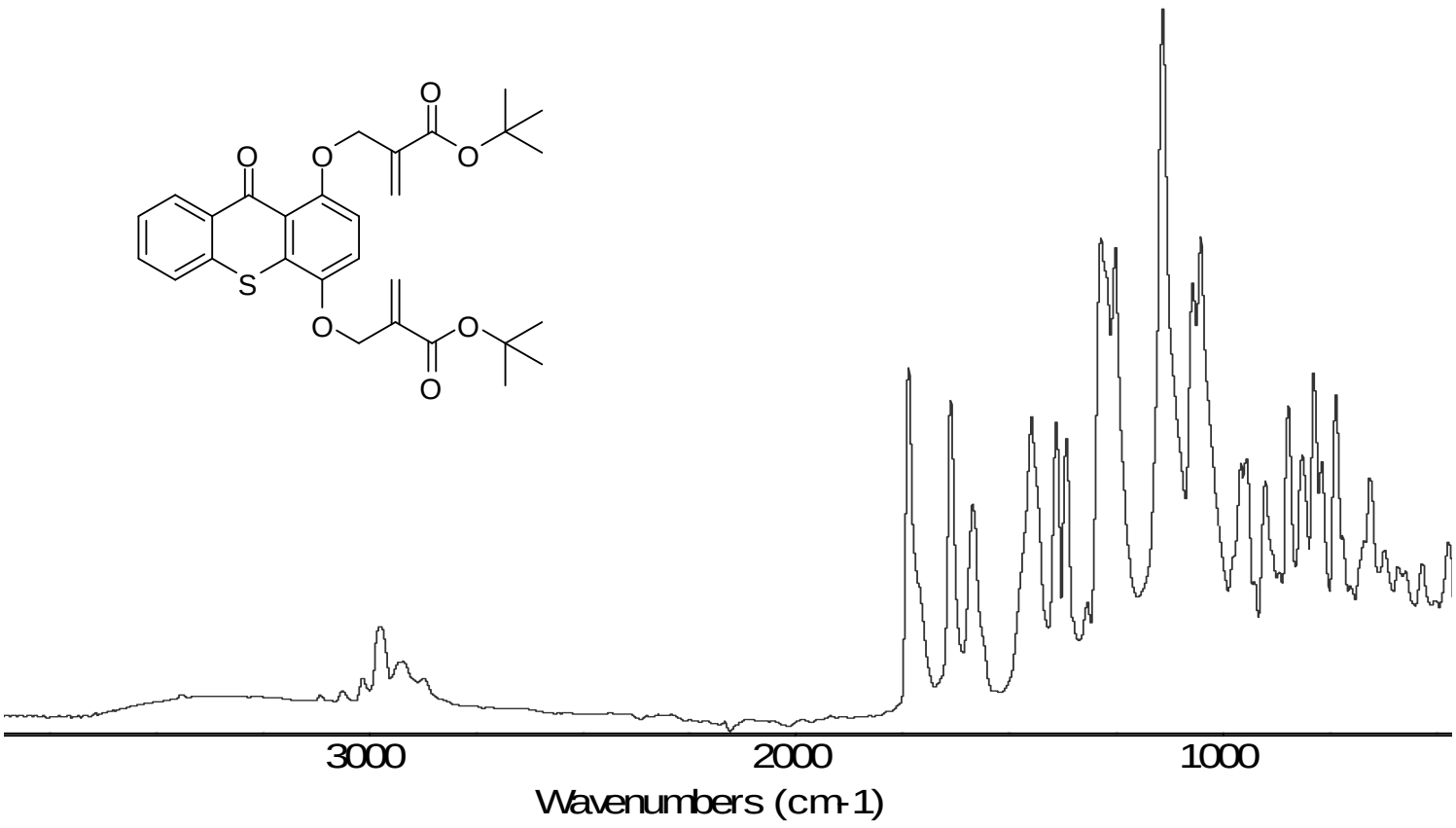

Figure A.4. FTIR spectrum of TX3.

APPENDIX B: PHOTOPOLYMERIZATION RESULTS

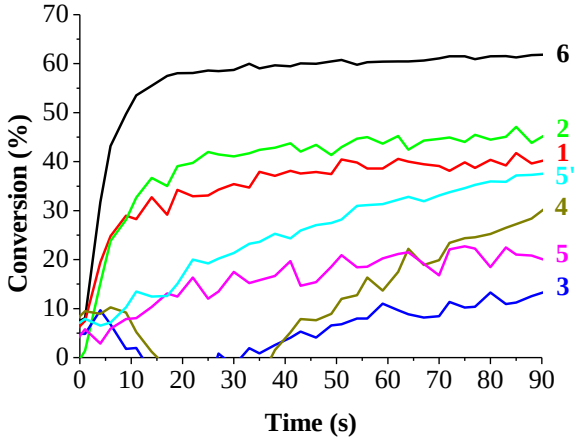

Figure B.1. Photopolymerization profiles of TMPTA under air upon the LED@385 nm exposure, TX1/MDEA (1), TX2/MDEA (2), TX3/MDEA (3), TX4/MDEA (4), TX5 alone (5), TX5/MDEA (5'), ITX/MDEA (6).

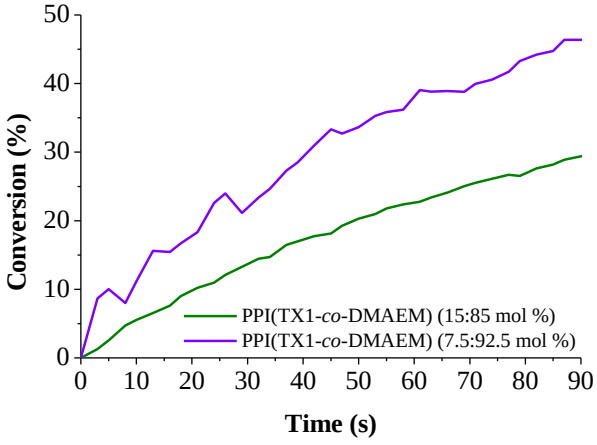

Figure B.2. Photopolymerization profiles of TMPTA under air upon the LED@385 nm exposure.

APPENDIX C: ESR ANALYSIS RESULTS

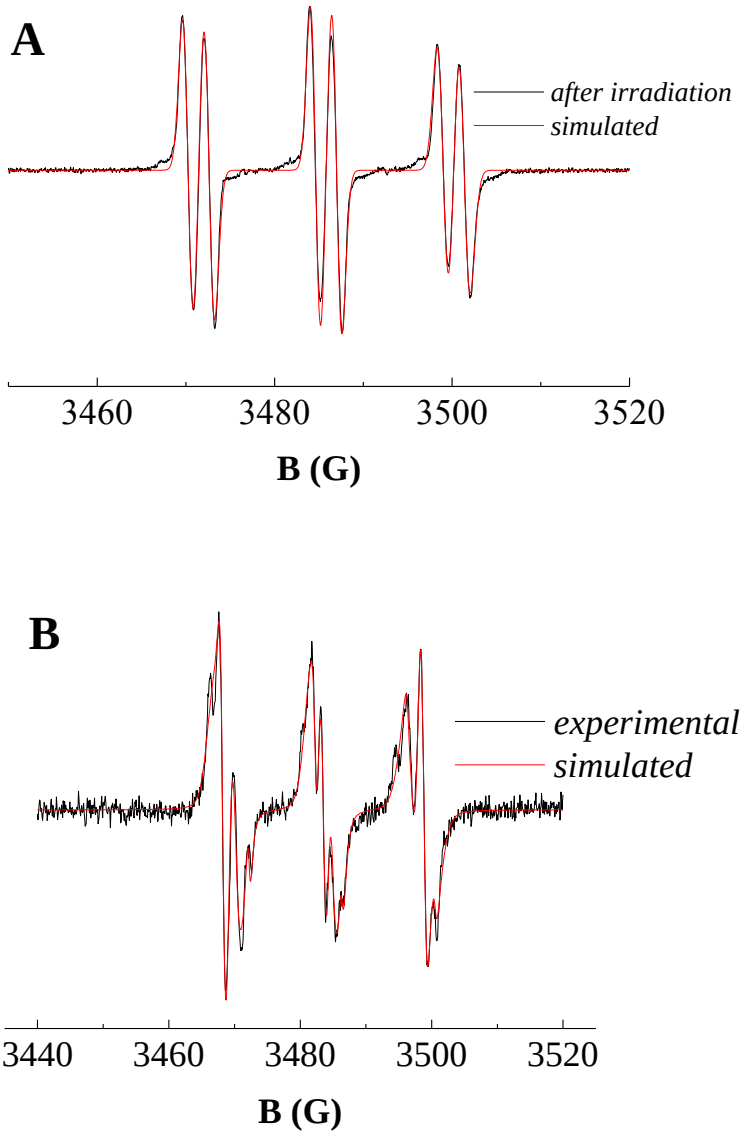

Figure C.1. ESR spectra of the radicals generated in (A) TX5/EDB, (B) TX5 upon the LED@385 nm exposure and trapped by PBN in *tert*-butylbenzene.

APPENDIX D: CYCLIC VOLTAMMETRY RESULTS

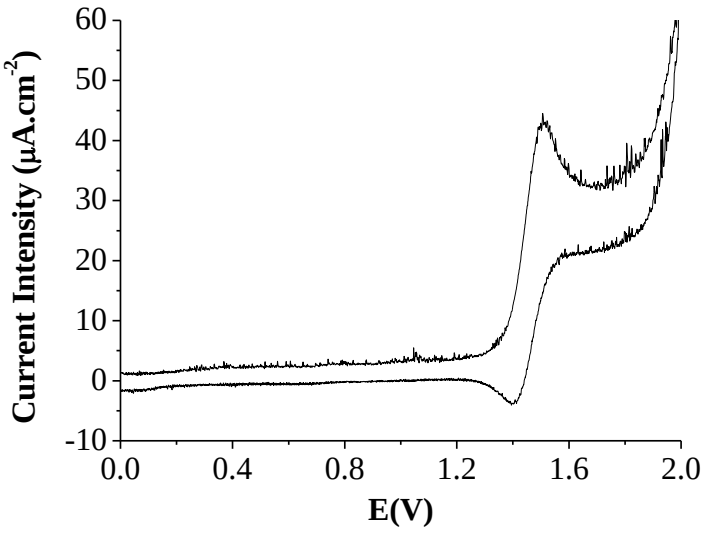

Figure D.1. Cyclic voltammogram of TX1 in acetonitrile.

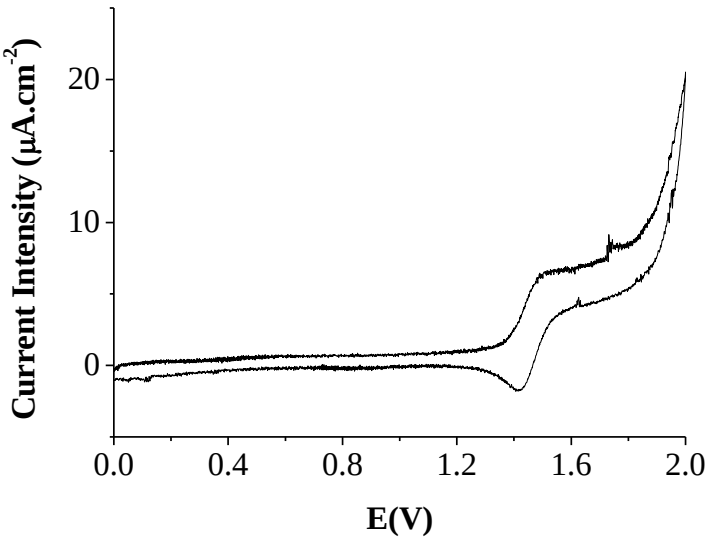

Figure D.2. Cyclic voltammogram of TX2 in acetonitrile.

REFERENCES

1. Fouassier, J. P. and J. Lalevée, *Photoinitiators for Polymer Synthesis: Scope, Reactivity and Efficiency*, First Edition, Wiley-VCH Verlag GmbH & Co. KGaA, Weinheim, pp. 21-22, 2012.

2. Dietliker, K., T. Jung, J. Benkhoff, H. Kura, A. Matsumoto, H. Oka, D. Hristova, G. Gescheidt and G. Rist, "New Developments in Photoinitiators", *Macromolecular Symposia,* Vol. 217, pp. 77-97, 2004.

3. Yagci, Y., S. Jockush and N. J. Turro, "Photoinitiated Polymerization: Advances, Challenges, and Opportunities", *Macromolecules* , Vol. 43, pp. 6245-6260, 2010.

4. Corrales, T., F. Catalina, C. Peinado and N.S. Allen, "Free Radical Macrophotoinitiators: An Overview on Recent Advances", *Journal of Photochemistry and Photobiology A: Chemistry*, Vol. 159, pp. 103-114, 2003.

5. Yilmaz, G., B. Aydogan, G. Temel, N. Arsu, N. Moszner and Y. Yagci, "Thioxanthone-Fluorenes as Visible Light Photoinitiators for Free Radical Polymerization", *Macromolecules,* Vol. 43, pp. 4520-4526, 2010.

6. Fouassier, J. P., F. Morlet Savary, J. Lalevée, X. Allonas and C. Ley, "Dyes as Photoinitiators or Photosensitizers of Polymerization Reactions", *Materials,* Vol. 3, pp. 5130-5142, 2010.

7. Odian, G., *Principles of Polymerization*, Wiley-Interscience Press, New York, 1981.

8. Hoyle, C. E. and J. F. Kinstle, *Radiation Curing of Polymeric Materials,* American Chemical Society, 1990.

9. Schwalm, R., *UV Coatings Basics, Recent Developments and New Applications,* 2006.

10. Andrzejewska E., "Photopolymerization Kinetics of Multifunctional Monomers", *Progress in Polymer Science,* Vol. 26, pp. 605-665, 2001.

11. Allonas, X., J. Lalevée, F. M. Savary and J. P. Fouassier, "Understanding the Reactivity of Photoinitiating Systems for Photopolymerization", *Polimery*, Vol. 51, pp. 491-498, 2006.

12. Wang, H., J. Wei, X. Jiang and J. Yin, "Novel Chemical-Bonded Polymerizable Sulfur-Containing Photoinitiators Comprising the Structure of Planar *N*-phenylmaleimide and Benzophenone for Photopolymerization", *Polymer*, Vol. 47, pp. 4967-4975, 2006.

13. Nayak, B. R. and L. J. Mathias, "A Novel Photoinimer for the Polymerization of Acrylates and Methacrylates", *Journal of Polymer Science: Part A: Polymer Chemistry,* Vol. 43, pp. 5661-5670, 2005.

14. Karahan, O., D. Karaca Balta, N. Arsu and D. Avci, "Synthesis and Evaluations of Novel Photoinitiators with Side-Chain Benzophenone, Derived from Alkyl α-hyrdoxymethacrylates", *Journal of Photochemistry and Photobiology A: Chemistry*, Vol. 274, pp. 43-49, 2014.

15. Yang, J., R. Tang, S. Shi and J. Nie, "Synthesis and Characterization of Polymerizable One-Component Photoinitiator Based on Sesamol" *Photochemical & Photobiological Sciences,* Vol. 12, pp. 923-929, 2013.

16. Karaca Balta, D., O. Karahan, D. Avci and N. Arsu, "Synthesis, Photophysical and Photochemical Studies of Benzophenone Based Novel Monomeric and Polymeric Photoinitiators" *Progress in Organic Coatings,* Vol. 78, pp. 200-207, 2015.

17. Cesur, B., O. Karahan, S. Agopcan, T. N. Eren, N. Okte, D. Avci, "Difunctional Monomeric and Polymeric Photoinitiators: Synthesis and Photoinitiating Behaviours", *Progress in Organic Coatings*, Vol. 86, pp. 71-78, 2015.

18. Corrales, T., C. Peinado, F. Catalina, M. G. Neumann, N. S. Allen, A. M. Rufs and M. V. Encinas, "Photopolymerization of Methyl Methacrylate Initiated by Thioxanthone Derivatives: Photoinitiation Mechanism", *Polymer,* Vol. 41, pp. 9103-9109, 2000.

19. Angiolini, L., D. Caretti and E. Salatelli, "Synthesis and Photoinitiation Activity of Radical Polymeric Photoinitiators Bearing Side-Chain Camphorquinone Moieties", *Macromolecular Chemistry and Phys*ics, Vol. 201, pp. 2646-2653, 2000.

20. Allonas, X., J. P. Fouassier, L. Angiolini and D. Caretti, "Excited-State Properties of Camhorquinone Based Monomeric and Polymeric Photoinitiators", *Helvetica Chimica Acta.*, Vol. *84*, pp. 2577-2588, 2001.

21. Wei, J. and F. Liu, "Novel Highly Efficient Macrophotoinitiator Comprising Benzophenone, Coinitiator Amine, and Thio Moieties for Photopolymerization", *Macromolecules*, Vol. 42, pp. 5486-5491, 2009.

22. Wang, J., J. Cheng, J. Liu, Y. Gao and F. Sun, "Self-floating Ability and Initiating Gradient Photopolymerization of Acrylamide Aqueous Solution of a Water-soluble Polysiloxane Benzophenone Photoinitiator", *Green Chemistry*, Vol. 15, pp. 2457-2465, 2013.

23. Jiang, X. and J. Yin, "Polymeric Photoinitiator Containing In-Chain Thioxanthone and Co-Initiator Amines", *Macromolecular Rapid Communications,* Vol. 25, pp. 748-752, 2004.

24. Temel, G., B. Aydogan, N. Arsu and Y. Yagci, "Synthesis and Characterization of One-Component Polymeric Photoinitiator by Simultaneous Double Click Reactions

and Its Use in Photoinduced Free Radical Polymerization", *Macromolecules,* Vol. 42, pp. 6098-6106, 2009.

25. Wang, Y., X. Jiang and J. Yin, "Novel Polymeric Photoinitiators Comprising of Side-Chain Benzophenone and Coinitiator Amine: Photochemical and Photopolymerization Behaviors", *European Polymer Journal*, Vol. 45, pp. 437-447, 2009.

26. Wang, K., Y. Lu, P. Chen, J. Shi, H. Wang and Q. Yu, "Novel One-Component Polymeric Benzophenone Photoinitiator Containing Poly (ethylene glycol) as Hydrogen Donor", *Materials Chemistry and Physics*, Vol.143, pp. 1391-1395, 2014.

27. Cheng, L. and W. Shi, "Synthesis and Photoinitiating Behaviour of Benzophenone-Based Polymeric Photoinitiators used for UV-Curing Coatings", *Progress in Organic Coatings,* Vol. 71, pp. 355-361, 2011.

28. Groot, H. D. J., K. Dillingham, H. Deuring, H. J. Haitjema, F. J. V. Beijama, K. Hodd and S. Norrby, "Hydrophilic Polymeric Acylphospine Oxide Photoinitiators/ Crosslinkers for in Vivo Blue-Light Photopolymerization", *Biomacromolecules*, Vol. 2, pp. 1271-1278, 2001.

29. Chen, Y., J. Loccufier, L. Vanmaele and H. Frey, "Novel Multifunctional Hyperbranched Polymeric Photoinitiators with Built-in Amine Coinitiators for UV-Curing", *Journal of Materials Chemistry*, Vol. 17, pp. 3389-3392, 2007.

30. Si, Q., X. Fan, Y. Liu, J. Kong, S. Wang and W. Qiao, "Synthesis and Characterization of Hyperbranched-Poly(siloxysilane)-Based Polymeric Photoinitiators" *Journal of Polymer Scince, Part A: Polymer Chemistry,* Vol. *44*, pp. 3261-3270, 2006.

31. Xie, H., L. Hu, Y. Zhang and W. Shi, "Sulfur-Containing Hyperbranced Polymeric Photoinitiator End-Capped with Benzophenone and Tertiary Amine Moiteies

Prepared via Simultaneous Double Thiol-Ene Click Reactions Used for UV Curing Coatings", *Progress in Organic Coatings*, Vol. 72, pp. 572-578, 2011.

32. Chen, Y., J. Loccufier, L. Vanmaele, E. Barriau and H. Frey, "Novel Multifunctional Polymeric Photoinitiators and Photo-Coinitiators Derived from Hyperbranched Polyglycerol", *Macromolecular Chemistry and Phys*ics, Vol. 208, pp. 1694-1706, 2007.

33. Wen, Y., X. Jiang, R. Liu and J. Yin, "Amphipathic Hyperbranched Polymeric Thioxanthone Photoinitiators (AHPTXs): Synthesis, Characterization and Photoinitiated Polymerization", *Polymer*, Vol. 50, pp. 3917-3923, 2009.

34. Gacal, B., H. Akat, D. K. Balta, N. Arsu and Y. Yagci, "Synthesis and Characterization of Polymeric Thioxanthone Photoinitiators via Double Click Reactions" *Macromolecules*, Vol. *41*, pp. 2401-2405, 2008.

35. Akat, H., B. Gacal, D. K. Balta, N. Arsu and Y. Yagci, "Poly(ethyleneglycol)-Thioxanthone Prepared by Diels-Alder Click Chemistry as One-Component Polymeric Photoinitiator for Aqeous Free-Radical Polymerization", *Journal of Polymer Science., Part A: Polymer Chemistry*, Vol. 48, pp. 2109-2114, 2010.

36. Jiang, X., J. Luo and J. Yin, "A Novel Amphipathic Polymeric Thioxanthone Photoinitiator" *Polymer*, Vol. 50, pp. 37-41, 2009.

37. Kork, S., G. Yilmaz and Y. Yagci, "Poly(vinylalcohol)-Thioxanthone as One-Component Type II Photoinitiator for Free Radical Polymerization in Organic and Aqeous Media" *Macromolecular Rapid Communications*, Vol. 36, pp. 923-928, 2015.

38. Jiang, X. And J. Yin, "Study of Macrophotoinitiator Containing In-Chain Thioxanthone and Coinitiator Amines", *Polymer*, Vol. 45, pp. 5057-5063, 2004.

39. Corrales, T., F. Catalina, N. S. Allen and C. Peinado, *Journal of Photochemistry & Photobioogy, A,* Vol. 169, pp. 95-100, 2005.

40. Jiang, X. and J. Yin, "Dendritic Macrophotoinitiator Containing Thioxanthone and Coinitiator Amine", *Macromolecules*, Vol. 37, pp. 7850-7853, 2004.

41. Jiang, X., H. Xu and J. Yin, "Copolymeric Dendritic Macrophotoinitiators", *Polymer,* Vol. 46, pp. 11079–11084, 2005.

42. Neglig, E., R. Schneider, L. Vidal, G. Clavier and L. Balan, "Silver Nanoparticles Coated with Thioxanthone Derivative as Hybrid Photoinitiating Systems for Free Radical Polymerization", *Langmuir,* Vol. 28, pp. 17795-17802, 2012.

43. Eken Korkut, E., G. Temel, D. Karaca Balta, N. Arsu and M. Kasım Sener, "Type II photoinitiator substituted zinc phthalocyanine: Synthesis, photophysical and photopolymerization studies", *Journal of Luminescence,* Vol. 136, pp. 389-394, 2013.

44. Jiang, X. and J. Yin, "Polymeric Photoinitiator Containing In-chain Thixanthone and Coinitiator Amines", *Macromolecular Rapid Communications,* Vol. 25, pp. 748-752, 2004.

45. Warren S. C. and L.J. Mathias, "Synthesis and Polymerization of ethyl α-chloromethylacrylate and Related Derivatives", *Journal of Polymer Science Part A: Polymer Chemistry,* Vol. 28, pp. 1637-1648, 1990.

46. Mathias L. J., S. C. Warren and S. Huang, "tert-Butyl .Alpha.-Hydroxymethylacrylate and Its Dimer: Multifunctional Monomers Giving Polymers With Easily Cleaved Ester Groups" *Macromolecules,* Vol. 24, pp. 2036-2042, 1991.

47. Lalevée, J., N. Blanchard, M. A. Tehfe, M. Peter, F. Morlet-Savary, D. Gigmes and J. P. Fouassier, "Efficient Dual Radical/Cationic Photoinitiator Under Visible Light: A New Concept", *Polymer Chemistry,* Vol.2, pp. 1986-1991, 2011.

48. Rehm, D. and A. Weller, *Israel Journal of Chemistry*, "Kinetics of Fluorescence Quenching by Electron and H-Atom Transfer", Vol. 8, pp. 259-271, 1970.

49. Hsio, Jiunn-Shyong and S. E. Webber, *Journal of Physical Chemistry*, "Triplet-State Electron Transfer from Anthracene and Pyrene Covalently Bound to Polyelectrolytes in Aqeous Solution", Vol. 96, pp. 2892-2901, 1992.

50. Brandrup, J. and E. H. Immergut, *Polymer Handbook*, Wiley-Interscience, New York, 1975.

51. Tehfe M. A., J. Lalevée, S. Telitel, J. Sun, J. Zhao, B. Graff, F. Morlet-Savary and J. P. Fouassier, "Iridium Complexes Incorporating Coumarin Moiety as Catalyst Photoinitiators: Towards Household Green LED Bulb and Hydrogen Lamp Irradiation", *Polymer,* Vol. 53, pp. 2803-2808, 2012.

52. Tehfe, M. A., J. Lalevée, F. Morlet-Savary, B. Graff, N. Blanchard and J. P. Fouassier, "Tunable Organophotocatalysts for Polymerization Reactions under Visible Light", *Macromolecules,* Vol. 45, pp. 1746-1752, 2012.

53. M. J. Frisch et al (2009) Gaussian 09, revision C.01. Gaussian, Inc., Wallingford.

54. Tehfe, M. A., F. Dumur, B. Graff, F. Morlet-Savary, J. P. Fouassier, D. Gigmes and J. Lalevée, "New Push-Pull Dyes Derived from Michler's Ketone For Polymerization Reactions Upon Visible Light", Macromolecules, Vol. 46, pp. 3761-3770, 2013.

55. Telitel, S., F. Dumur, D. Gigmes, B. Graff, J. P. Fouassier and J. Lalévee, "New Functionalized Aromatic Ketones as Photoinitiating Systems for Near Visible and Visible Light Induced Polymerizations", *Polymer,* Vol. 54, pp. 2857-2864, 2013.